Spectroelectrochemical Study of Electron Transfer Steps at ITO Electrode Modified by Molecular Layer with Viologen Moieties with and without Pt complexes

（ITO 電極上に構築したビオロゲン分子層における白金錯体での電子移動過程の分光電気化学測定による研究　－白金錯体存在の効果－）

Cepi Kurniawan

Graduate School of Chemical Sciences and Engineering
Hokkaido University

2016

ACKNOWLEDGEMENT

CONTENT

CHAPTER 1

INTRODUCTION

1.1. General Introduction

The rising energy demand based on fossil fuel in many countries will affect to two interconnected energy and climate change crises shortly.[1] The invention of carbon-neutral energy resources brings us both in reducing our dependencies on fossil fuel and in limiting the carbon dioxide/monoxide emitted to the environment. Further, in response to the global energy challenges, scientists are going to extent the development of renewable energy resources that able to meet projected energy demands. One of the most promising study results has been focused on hydrogen generation.[2] It show a high efficiency, environmentally friendly fuel that can be produced safely, versatile, and has many potential energy uses, including powering homes, a variety of industrial activities, electric utilities, and non-polluting vehicles. Moreover, hydrogen is anticipated to join electricity as the foundation for a globally sustainable energy system using renewable energy making it the cleanest and simplest sustainable fuel. Therefore, hydrogen is increasingly considered as the fuel of the future.[3-5]

There are various possible pathways to generate hydrogen, but the most common and least expensive way to produce hydrogen at present is by steam reforming reaction from fossil fuel.[6, 7] However, this technology also generates CO or CO_2, which is dangerous to health and represents the great poison for hydrogen fuel-cell catalysts.[8] Water splitting is one of the most promising methods to generate hydrogen. Since the first discovery of electrolytic water splitting into hydrogen and oxygen, water electrolysis both in scientific study and technological application has been continuously showing an improvement.[9, 10]

Water splitting is represented by:

$$2H_2O \rightarrow O_2 + 4H^+ + 4\ e^- \hspace{4cm} \textit{(1-1)}$$

$$4H^+ + 4\ e^- \rightarrow 2H_2 \hspace{5cm} \textit{(1-2)}$$

where Eq. 1-1 takes place at the anode and Eq. 1-2 takes place at the cathode of an electrochemical cell. The standard potential (E^0) is 1.23 V and 0.00 V (vs. NHE) for eq. (1-1) and eq. (1-2), respectively. As dictated by the Nernst equations, both reactions are pH dependent and change by 60 mV per pH unit. Toward the development of an electrochemical cell for water splitting, catalysts are needed to decrease the high activation energy.

Most research in this field has been focused on the development of efficient catalysts to minimize the energy barrier of water splitting reactions. Platinum (Pt) metal efficiently catalyzes hydrogen evolution (HER).[11-16] The main issue in Pt utilization is cost, and thus, various approaches such as controlling Pt loading and use of non-Pt catalyst have been proposed to achieve the sufficient performance, which can overcome the cost issue.

Some metal-free catalysts on HER have been developed.[17-21] Carbon is the most abundant element on the earth and carbon-based materials can be fabricated on a large scale with lower manufacturing cost compared to metal-based. Cui and coworkers reported that carbon nanotubes act as a highly-active metal-free electrocatalyst for HER.[22] Melem, the building unit of g-C_3N_4, was also reported for the first time as a metal-free photocatalyst for hydrogen evolution.[23] In advance, Chu and coworkers demonstrated that incorporation of transition metals within melem sheets could increase their catalytic activity. [24] However, to my knowledge, there is no report about a catalyst for electrocatalytic hydrogen evolution beyond metals.

The transition metals are very likely owing to their stability and abundance, and low cost.[25-31] Nickel(Ni) is one of the most promising materials identified so far.[32-34] Ni

alloys have been proposed to replace Pt because of their low cost, high availability, low overpotential, and stability in alkaline solutions.[35, 36] This consideration also applies to other non-noble-metal catalysts. However, group VI transition metal chalcogenides[37, 38], nitrides and carbides[39, 40] exhibit similar properties such as corrosion resistance, stable, and high melting point, in which the research interest during the past few decades was increased in the context of their potential utilization as electrocatalysts. Metal complexes have been introduced due to their high activity and tenability as well as Pt.[41-44] Many fundamental studies on both electrochemical and photoelectrochemical of HER catalyzed by Ni and cobalt (Co) complexes have been reported.[45-47]

However, The Pt metal is still important, thus, Pt complex based catalyst is being developed for HER catalyst. To extend the studies on Pt complex catalysis, Uosaki and coworkers have been made continuous efforts to better understand the hydrogen evolution reaction (HER) from water catalyzed by Pt-based molecular catalysts by employing the so-called "confined molecular catalyst".[48-50]

1.2. Molecular Catalyst

1.2.1. Homogeneous and heterogeneous catalyst

Catalyst plays a significant role in various chemical and biological reactions. Catalysts categorize into homogeneous and heterogeneous catalyst based on their utilization condition. The former is exists in the same a phase as the reactants and/or products, whereas the latter catalyst is defined to be in the different phase with the reactants and products.

The major advantage of homogeneous catalyst is every single point of catalyst can act as a single active site. This provides homogenous catalyst intrinsically more active and selective at molecular level. Thus, the term of molecular catalyst bind to the homogenous

catalyst.[51] Enzymes,[52, 53] organometallic compounds,[54-56] and various transition metal complex, are various typical homogenous catalyst mostly studied and utilized in the industrial process. Practically, in general, they perform high activity and selectivity under mild reaction conditions. Unfortunately, homogenous catalyst is difficult to recycle and to separate from the products.

On the other hand, heterogeneous catalyst serves features to reuse within another catalysis cycle. Commonly, heterogeneous catalyst exists in the solid state. An extensive range of solid state materials have been evaluated for various catalysis reactions, including a metal and semiconductor.[57] Compare to active site of homogeneous catalyst, heterogeneous catalysts usually contain a broad range of active sites, thus, the molecular-level approaches to heterogeneous catalysis are challenging.

Fabrication of heterogeneous catalyst with molecular active site takes advantage not only to improve the selectivity of close to homogeneous catalyst but also it is easy to separate the product from the catalyst in the heterogeneous system. The heterogeneous molecular catalyst, at least, minimizes waste generated for catalyst separation and allowing recyclability of the catalyst. From the economic view, recyclability is an importance part since the catalysts are, sometimes, being the most expensive component. In scientific aspects, a future interest in the design of catalysis will probably focus in the investigation of deep mechanistic understanding down to the atomic scale.

1.2.2. Confined molecular catalyst

Molecular catalysts are interesting due to their high activity achievement and tenability.[58] Attachment of molecular catalyst means to combine homogeneous and heterogeneous catalytic. Such confined molecular catalyst typically attaches over solid

supports with high surface area. They present general features such as consist of one or few atoms; spatially separated from one another; active sites are well-characterized.[59] However, the immobilized molecular catalyst usually performs less than their homogeneous catalyst.

There are several ways for the synthesis of immobilized molecular catalysts. Anchoring catalyst onto porous material has been well-known for many years. Ordered mesoporous silica, for example, provides excellent opportunities for the immobilization of homogeneous catalysts via covalent binding because of the availability of silanol groups.[60-63] These silanol groups provide reactive sites for functionalization[63] and offer tunable surface properties that allow us to control both position and density of the immobilized catalyst precisely.

Schubert and coworkers anchoring the metal complex via polymerization or copolymerization.[64] They reported various metal-containing systems, including polypyridyl complexes, metallocenes, porphyrin, and salen compounds incorporated into polymeric frameworks by applying electropolymerization techniques. The similar work also reported by Serge[65] and Schuhmann[66] by performed oxygen reduction reaction at electropolymerized films of containing a number of different manganese, iron, and cobalt porphyrins supported on multi-walled carbon nanotubes (MW-CNTs). Another way to incorporate the active catalyst via polymer binding is by using layer-by-layer assembling as it reported by Uosaki and coworkers.[67] The well-controlled of gold nanoclusters in a layer-by-layer assembly with polymer binding layers had been demonstrated to be affected by pH and ionic strength of the polymer solution when nanoparticles covered with mercaptoundecanoic acid layer.

The incorporation of molecular catalyst via ionic interaction by using ion exchange

also widely developed. The immobilization of homogeneous catalysts such as metal complex to solid-support has received considerable attention. Metal complex or organometallic compounds, a typical homogeneous catalyst, is ionic species, and then ionic bond immobilization of such molecular complex ions to opposite ionic charge layer-modified surfaces was known. Figure 1-1 illustrates the ion exchange mechanism on viologen modified Si(111).[50] Viologen moieties are positively charged; then the halide ions neutralize the charge. The halide ion was exchanged by using the molecules with the same charge, in this case [$PtCl_4^{2-}$] ions. [50, 68, 69]
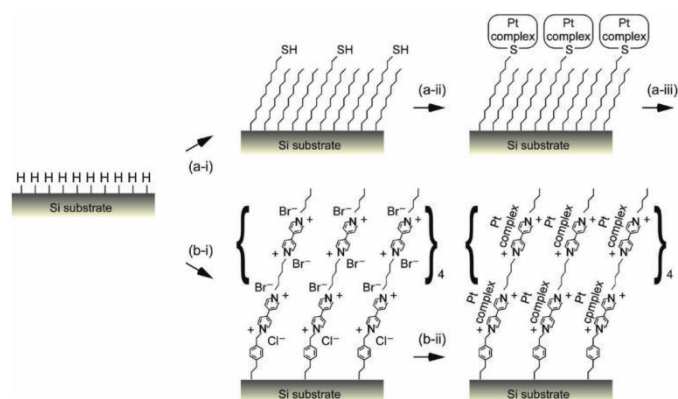
Figure 1-1. Immobilization of $PtCl_4^{2-}$ into viologen layers constructed on silicon surfaces.[69]

Incorporation of Pt complex within viologen layers reported by Uosaki and coworkers demonstrated that the H_2-evolving activity of immobilized Pt complexes (Figure 1-2(i)). Further, extensive efforts have been devoted understanding the mechanism of hydrogen evolution (HER) catalyzed platinum(II) complexes was proposed.[69] The state of Pt complex was investigated by XPS (Figure 1-2(ii)). The SEM image obtained after $NaBH_4$ treatment shows no Pt particles was formed; indicate that Pt complex was well organized within viologen layers (Figure 1-2(iii)). The fact that Pt complex is well controlled within

organic layer was proved from in-situ EXAFS spectra results showing that during HER (by applying potential -0.6 and -0.8 V) no Pt-Pt bond was observed (Figure 1-2(iv)).

(i)

(ii)

(iii)

(iv)
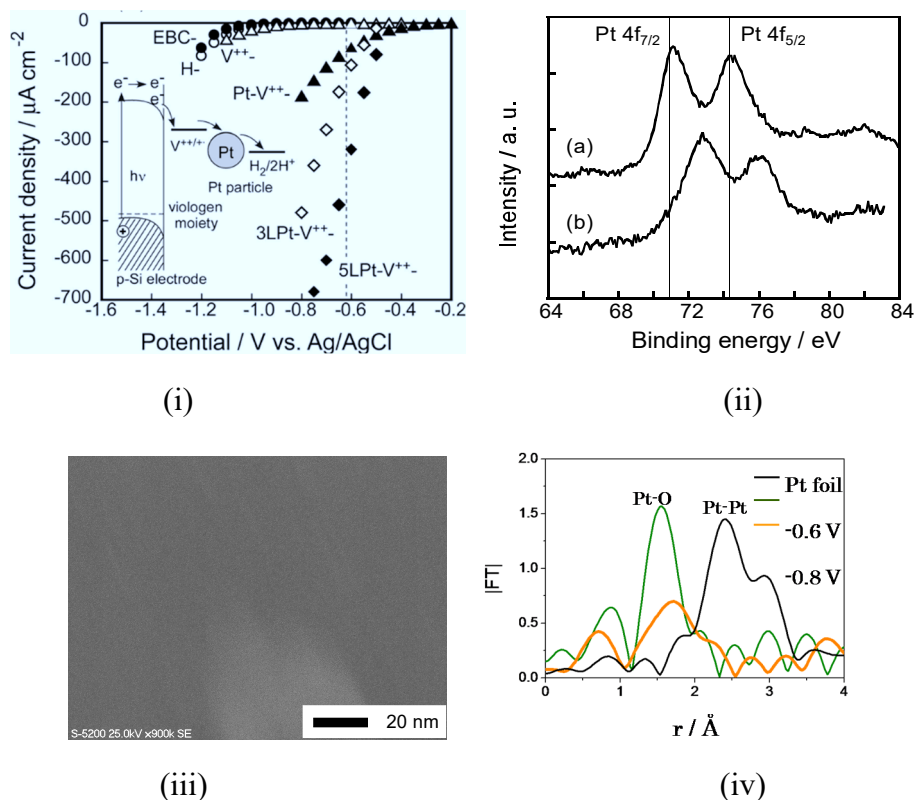
Figure 1-2. (i) I-V curve of Pt complex incorporated within viologen layer,[68, 69] (ii) XP-spectra of (a) Pt-complex and (b) Pt metals within viologen layers,[70] (iii) SEM image of Pt within viologen layer, and (iv) comparison of Fourier transformed EXAFS spectra of Pt foil (black line), Pt-complex at -0.6 V (green line) and -0.8V (orange line)).

1.3. Viologen

Viologens is the common name for compounds related to the N,N`-disubstituted-4,4`-bipyridium salt. It was originally investigated as a redox indicator in biological studies. Further, they were also found to be a good herbicide.[71] Later, there were many fundamental and applied investigation due to the electrochromic properties of these

compounds. Recently, they have been utilized as an electroactive component, both in free form or bound to the electrode surface, in the solar energy conversion devices.[72]

Viologens are the most intensively studied molecular building blocks in supramolecular chemistry. Their solution electrochemistry is well documented in the literature.[73] Certain attention was paid to the surface chemistry of viologens using standard electrochemical methods such as cyclic voltammetry (CVs), [74-77] quartz crystal microbalance (QCM)[78] and various spectroscopic methods, e.g. FTIR [79] Raman spectroscopy [80, 81] or UV spectroscopy [75, 82, 83] in order to obtain structural information on the particular viologen redox-states.

1.3.1. Physical and electrochemical properties

The main characteristic of the viologens family is their ability to exist in three common oxidation states, viologen dication (V^{2+}), viologen radical cation ($V^{\bullet+}$), and its neutral form (V^0). The formation of different redox states of viologen and their molecular structure is shown in Figure 1-3.[84]
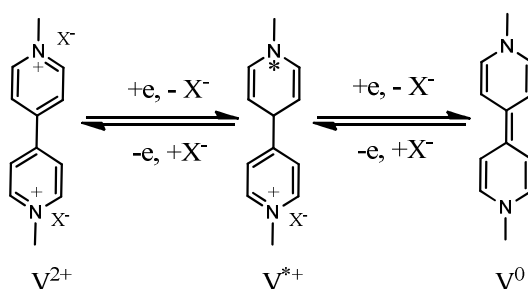
Figure 1-3. Schematic structure of viologen at different oxidation states.[84]

The $V^{\bullet+}$ species is soluble in organic solvents such as methanol, acetonitrile, and dimethylformamide. However, viologen only soluble if the counter anion (X^-) is large, such

as NO_3^-, PF_6^- or ClO_4^-. On the other hand, their solubility in water is slightly more complicated. Some anion imparts a high solubility to the V^{2+} but causes ion pairing with the $V^{\bullet+}$ species to make the $V^{\bullet+}$ precipitated.

Aqueous solutions of the $V^{\bullet+}$ species vary in color from blue to purple depend on the concentration and temperature. Kosower and Cotter (1964) proposed the monomer-dimer equilibrium.[85] They found that the $V^{\bullet+}$ is violet in cold solution but become blue upon warming. This color change is fully reversible. The equilibrium is expressed in Eq. (1-3).

$$(V_2)^{2+} \rightleftharpoons 2V^{\bullet+} \tag{1-3}$$

Other unique properties of $V^{\bullet+}$ species are their ability to form radical micelles in aqueous solution. The asymmetric viologens are the most commonly studied owing to their capacity to facilitate the assembly process by providing the hydrophobic interactions. The presence of micelles can affect dramatically on the electrochemistry of viologen. Lee and coworkers have reported that N-methyl-N′- hexadecyl viologen systems became significantly changes when the surfactant was mixed in an anionic system.[86]

The viologen species are easy to detect by using voltammetry.[87-89] Figure 1-4 shows the cyclic voltammograms (CVs) of a gold electrode in 1 mM methyl viologen (MV^{2+}) and 0.1 M K_2SO_4 supporting electrolyte solution. Two pairs of redox peaks a/a` and b/b` are associated with the redox couple $MV^{2+}/MV^{\bullet+}$ and $MV^{\bullet+}/MV^0$, respectively. The appearance of the peak c is related to the formation of the dimer ($MV_2^{2+)}$.[84]
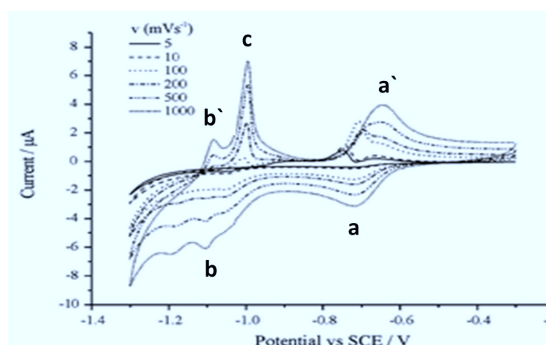
Figure 1-4. Overlaid CVs of 1 mM MV^{2+} in 0.1 M K_2SO_4 solution at a gold electrode, scan rate (v) was ranged from 0.005 to 1 V s^{-1}.[89]

1.3.2. Spectroscopic properties of viologen

1.3.2.1. UV-visible spectra

UV-vis spectroscopic data of viologen always quoted to the intense blue color of $V^{\bullet+}$. A detailed information related to all the three viologen redox states are well studied.[90] The typical UV-vis spectra of methyl viologen (MV) are shown in Figure 1-5.

While aqueous solutions of MV^{2+} do not absorb light to an appreciable extent above 260 nm ($\varepsilon_{260} = 20.700$ $M^{-1}cm^{-1}$), both $MV^{\bullet+}$ and MV^0 exhibit well-characterized UV-visible spectra with maxima at 400 nm ($\varepsilon_{400} = 42.100$ $M^{-1}cm^{-1}$) and 600 nm ($\varepsilon_{600} = 13.700$ $M^{-1}cm^{-1}$) for $MV^{\bullet+}$ and at 375 nm ($\varepsilon_{370} = 34.500$ $M^{-1}cm^{-1}$) and 400 nm ($\varepsilon_{400} = 42.500$ $M^{-1}cm^{-1}$) for MV^0.[91, 92] Kosower and Cotter also reported that $MV^{\bullet+}$ are in equilibrium with the dimer (MV_2^{2+}).[91] The presence of MV_2^{2+} has been characterized by the presence of absorption 375, 550 and 870 nm with decreasing of the $V^{\bullet+}$ absorption and it was attributed to the dimerization of $MV^{\bullet+}$ (inset in Figure 1-5).[91]

Wavelength / nm
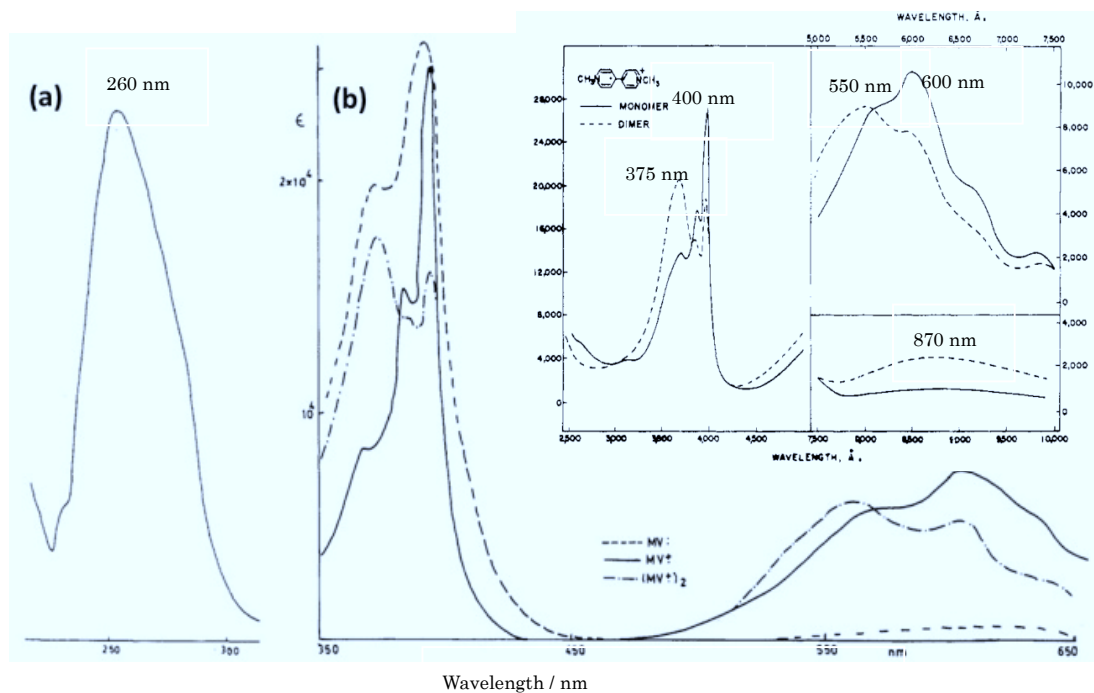
Figure 1-5. UV-Vis spectra of (a) MV^{2+} and (b) monomer $MV^{\bullet+}$ (solid line), MV^0 (dashed line) and dimer $(MV^{\bullet+})_2$ (dot-dashed line) in acetonitrile.[90] Onset: Enlarge scale of viologen radical cation monomer and dimer.

The dimerization of $V^{\bullet+}$ affects the electrochromic properties of viologen and further reactions where $V^{\bullet+}$ involved. Many electroactive organic materials performed distinct UV-Vis absorption spectra when they switched to different redox states. This such material named as electrochromic materials. Commonly, the color changes from colorless (chromophore only absorb UV energy, "bleach mode") to colored states (chromophore absorb visible energy, "write mode").[93] Electrochromic devices are a typical application of electrochemical cells. It consists in two-electrode configuration and, where the electrodes are separated by supporting electrolyte. Application of electrochromic materials includes displays,[94] smart windows,[95] and optical shutter.

The utilization of viologen in electrochromic devices has been explored. Among viologens compounds, 1,1`-diheptyl-4,4`-viologen; (HV^{2+}) is usually used for

11

electrochromic applications because its radical cation (HV$^{\bullet+}$) can form an insoluble violet film on an electrode surface.[83, 96, 97] The nature of the alkyl chain of viologen does affect the solubility properties of the resulting reduced form. However, recently, the derivatization of viologen to explore their electrochromic properties dramatically increase.[98] The V$^{\bullet+}$ species, with their long alkyl substituents, are also often electrodeposited due to an increase in the hydrophobic character of the substituents. [4,5,10] Furue and Nozakura reported UV-vis spectra of electrodeposited l e$^-$ reduction products of V^{2+} are similar to those of (V$^{\bullet+}$)$_2$ and the UV-Vis spectra of 2 e$^-$ reduced bisviologen (C$_1$V$^{\bullet+}$C$_n$V$^{\bullet+}$C$_1$: n = 2, 3, 4, 5), which can form intramolecular dimers as well as intermolecular dimers. Close examination of the reported (V$^{\bullet+}$)$_2$ spectra reveals a considerable difference in the shape of the 550 nm band and the absorption in the near-IR region. However, little attention has been given to these, and most of the studies on absorption spectra have been carried out up to 800 to 900 nm.[99]

1.3.2.2. FTIR spectra of viologen

The viologen structure and redox functionality have been studied by vibrational spectroscopy.[79, 100, 101] Figure 1-6(A) shows the in situ surface-enhanced infrared absorption spectroscopy (SEIRAS) studies of viologen with different alkyl chain (nVn, n = number of the carbon atom in alkyl chain). Three main regions of viologen-related vibration modes that are, ring vibrational mode of bipyridine (1000~1750 cm^{-1}), CH- stretching of alkyl chain (2800~3000 cm^{-1}), and CH-stretching in aromatic ring of bipirydine (3000~3100 cm^{-1}). The characteristic vibration mode of viologen species are below 1750 cm^{-1} region. The in-plane dipole moment either parallel to the long molecular axis (B3u in D2h symmetry: 1642, 1508, 1225, 1180 cm^{-1}) or parallel to the short molecular axis (B2u modes in D2h symmetry: 1450, 1355, 1280 cm-1).[102]

Figure 1-6(B) are shown the reflection absorption spectra (IRRAS) of three redox state of viologen in aqueous solution, MV^{2+}, and the electrogenerated species, $MV^{\bullet+,}$ and MV^0. The bands at 1605, 1511, 1340, 1201, and 1184 cm^{-1} appeared with large intensities at 0 V. All of those bands intensity were growth at -1.0 V, in which $V^{\bullet+}$ is exist, and decrease in intensities at -1.4V, as the V^0 was formed. The reversible evolution of the IR bands in the range of the ring vibrations for $V^{2+}/V^{\bullet+}$ agrees with the conclusions drawn from CVs.[101]
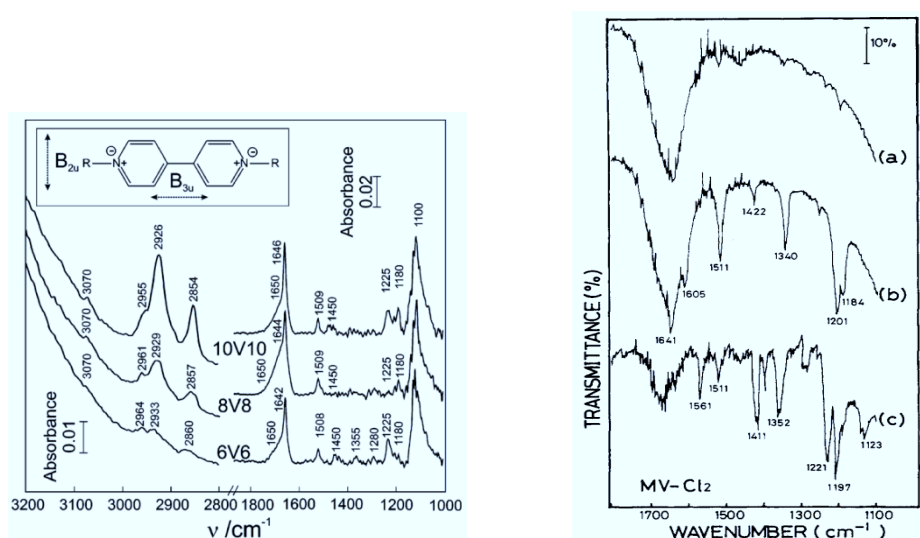
Figure 1-6. (A) In situ SEIRA spectra of viologen with different alkyl chain.[102] (B) IR spectra for 0.1 M MVCl$_2$ in aqueous solution at (a) 0 (MV^{2+} state), (b) -1.0 V ($MV^{\bullet+}$ state), and (c) -1.4 V (MV^0 state).[101]

1.3.3. Electron mediator behavior of viologen

Viologen is one of the most extensively used electron transfer mediator groups for reduction of various biological molecules such as cytochrome-c, [103-105] hydrogenase, [106, 107] horseradish peroxidase, [108] NADH, [109] myoglobin, [110] ferredoxin, [111, 112] and other proteins.[113] Figure 1-7(a) are shown a schematic representation of the electron transfer mediation function of viologen in a biological system. Three component photochemical have been developed as an artificial biological system, which is consist of an

aqueous solution of ruthenium (II) tris (2, 2'-bipyridine) [114-120] or an alternative photosensitizer such as porphrin[121-125] as a photosensitizer, methyl viologen as an electron-transfer mediator, and the last component is catalyst.[126, 127]
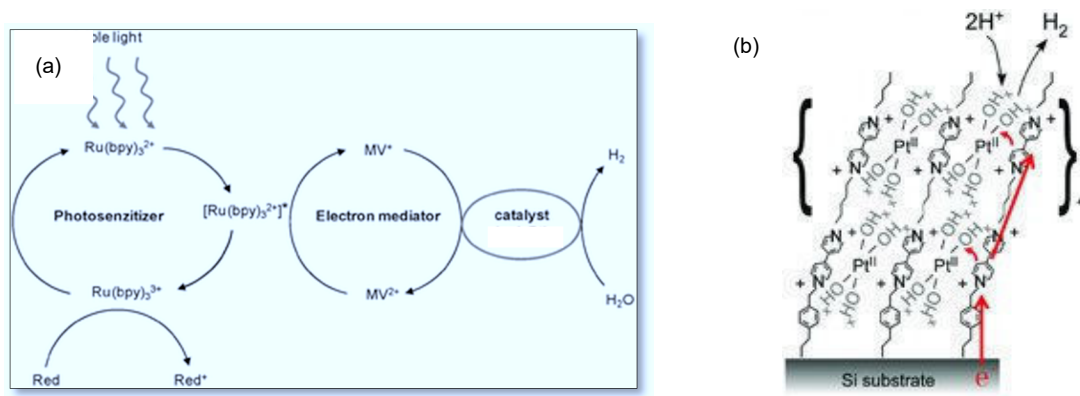
Figure 1-7. Overview of the photoinduced reduction of water mediated by MV^{2+}.[106] and (b) hydrogen evolution reaction catalyzed by Pt complex suggesting that electron was transferred via viologen moiety.[69, 70]

There are a wide variety approach to immobilize viologen onto electrode surfaces including metals,[128, 129] Nafion membrane,[130] glassy carbon,[131-133] zeolite-modified carbon-paste electrode,[134, 135], titanium dioxide [136] and silicon surfaces.[68, 137] In advanced, both for practical and fundamental studies, electron transfer mediator properties of viologen has been addressed on the chemical attachment of viologen compounds on the gold electrode surface.[138] a numerous work related to the utilization of gold as a substrate for viologen immobilization has been reported.[139-145] Such stable and well-ordered self-assembled monolayer (SAMs) of viologen-functionalized thiol was used to immobilize and electrically connect various protein and enzyme such as cytochrome[143] and horseradish peroxidase (HRP)[139]. Hawkridge and coworkers have extended their studies to immobilize cytochrome on polymeric viologen.[146] the similar work was also

reported by Simon and Moore. They were reported that the polyviologen is stable in air for some days but at the same time is electro-active in that it can act as a mediator. [147]
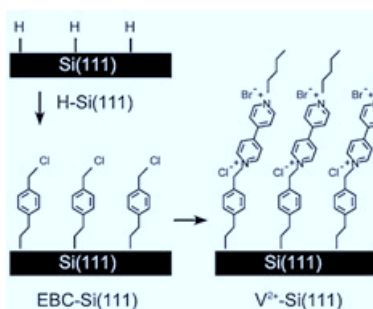
Figure 1-8. Schematic illustration of modification steps of hydrogen-terminated Si(111) surface to obtain metal complex-V^{2+}-Si(111) surfaces.[68]

Uosaki and coworkers reported more recent studies on the viologen immobilization (Figure 1-8). Silicon is a more attractive substrate to construct functional surfaces than gold in conjunction with technological applications. Recently, the formation of monolayer via Si-C bond via photochemical[148, 149], electrochemical reactions,[150, 151] and reactions with radical initiators[151-154] has extensively attracted much attention. Mono- and multilayer of viologen monolayer was constructed on hydrogen-terminated n- and p-type Si(111) surfaces via Si-C bond. In the work of Uosaki and Masuda [68], Si(111) was functionalized via surface coupling reactions that involve the attachment of 4-vinylbenzyl chloride on Si-H terminated surface followed by 1-methyl-4,4`-bipyridine coupling (Figure 1-8). Further, they also prepare multilayers of viologen via the surface coupling reactions.[69] Stepwise surface coupling reaction for surface modification is beginning to fabricate enormous interest because of the potential for achieving quantitative coupling of species to a surface with no side reactions.[155]

1.4. Functionalization of Indium Tin Oxide (ITO)

Considerable development in spectroelectrochemistry had taken place since 1964 when Kuwana introduced the basis of this analytical method [156]. The advantage of spectroelectrochemical techniques is they can provide spectral data that are complementary to the current or voltage response of conventional electroanalytical techniques. Spectroelectrochemical techniques also provide molecular specificity and structural information of the species under interest and the selective control of oxidation state by varying potentials. A transparent conducting electrode (TCE) is needed to conduct spectroelectrochemical measurements. Among various TCE studied, indium tin oxide (ITO) is a very promising material and attracted a great deal of research. ITO known as a non-stoichiometric and doped of tin and indium oxide and shows high transmittance and conductivity.[157]

The attachment of organic moieties to the surface of indium-tin-oxide (ITO) has been the subject of interest due to the potential applications in fabricating transparent contacts for organic optoelectronic devices and in sensors for chemical and/or biological reagents. The particular application that motivated the present investigation is an interest in using organic molecules in a stepwise surface reaction coupling procedure to tether molecular catalyst to an ITO surface. For this purpose, it is necessary to establish the chemical and geometrical structure of the organic adlayer. Some work in this area has been done largely or entirely in ultrahigh vacuum (UHV) [158-160]. However, the majority of ITO functionalization studies have been performed wet-chemically using a wide variety of reagents including organic and organometallic alkoxysilanes [161-164], amines [165-168], carboxylic acids [169-172], phosphonic acids[172-175], and thiols[158, 175].

Figure 1-10 show a confinement of aklylsilane on ITO. Functionalization of ITO with alkylsilane with various end groups is still important.[176-178] ITO functionalized alkylsilanes, such as aminopropyl-trimethoxysilane, have been used mainly for attaching organic and biological molecules onto ITO. [179] 3-Aminopropyl-triethoxysilane (APTES) has been commonly used to prepare amine-functionalized self-assembled monolayers on ITO electrodes.[180]
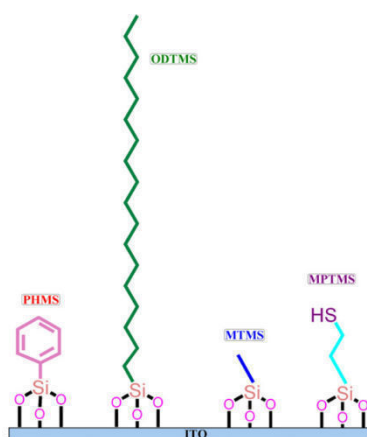
Figure 1-9. Various silane molecules such as phenyl trimethoxysilane (PHMS), octadecyl-trimethoxysilane (ODTMS), methyl tri-methoxysilane (MTMS) and 3-mercaptopro-pyltrimethoxysilane (MPTMS) used for SAM formation on ITO electrodes.[178]

Various approaches have been carried out to immobilize viologen on ITO. Liu and coworkers [181] reported the functionalization of ITO surfaces with viologen moieties by using graft polymerization from vinyl benzyl viologen (VBV) monomers. They demonstrate that viologen moiety was stable on ITO surface based on voltammogram of viologen species and utilize it as electrochromic electrodes. Polymerization of viologen is potential to be used in electrochemics devices. Jain and coworkers reported the ionic self-assembled multilayer of polyviologen (PV) polyacrylamido-methylpropanesulfonic acid (PAMPS) on ITO. PV was synthesized by polymerization of N,N'-bis(aminopropyl)-4,4'-bipyridinium bromide

hydrobromide (APD) and isophthaloyl chloride (ISP). [182] Formation of viologen polymer was also reported by Ng and coworkers.[183] Unfortunately, most of polymeric viologen with short alkyl substituent is soluble in water then it will be washed away during application.[184, 185]

Langmuir-Blodgett film method to form heterogeneous viologen and hydrogenase film on ITO was also reported.[106, 186] Qian and coworkers compare the hydrogenase activity that directly deposited on ITO surfaces (without viologen), the result shows that concentration of hydrogen produced was similar. This similarity implies that the hydrogenase covered on the viologen layers on the electrode dominates the yield of hydrogen. On the other word, the coverage of viologen on ITO prepared by using Langmuir-Blodgett is lower than the expected number.[106]

Figure 1-10. Immobilization of DAPV on ITO.[180]
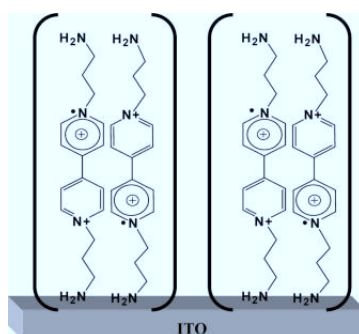
Self-assembled monolayers (SAMs) have attracted great attention due to their potential applications as well as fundamental research. SAMs have many advantages such as exceptional stability, a highly packed and ordered nature, good insulating power, and other unique properties, which use perspective scaffolds for a wide range of applications. However, the interaction of head-group of the assembled molecules should strong enough to obtain well-defined and stable monolayer. SAM of diaminoprophyl-viologen on ITO (DAPV/ITO)

was reported.[180, 187] The DAPV/ITO was then used as a solar cell electrode. The photocurrent of solar cell was improved after ITO modified with viologen. However, the disadvantage of amine group as a linker group was also reported. The bond of amine group on ITO is weak because of N atom will form coulombic interaction with oxygen atoms on ITO surfaces, not a covalent bond.[180]

1.5. Characterization Techniques of Modified ITO Surfaces

Many physical and chemical techniques have been employed to study molecular layer formed on surfaces, such as FTIR Spectroscopy, X-ray photoelectron spectroscopy, and ellipsometry, The presence of conductive surfaces as a conductive substrate makes electrochemistry a powerful approach for characterizing molecular assemblies on the surface.

1.5.1. Voltammetric characterization

Cyclic voltammetry is one of the most widely used methods in the inorganic, physical and biological area for study of fundamental oxidation and reduction reactions. However, in general, it is widely used for qualitative information on electron transfer processes, from the relationship between current and voltage observed in an electrochemical process. Cyclic voltammetry is an important method for characterizing electrode surfaces and testing the cleanliness and reproducibility of an electrochemical system. The applied potential is increased and decreased in a sawtooth waveform (Figure 1-11(a)) and the current response are shown in Figure 1-11(b).

When chemical species are attached to a surface, reversible electron transfer can be recorded. The redox potential, E^0, is determined from the average of the anodic and cathodic

peak potentials, $(E_{pa}+E_{pc})/2$, and the peak separation, ΔE_p, is calculated by $E_{pa}-E_{pc}$. As scan rate increases, peak separation increases. At slow scan rates the peak separation is 0 because the redox center is adsorbed onto the electrode and diffusion does not play a role as well the reaction is controlled only by electron transfer kinetics, the areas under both peaks are equal. The area gives the amount of charge required (Q) to carry out the electrochemical process, which gives the amount of material bonded to the surface.
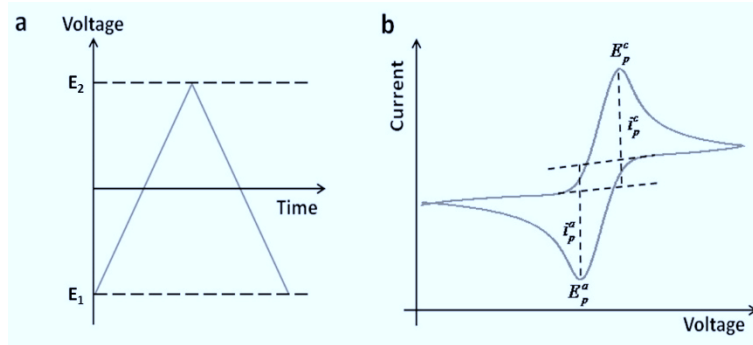
Figure 1-11. Potential waveform applied to working electrode in cyclic voltammetry and (b) Diagram of cyclic voltammogram (CV) for a simple reversible redox couple.

The integrated voltammetric charge recorded under the current peak can be used to estimate the surface coverage (Γ) of electroactive species using Eq. (1-5):

$$\Gamma = \frac{Q}{nFA}$$

(1-5)

where Γ = surface coverage (mol cm^{-2}), Q = charge (C cm^{-2}), n = number of electron involve, and F = Faraday constant (96.485 J per Volt gram equivalent) and A electrode area (cm^2).

1.5.2. UV-vis spectroscopy

A molecule of any substance has an internal energy that can be considered as the total of the energy of its electrons, the vibration energy between atoms and the energy associated with rotation of the molecule. In absorption spectroscopy, though the mechanism of absorption of energy is different in the ultraviolet, infrared and nuclear magnetic resonance regions, the fundamental process is the absorption of a discrete amount of energy. The energy required for the transition from a state of lower energy to state of higher energy is exactly equivalent to the energy of electromagnetic radiation that causes transition. The typical electronic transition for several functional groups shown in Figure 1-12.
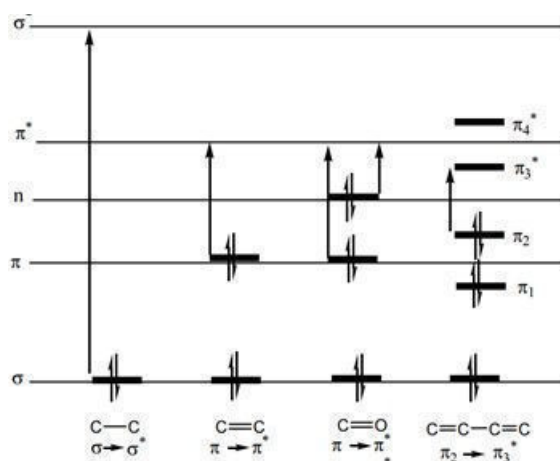
Figure 1-12. Relative energies of orbitals most commonly involved in electronic spectroscopy of organic molecules.

Ultraviolet – visible spectroscopy (λ=200 - 800 nm) studies the changes in electronic energy levels within the molecule arising due to transfer of electrons from π- or non-bonding orbitals. It commonly provides the knowledge about π-electron systems, conjugated unsaturated systems, aromatic compounds and conjugated non-bonding electron systems, etc. This absorption spectroscopy uses electromagnetic radiations between 190 nm to 800

nm and is divided into the ultraviolet (UV, 190-400 nm) and visible (VIS, 400-800 nm) regions. Since the absorption of ultraviolet or visible radiation by a molecule leads transition among electronic energy levels of the molecule, it is called as electronic spectroscopy. The information provided by this spectroscopy when combined with the information provided by NMR and IR spectral data leads to valuable structural determination.

The greater the number of molecules that absorb light of a given wavelength, the greater the extent of light absorption and higher the peak intensity in the absorption spectrum. If there are only a few molecules that absorb radiation, the total absorption of energy is less and consequently lower intensity peak is observed. This makes the basis of Beer-Lambert Law, which states that the fraction of incident radiation absorbed is proportional to the number of absorbing molecules in its path. When the radiation passes through a solution, the amount of light absorbed or transmitted is an exponential function of the molecular concentration of the solute and a function of the length of the path of radiation through the sample. Therefore,

$$-\log I_0 / I = Abs = \varepsilon\, c\, b \qquad\qquad (1\text{-}6)$$

where I_0 = Intensity of the incident light (or the light intensity passing through a reference cell) I = Intensity of light transmitted through the sample solution c = concentration of the solute in M, b = path length of the sample in cm.

As mentioned earlier that viologen radical cation ($V^{+\bullet}$) and neutral (V^0) species are strong chromophores in the visible region. In addition, the Beer–Lambert law can be applied to viologen in solutions and the resulting solution concentration, c, determined as:

$$C = \frac{Abs}{b \times \varepsilon} \qquad\qquad (1\text{-}7)$$

$$\Gamma_{monolayer} = \frac{Abs}{1000 \times \varepsilon} \qquad\qquad (1\text{-}8)$$

For a surface-confined molecule, the path length b is the thickness of the viologen layers, which is also difficult to evaluate. Reducing the resulting solution to a defined volume, V $(0.001\ b)$, and measuring the $V^{\bullet+}$ or V^0 band absorbance, the Beer–Lambert law can be applied to determine the viologen concentration on the surface. Noting that the concentration C multiplied by the path length b is proportional to the surface concentration $\Gamma_{monolayer}$, the Lambert-Beer law can be modified as shown in Eq. 1-8.

1.5.3. Fourier transform infrared (FTIR) spectroscopy

The FTIR spectroscopy is used in material science to identify the chemical composition of materials quickly. This technique identifies molecules by measuring their infrared absorption spectra. In an FTIR spectrometer, molecules are illuminated with two IR beams (one with fixed length and other with variable length). The energy of the IR irradiation is absorbed by molecules and is transformed into molecular vibrations. This absorption is quantized and specific to different covalent bonds within various chemical functional groups. The combination of the two IR beams produces a series of constructive and destructive interference pattern and the results in variation in the intensities of the IR irradiation forming an interferogram. Fourier transform converts this interferogram to IR spectra, which can be used to identify the functional group present on the surface.

There are many advantages in using FTIR spectroscopy, for instance, it allows simultaneous analysis of multiple frequencies. It has a high S/N ratio, high resolution (<0.001 cm^{-1}), and low detection limit (micro or nanograms of the sample) makes it quick and qualitative measurement to identify the presence of organic compounds in self-assembled monolayers, but it is not useful for identifying the defect in SAMs.

It is necessary to include backside reflection into the model for a semitransparent film

if the glass substrate is not roughened or reflections from the backside are avoided by some other method (Figure 1-13). For ellipsometry and FTIR measurement, we roughened the back surface of the samples by means of sandblasting/polishing, except for those samples intended for spectroelectrochemical treatment for which transmittance measurements.[188]
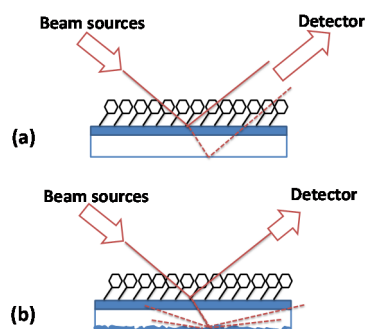
Figure 1-13. Unwanted reflections from the back surface on a smooth surface (a) and suppressed by roughening (b).[188]

1.5.4. Ellipsometry

Spectroscopic ellipsometry is a method of accurately measuring various properties such as thickness, refractive index, and extinction coefficient of thin metal, polymer or semiconductor film [189, 190]. The vertical resolution of this technique is < 0.1 A. This technique enables researchers to identify the average thickness of individual layers in a multilayered sample [190-192].

Spectroscopic Ellipsometry measures the properties of a substrate by illuminating the surface with linear polarized light (Figure 1.14); this light may reflect from or transmit through the substrate at the surface-air interface.
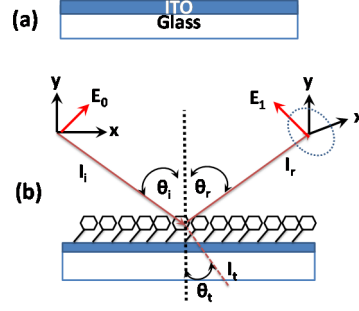
Figure 1-14. (a) ITO substrate model and (b) a schematic representation of the incident light (I_i), the reflected light (I_r) and transmitted light (I_t) shows the change in their polarization in an ellipsometry measurement.

The interaction of the light and results in the polarization of the reflected light being modified from linear to elliptical. Knowing the polarization of incident beam and measuring polarization of reflected beam, the relative phase change (Δ) and the relative amplitude change (Ψ) can be calculated. Ψ and Δ are used to determine s-polarized and p-polarized light ratio reflected off the surface:

$$e^{i\Delta} \tan \Psi = \frac{E_{reflected(p)} / E_{incident(p)}}{E_{reflected(s)} / E_{incident(s)}} \tag{1-9}$$

$$e^{i\Delta} \tan \Psi = \frac{r_p}{r_s} \tag{1-10}$$

Ψ and Δ are related to the Fresnel's equation:

$$r_p = \frac{n_1 \cos \Theta_0 - n_0 \cos \Theta_1}{n_1 \cos \Theta_0 + n_0 \cos \Theta_1} \tag{1-11}$$

$$r_s = \frac{n_1 \cos \Theta_0 - n_0 \cos \Theta_1}{n_1 \cos \Theta_0 + n_0 \cos \Theta_1} \tag{1-12}$$

where Θ_0 and Θ_1 are incident angle and refraction angle, respectively. n_0 and n_1 ($n \equiv N-iK$) is a complex index of refraction of medium and film, respectively. For the simplest three layers model (ambient, film, and substrate) one defines the Fresnel reflection coefficient between medium and film as $r_{01}{}^{p}$ and $r_{01}{}^{s}$ similarly between film and substrate as $r_{12}{}^{p}$ and $r_{12}{}^{s}$, then:

$$ei\Delta \tan \Psi = \frac{(r_{01}{}^{p} + r_{12}{}^{p} e^{-2i\beta})(r_{01}{}^{s} + r_{12}{}^{s} e^{-2i\beta})}{(1 + r_{01}{}^{p} r_{12}{}^{p} e^{-2i\beta})(1 + r_{01}{}^{s} r_{12}{}^{s} e^{-2i\beta})}$$ (1-13)

Where

$$\beta = \sqrt{2\pi(d/\lambda)(n_1{}^{2} - n_0{}^{2} \sin^2 \Theta)}$$ (1-14)

and d is the film thickness. This equation is known as the Drude extension to the Fresnel model.[193]

1.5.5. X-ray photoelectron spectroscopy (XPS)

XPS is a surface chemical analysis technique. XPS spectra are obtained by irradiating a sample with a beam of X-rays while simultaneously measuring the kinetic energy (E_K) and a number of electrons that escape from the top of the material being analyzed. X-rays are generated by bombarding a metallic target (usually Al: 1486 eV, or Mg: 1254 eV) with high-energy electrons. The incoming photons hit the sample causes a photo-ejection ionization of the electrons from the inner shell orbitals. There is certain energy between the core level electrons and the nucleus call binding energy (BE). When the electron is pulled away from the nucleus, the attraction between the electron and the nucleus decreases and the BE decreases until a point is reached when the electron will be free of the nucleus. This is the

point with zero energy of attraction between the electron and the nucleus. The equation describes the kinetic energy of emitted photoelectrons.

$$EK = \text{hv} - BE \tag{1-15}$$

The core level energy depends on the chemical state of the atom. When the element is in different chemical state, e.g. oxidation state, its corresponding energy level will be different, thus giving out photoelectrons at slightly different energies. The energy shift is the correlated with the overall charge on the atom and with the presence of any chemical bonding. This can be interpreted by XPS data to give information of a chemical nature of the sample such as the oxidation state of the atom, number, and type of surrounding atoms, and the electronegativity of atoms.

XPS is chosen when surface composition and the composition as a function of depth are under investigation. XPS has proven to be a very useful technique for the characterization of modified surface. The quality of monolayers constructed on different substrates can be identified by comparing intensities of photoelectrons emitted from samples.[44] XPS has also been used to quantify the atomic ratio and chemical shifts for monolayers.[89] Angle-resolved XPS (AR-XPS) has also been employed to determine the monolayer thickness.[95-101]

From the XPS intensities, we can calculate the elemental composition of the surface. The integrated area of an XPS peak of an atomic species in the bulk is given by:

$$I_X = F\left(hv\right)\sigma_X\left(hv\right)\rho_X V_s T\left(E_X\right)D\left(E_X\right)W_X\left(\beta,\phi\right)\Delta\Omega \tag{3-1}$$

where $F(hv)$ is a photon flux from the x-ray source, $\sigma_X(hv)$ is a photoionization energy, ρ_X is density of emitting species, V_s is volume of sample, $T(E_X)$ is an analyzer transmission at the photoelectron kinetic energy (E_X), $D(E_X)$ is detector efficiency. The $W_X(\beta,\phi)$ is an angular

distribution which depends on an asymmetry factor *(β)* and on the angle between the incident photon beam and the direction of the collected photoelectrons (ϕ). ΔΩ is a solid angle of analyzer acceptance. "X" is refers to a specific core level of a given atomic species. The terms *F(hv)* and ΔΩ are the same for all core levels in a given spectrum, and the analyzer operates in the retard mode in which the energy of the electrons incident on the detector (and, therefore, *D(E$_X$)*) is a constant. All such constant terms cancel in the computation of peak area ratios. The σ_X*(hv)* values are obtained from standard tabulations,[1,2] and the analyzer transmission is obtained by calibration. The angle ϕ ≈ 60° is used, for which W_X*(β,ϕ)* is unity for all "X".

1.6. Objective and Thesis Outline

The role of Pt complex as a molecular catalyst confined within viologen layers has been well understood. However, the electron transfer steps from electrode to Pt complex are still needed to be clarified. The objective of this thesis is to obtain direct prove that electron was transferred via viologen moiety by employing in situ UV-vis spectroelectrochemical technique. Emphasis is addressed on the electrogenerated viologen intermediate formation of in the absence and the presence of Pt complex as a catalyst during HER.

The structure of the present thesis is as follows:

Chapter 1 briefly introduces the important of confined molecular catalysts to overcome the cost issue of platinum catalyst. The viologen properties and immobilization approaches are also reviewed. Some practical consideration in choosing ITO electrode for spectroelectrochemical measurement, ITO surface modification, and related characterization techniques are briefly explained.

Chapter 2 describes the experimental detail such as materials used in this work,

surface modification steps, spectroelectrochemical setup and measurement, and physical characterization are explained.

Chapter 3 deal with viologen layer formation on ITO using a step by step surface coupling reaction. The first step is formation a bromoalkylsilane as a linker layer via hydrolysis of bromoundecyltrichlorosilane on OH-terminated ITO surface to yield Br-ITO. The silane coupling reaction time is followed by FTIR and then the formation of bromo-terminated ITO is confirmed by XPS. The second step is formation of mono- and multi-viologen layers by bipyridine followed by bromoalkyl coupling reactions. The viologen formation is examined from the FTIR and XP spectra. The electrochemical response of $Fe^{3+/4+}$ on modified ITO is also discussed.

In **Chapter 4**, the voltammetric behavior of mono- and multi-viologen layers on ITO and their UV-vis spectroelectrochemical properties are examined. The spectroelectrochemical properties of methyl viologen in solution are discussed for comparison of the free and surface-bound viologen moiety. Potential dependent of steady state UV-vis absorbance spectra of viologen modified ITO are also explained. The time-resolved UV-vis absorbance spectra are also presented.

Chapter 5 present the confinement of Pt complex within viologen layers and their electrochemical and spectroelectrochemical properties are discussed. The HER catalyzed by Pt complex incorporated within viologen monolayer on ITO is checked as a function of number of viologen layers. The UV-vis absorbance spectra of viologen species in the presence of Pt complex is monitored as a function of applied potential. The steady state and time-resolve absorbance spectra of viologen layers with Pt complex are discussed by comparing the results presented in chapter 4. The electrogenerated viologen transient-spectra during double potential steps are analyzed to clarify the role of viologen moiety during HER

catalyzed by Pt complex.

In **Chapter 6**, the conclusions are summarized and future work briefly presented.

1.7. References

1.   McKittrick, E., *Environment* **2014,** *56* (3), 25-35.

2.   Midilli, A.; Dincer, I., *Int J Hydrogen Energy* **2008,** *33* (16), 4209-4222.

3.   Jacques, P. A.; Artero, V.; Pecaut, J.; Fontecave, M., *Proc Natl Acad Sci U S A* **2009,** *106* (49), 20627-32.

4.   Tanaka, K., *Chem Rec* **2009,** *9* (3), 169-86.

5.   Fukuzumi, S.; Yamada, Y., *J Mater Chem* **2012,** *22* (46), 24284-24296.

6.   Busser, G. W.; Mei, B.; Muhler, M., *ChemSusChem* **2012,** *5* (11), 2200-6.

7.   Pan, W.; Zheng, T.; Song, C. S., *Abstracts of Papers of the American Chemical Society* **2002,** *223*, U576-U576.

8.   Besancon, B. M.; Hasanov, V.; Imbault-Lastapis, R.; Benesch, R.; Barrio, M.; Molnvik, M. J., *Int J Hydrogen Energy* **2009,** *34* (5), 2350-2360.

9.   Carmo, M.; Fritz, D. L.; Merge, J.; Stolten, D., *Int J Hydrogen Energy* **2013,** *38* (12), 4901-4934.

10.   Ursua, A.; Gandia, L. M.; Sanchis, P., *Proceedings of the IEEE* **2012,** *100* (2), 410-426.

11.   Abe, T.; Fujita, T.; Sekimoto, K.; Tajiri, A.; Kaneko, M., *J Mol Catal* **2003,** *201* (1-2), 55-62.

12.   Adamiec, J.; Beszterda, S.; Fiedorov, R., *React Kinet Catal L* **1986,** *31* (2), 371-376.

13.   Cretu, R.; Kellenberger, A.; Vaszilcsin, N., *Int J Hydrogen Energy* **2013,** *38* (27), 11685-11694.

14.   Doner, A.; Taskesen, E.; Kardas, G., *Int J Hydrogen Energy* **2014,** *39* (22), 11355-11359.

15.   Himeshima, N.; Amao, Y., *Energy & Fuels* **2003,** *17* (6), 1641-1644.

16.   Ioroi, T.; Fujiwara, N.; Siroma, Z.; Yasuda, K.; Miyazaki, Y., *Electrochem Commun* **2002,** *4* (5), 442-446.

17.   Chen, Y.; Lin, B.; Wang, H.; Yang, Y.; Zhu, H. B.; Yu, W. L.; Basset, J. M., *Chem Eng J* **2016,** *286*, 339-346.

18.   Chen, Y.; Lin, B.; Yu, W. L.; Yang, Y.; Bashir, S. M.; Wang, H.; Takanabe, K.; Idriss, H.; Basset, J. M., *Chem Eur J* **2015,** *21* (29), 10290-+.

19.   Gao, G. P.; Jiao, Y.; Ma, F. X.; Jiao, Y. L.; Waclawik, E.; Du, A. J., *J Catal* **2015,** *332*, 149-155.

20.   Magdic, K.; Kvastek, K.; Horvat-Radosevic, V., *Electrochim Acta* **2015,** *167*, 455-469.

21.   Yuan, Y. J.; Lu, H. W.; Ji, Z. G.; Zhong, J. S.; Ding, M. Y.; Chen, D. Q.; Li, Y. H.; Tu, W. G.; Cao, D. P.; Yu, Z. T.; Zou, Z. G., *Chem Eng J* **2015,** *275*, 8-16.

22.   Cui, W.; Liu, Q.; Cheng, N.; Asiri, A. M.; Sun, X., *Chem Commun (Camb)* **2014,** *50* (66), 9340-2.

23.   Chu, S.; Wang, C. C.; Feng, J. Y.; Wang, Y.; Zou, Z. G., *Int J Hydrogen Energy* **2014,** *39* (25), 13519-13526.

24.   Cao, S. W.; Liu, X. F.; Yuan, Y. P.; Zhang, Z. Y.; Fang, J.; Loo, S. C.; Barber, J.; Sum, T. C.; Xue, C., *Phys Chem Chem Phys* **2013,** *15* (42), 18363-6.

25.   Meyer, S.; Nikiforov, A. V.; Petrushina, I. M.; Kohler, K.; Christensen, E.; Jensen, J. O.; Bjerrum, N. J., *Int J Hydrogen Energy* **2015,** *40* (7), 2905-2911.

26.   Bonde, J.; Moses, P. G.; Jaramillo, T. F.; Norskov, J. K.; Chorkendorff, I., *Faraday Discusss* **2008,** *140*, 219-231.

27.   Medvedev, I. G., *Russ J Electrochem+* **2004,** *40* (11), 1123-1131.

28.   Heyrovsky, M., *Collection of Czechoslovak Chemical Communications* **2001,** *66* (1), 67-80.

29.   Medvedev, I. G., *Russ J Electrochem+* **1993,** *29* (9), 956-960.

30.   Raj, I. A.; Vasu, K. I., *J Appl Electrochem* **1992,** *22* (5), 471-477.

31.   Sellmann, D.; Geck, M.; Moll, M., *J Am Chem Soc* **1991,** *113* (14), 5259-5264.

32.   Grubac, Z.; Metikos-Hukovic, M.; Babic, R., *Int J Hydrogen Energy* **2013,** *38* (11), 4437-4444.

33.   Herraiz-Cardona, I.; Ortega, E.; Anton, J. G.; Perez-Herranz, V., *Int J Hydrogen Energy* **2011,** *36* (16), 9428-9438.

34.   Hall, D. S.; Bock, C.; MacDougall, B. R., *J Electrochem Soc* **2013,** *160* (3), F235-F243.

35.   Anastasopoulos, A.; Blake, J.; Hayden, B. E., *J Phys Chem C* **2011,** *115* (39), 19226-19230.

36.   Chen, L. L.; Lasia, A., *J Electrochem Soc* **1993,** *140* (9), 2464-2473.

37.   Hou, Y.; Zhang, B.; Wen, Z. H.; Cui, S. M.; Guo, X. R.; He, Z.; Chen, J. H., *J Mater Chem A* **2014,** *2* (34), 13795-13800.

38.   Chang, Y. H.; Nikam, R. D.; Lin, C. T.; Huang, J. K.; Tseng, C. C.; Hsu, C. L.; Cheng, C. C.; Su, C. Y.; Li, L. J.; Chua, D. H., *ACS Appl Mater Interfaces* **2014,** *6* (20), 17679-85.

39.   Chen, W. F.; Muckerman, J. T.; Fujita, E., *Chem Commun (Camb)* **2013,** *49* (79), 8896-909.

40.   Chen, W. F.; Schneider, J. M.; Sasaki, K.; Wang, C. H.; Schneider, J.; Iyer, S.; Iyer, S.; Zhu, Y.; Muckerman, J. T.; Fujita, E., *ChemSusChem* **2014,** *7* (9), 2414-8.

41.   Bercaw, J. E.; Chen, G. S.; Labinger, J. A.; Lin, B. L., *J Am Chem Soc* **2008,** *130* (52), 17654-+.

42. Du, P. W.; Knowles, K.; Eisenberg, R., *J Am Chem Soc* **2008,** *130* (38), 12576-+.

43. Du, P. W.; Schneider, J.; Jarosz, P.; Eisenberg, R., *J Am Chem Soc* **2006,** *128* (24), 7726-7727.

44. Kobayashi, M.; Masaoka, S.; Sakai, K., *Molecules* **2010,** *15* (7), 4908-4923.

45. Muresan, N. M.; Willkomm, J.; Mersch, D.; Vaynzof, Y.; Reisner, E., *Angew Chem Int Ed Engl* **2012,** *51* (51), 12749-53.

46. Rao, H.; Wang, Z. Y.; Zheng, H. Q.; Wang, X. B.; Pan, C. M.; Fan, Y. T.; Hou, H. W., *Catal Sci Technol* **2015,** *5* (4), 2332-2339.

47. Zhao, X.; Duan, H. F.; Que, C. L.; Yang, M.; Abubakar, K.; Baker, D. L.; Yan, B.; Webster, C. E., *Abstracts of Papers of the American Chemical Society* **2013,** *245*.

48. Uosaki, K.; Fukumitsu, H.; Masuda, T.; Qu, D., *Phys Chem Chem Phys* **2014,** *16* (21), 9960-5.

49. Masuda, T.; Uosaki, K., *Chem Lett* **2004,** *33* (7), 788-789.

50. Masuda, T.; Shimazu, K.; Uosaki, K., *J Phys Chem C* **2008,** *112* (29), 10923-10930.

51. Das, S.; Brudvig, G. W.; Crabtree, R. H., *Chem Commun (Camb)* **2008,** (4), 413-24.

52. Karyakin, A. A., *Bioelectrochemistry* **2012,** *88*, 70-5.

53. Morozov, S. V.; Vignais, P. M.; Cournac, V. L.; Zorin, N. A.; Karyakina, E. E.; Karyakin, A. A.; Cosnier, S., *Int J Hydrogen Energy* **2002,** *27* (11-12), 1501-1505.

54. Zhang, G. G.; Wang, X. C., *J Catal* **2013,** *307*, 246-253.

55. Torresan, I.; Michelin, R. A.; Marsella, A.; Zanardo, A.; Pinna, F.; Strukul, G., *Organometallics* **1991,** *10* (3), 623-631.

56. Abe, T.; Chiba, J.; Ishidoya, M.; Nagai, K., *Rsc Advances* **2012,** *2* (21), 7992-7996.

57. Brimblecombe, R.; Dismukes, G. C.; Swiegers, G. F.; Spiccia, L., *Dalton Trans* **2009,** (43), 9374-84.

58. Sheehan, S. W.; Thomsen, J. M.; Hintermair, U.; Crabtree, R. H.; Brudvig, G. W.;

Schmuttenmaer, C. A., *Nat commun* **2015,** *6*, 6469.

59. Dal Santo, V.; Liguori, F.; Pirovano, C.; Guidotti, M., *Molecules* **2010,** *15* (6), 3829-56.

60. Zhao, X. S.; Lu, G. Q.; Whittaker, A. K.; Millar, G. J.; Zhu, H. Y., *J Phys Chem B* **1997,** *101* (33), 6525–6531.

61. Zhao, X. S.; Lu, G. Q., *J Phys Chem B* **1998,** *102* (9), 1556-1561.

62. Zhao, X. S.; Bao, X. Y.; Guo, W.; Lee, F. Y., *Materials Today* **2006,** *9* (3), 32-39.

63. Thomas, J. M.; Raja, R.; Lewis, D. W., *Angew Chem Int Ed Engl* **2005,** *44* (40), 6456-82.

64. Friebe, C.; Hager, M. D.; Winter, A.; Schubert, U. S., *Adv Mater* **2012,** *24* (3), 332-45.

65. Le Goff, A.; Holzinger, M.; Cosnier, S., *Electrochim Acta* **2011,** *56* (10), 3633-3640.

66. Okunola, A.; Kowalewska, B.; Bron, M.; Kulesza, P. J.; Schuhmann, W., *Electrochim Acta* **2009,** *54* (7), 1954-1960.

67. Song, W.; Okamura, M.; Kondo, T.; Uosaki, K., *J Electroanal Chem* **2008,** *612* (1), 105-111.

68. Masuda, T.; Uosaki, K., *Chem Lett* **2004,** *33* (7), 2.

69. Masuda, T.; Fukumitsu, H.; Takakusagi, S.; Chun, W. J.; Kondo, T.; Asakura, K.; Uosaki, K., *Adv Mater* **2012,** *24* (2), 268-72.

70. Fukumitsu, H.; Masuda, T.; Qu, D.; Waki, Y.; Noguchi, H.; Shimazu, K.; Uosaki, K., *Chem Lett* **2010,** *39* (7), 768-770.

71. Bannon, J. S.; White, J. C.; Long, D.; Riley, J. A.; Baragona, J.; Atkins, M.; Crowley, R. H., *Acs Symposium Series* **1990,** *439*, 305-319.

72. Young Jo, M.; Eun Ha, Y.; Hyun Kim, J., *Sol Energ Mat Sol C* **2012,** *107*, 1-8.

73. Monk, P. M. S., *The Viologen: Physicichemical Properties, Synthesis, and Applications of the Salt of 4,4`-Bipyridine*. John Wiley & Sons Ltd.: BaffinsLane,

England, 1998.

74. Tanaka, Y.; Sagara, T., *Electrochem Commun* **2007,** *9* (4), 741-746.

75. sagara, T.; Maeda, H.; Yuan, Y.; Nakashima, N., *Langmuir* **1999,** *15*, 8.

76. Monk, P. M. S.; Turner, C.; Akhtar, S. P., *Electrochim Acta* **1999,** *44*, 4817-4826.

77. Ock, J.-Y.; Shin, H.-K.; Kwon, Y.-S.; Miyake, J., *Colloid Surface A* **2005,** *257-258*, 351-355.

78. Huang, H. X.; Qian, D. J.; Nakamura, N.; Nakamura, C.; Wakayama, T.; Miyake, J., *Electrochim Acta* **2004,** *49* (9-10), 1491-1498.

79. Han, B.; Li, Z.; Wandlowski, T.; Blaszczyk, A.; Mayor, M., *J Phys Chem C* **2007,** *111* (37), 13855-13863.

80. Lee, C.; Lee, Y. M.; Moon, M. S.; Park, S. H.; Park, J. W.; Kim, K. G.; Jeon, S.-J., *J Electroanal Chem* **1996,** *416*, 139-144.

81. Kumar, R.; Pillai, R. G.; Pekas, N.; Wu, Y.; McCreery, R. L., *J Am Chem Soc* **2012,** *134* (36), 14869-76.

82. Stargardt, J. F.; Hawkridge, F. M., *Anal Chim Acta* **1983,** *146*, 8.

83. Ayato, Y.; Takatsu, A.; Kato, K.; Matsuda, N., *J Electroanal Chem* **2006,** *595* (1), 87-93.

84. Monk, P. M. S., *The Viologens: Physicochemical Properties, Synthesis and Applications of the Salts of 4,4'-Bipyridine.* John Wiley & Sons: Chichester, 1998.

85. Kosower, E. M.; Cotter, J. L., *J. Am. Chem. Soc.* **1964,** *86* (24), 5524-5527.

86. Lee, D. K.; Kang, Y. S., *J Phys Chem B* **2004,** *108* (13), 4063-4070.

87. Lezna, R. O.; Centeno, S. A., *Langmuir* **1996,** *12* (2), 591-593.

88. Bird, C. L.; Kuhn, A. T., *Chem Soc Rev* **1981,** *10* (1), 49-82.

89. Xiao, L.; Wildgoose, G. G.; Compton, R. G., *New J Chem* **2008,** *32* (9), 1628-1633.

90. Mohammad, M., *J Org Chem* **1987,** *52* (13), 2779-2782.

91. Kosower, E. M.

92. Watanabe, T.; Honda, K., *J Phys Chem* **1982,** *86*, 2617-2619.

93. Rosseinsky, D. R.; Monk, P. M. S., *J Appl Electrochem* **1994,** *24*, 1213-1221.

94. Vlachopoulos, N.; Nissfolk, J.; Moller, M.; Briancon, A.; Corr, D.; Grave, C.; Leyland, N.; Mesmer, R.; Pichot, F.; Ryan, M.; Boschloo, G.; Hagfeldt, A., *Electrochim Acta* **2008,** *53* (11), 4065-4071.

95. Kavanagh, A.; Fraser, K. J.; Byrne, R.; Diamond, D., *ACS Appl Mater Interfaces* **2013,** *5* (1), 55-62.

96. Mortimer, R. J.; Reynolds, J. R., *Displays* **2008,** *29* (5), 424-431.

97. Lin, C.-F.; Hsu, C.-Y.; Lo, H.-C.; Lin, C.-L.; Chen, L.-C.; Ho, K.-C., *Sol Energ Mat Sol C* **2011,** *95* (11), 3074-3080.

98. Liu, M. O.; Chen, I.-M.; Lin, J.-L., *Mater Lett* **2007,** *61* (30), 5227-5231.

99. Bodappa, N.; Broekmann, P.; Fu, Y. C.; Furrer, J.; Furue, Y.; Sagara, T.; Siegenthaler, H.; Tahara, H.; Vesztergom, S.; Zick, K.; Wandlowski, T., *J Phys Chem C* **2015,** *119* (2), 1067-1077.

100. Sariciftci, N. S.; Mehring, M.; Gaudl, K. U.; Bauerle, P.; Neugebauer, H.; Neckel, A., *J Chem Phys* **1992,** *96* (9), 7164-7170.

101. Ito, M.; Sasaki, H.; Takahashi, M., *The J Phys Chem* **1987,** *91* (15), 3932-3934.

102. Han, B.; Li, Z.; Wandlowski, T.; Błaszczyk, A.; Mayor, M., *The J Phys Chem C* **2007,** *111* (37), 13855-13863.

103. Haladjian, J.; Pilard, R.; Bianco, P., *J Electroanal Chem* **1985,** *184* (2), 391-400.

104. Castner, J. F.; Hawkridge, F. M., *J Electroanal Chem* **1983,** *143* (1-2), 217-232.

105. Wei, J. F.; Ryan, M. D., *Anal Biochem* **1980,** *106* (1), 269-277.

106. Qian, D. J.; Nakamura, C.; Noda, K.; Zorin, N. A.; Miyake, J., *App Biochem Biotechnol* **2000,** *84-6*, 409-418.

107. Bagyinka, C.; Osz, J.; Szaaraz, S., *J Biol Chem* **2003,** *278* (23), 20624-7.

108. Li, J. H.; Yan, J. C.; Deng, Q.; Cheng, G. J.; Dong, S. J., *Electrochim Acta* **1997,** *42* (6), 961-967.

109. Karatani, H.; Wada, N.; Sugimoto, T., *Bioelectrochemistry* **2003,** *60* (1-2), 57-64.

110. Aono, S.; Ohtaka, A.; Okura, I., *J Mol Catal* **1995,** *96* (1), 87-92.

111. Bock, A. K.; Kunow, J.; Glasemacher, J.; Schonheit, P., *Eur J Biochem* **1996,** *237* (1), 35-44.

112. Yoon, K. S.; Ishii, M.; Igarashi, Y.; Kodama, T., *J Bacteriol* **1996,** *178* (11), 3365-3368.

113. Crawley, C. D.; Hawkridge, F. M., *Biochem Biophys Research Comm* **1981,** *99* (2), 516-522.

114. Moradpour, A.; Amouyel, E.; Keller, P.; Kagan, H., *Nouv J Chim* **1978,** *2*, 547.

115. Mau, A. W. H.; Overbeek, J. M.; Loder, J. W.; Sasse, W. H. F., *J Chem Soc* **1986,** *82*, 869-876.

116. Keller, P.; Moradpour, A., *J Am Chem Soc* **1980,** *102* (24), 7193-7196.

117. Keller, P.; Moradpour, A.; Amouyal, E.; Kagan, H. B., *New J Chem* **1980,** *4* (6), 377-384.

118. Lehn, J. M.; Sauvage, J. P., *Nouv J Chim* **1977,** *1*, 449.

119. Kiwi, J.; Gratzel, M., *Nature* **1979,** *281*, 657.

120. Miller, D.; Mclendon, G., *Inorganic Chemistry* **1981,** *20* (3), 950-953.

121. Kalyanasundaram, K.; Gratzel, M., *Helv Chim Acta* **1980,** *63* (2), 478-485.

122. Harriman, A.; Porter, G.; Richoux, M. C., *J Chem Soc* **1981,** *77*, 1939-1948.

123. Harriman, A.; Richoux, M. C.; Porter, G., *J Photochem* **1981,** *17* (1-2), 181-181.

124. Harriman, A.; Porter, G.; Richoux, M. C., *J Chem Soc* **1981,** *77*, 1175-1187.

125. Mercersmith, J. A.; Mauzerall, D., *Photochem Photobiol* **1981,** *34* (3), 407-410.

126. Wang, G. M.; Fu, X. K.; Deng, J.; Huang, X. M.; Miao, Q., *Chem Phys Lett* **2013,** *579*,

105-110.

127. Asakura, N.; Hiraishi, T.; Kamachi, T.; Okura, I., *J Mol Catal* **2001,** *172* (1-2), 1-7.

128. Fernandez, A.; Innocenti, M.; Guidelli, R., *J Electroanal Chem* **2002,** *532*, 9.

129. Arihara, K.; Kitamura, F., *J Electroanal Chem* **2003,** *550-551*, 10.

130. Barroso-Fernandez, B.; Lee-Avarez, M. T.; Selisker, C. J.; Heinmen, W. R., *Anal Chim Acta* **1998,** *370*, 9.

131. Quan, D.; Min, D. G.; Cha, G. S.; Nam, H., *Bioelectrochemistry* **2006,** *69*, 8.

132. Maalouf, R.; Chebib, H.; Saikali, Y.; Vittori, O.; Sigaud, M.; Jaffrezic-Renault, N., *Biosensors and Bioelectronics* **2007,** *22*, 6.

133. Komura, T.; Kijima, K.; Yamaguchi, T.; Takahashi, K., *J Electroanal Chem* **2000,** *486*, 8.

134. Walcarius, A.; Lamberts, L.; Derouane, E. G., *Electrochim Acta* **1993,** *38*, 9.

135. Walcarius, L. L. A.; Derouane, E. G., *Electrochim Acta* **1993,** *38*, 9.

136. Vlachopoulos, N.; Nissfolk, J.; Möller, M.; Briançon, A.; Corr, D.; Grave, C.; Leyland, N.; Mesmer, R.; Pichot, F.; Ryan, M.; Boschloo, G.; Hagfeldt, A., *Electrochim Acta* **2008,** *53*, 6.

137. Sun, Y.; Masuda, T.; Uosaki, K., *Chem Lett* **2012,** *41* (3), 328-330.

138. John, S. A.; Kitamura, F.; Tokuda, K.; Ohsaka, T., *Electrochim Acta* **2000,** *45*, 8.

139. Li, J.; Yan, J.; Deng, Q.; Cheng, G.; Dong, S., *Electrochim Acta* **1997,** *42* (6), 961-967.

140. Zotti, G.; Schiavon, G.; Zecchin, S.; Berlin, A.; Canavesi, A.; Pagani, G., *Synthetic Met* **1997,** *84* (1-3), 239-240.

141. Murakami, H.; Chifu, H.; Sagara, T., *Chem Lett* **2007,** *36* (10), 1218-1219.

142. Sagara, T.; Kato, N.; Toyota, A.; Nakashima, N., *Langmuir* **2002,** *18* (18), 6995-7001.

143. Sagara, T.; Murakami, H.; Igarashi, S.; Sato, H.; Niki, K., *Langmuir* **1991,** *7*, 7.

144. Sagara, T.; Tsuruta, H.; Nakashima, N., *J Electroanal Chem* **2001,** *500*, 9.

145. Arihara, K.; Ohsaka, T.; Kitamura, F., *Phys Chem Chem Phys* **2002,** *4* (6), 1002-1005.

146. Hawkridge, F. M.; Kuwana, T., *Anal Chem* **1973,** *45* (7), 1021-1027.

147. Simon, M. S.; Moore, P. T., *J Poly Sci* **1975,** *13* (1), 1-16.

148. Terry, J.; Linford, M. R.; Wigren, C.; Cao, R. Y.; Pianetta, P.; Chidsey, C. E. D., *App Phys Lett* **1997,** *71* (8), 1056-1058.

149. Effenberger, F.; Gotz, G.; Bidlingmaier, B.; Wezstein, M., *Angew Chem Int Ed Engl* **1998,** *37* (18), 2462-2464.

150. deVilleneuve, C. H.; Pinson, J.; Bernard, M. C.; Allongue, P., *J Phys Chem B* **1997,** *101* (14), 2415-2420.

151. Fidelis, A.; Ozanam, F.; Chazalviel, J. N., *Surface Science* **2000,** *444* (1-3), L7-L10.

152. Linford, M. R.; Fenter, P.; Eisenberger, P. M.; Chidsey, C. E. D., *J Am Chem Soc* **1995,** *117* (11), 3145-3155.

153. Bansal, A.; Li, X. L.; Lauermann, I.; Lewis, N. S.; Yi, S. I.; Weinberg, W. H., *J Am Chem Soc* **1996,** *118* (30), 7225-7226.

154. Bansal, A.; Lewis, N. S., *J Phys Chem B* **1998,** *102* (7), 1067-1070.

155. Ciampi, S.; Bocking, T.; Kilian, K. A.; James, M.; Harper, J. B.; Gooding, J. J., *Langmuir* **2007,** *23* (18), 9320-9.

156. Kuwana, T.; Heineman, W. R., *Acc Chem Res* **1976,** *9* (7), 241-248.

157. Chopra, K. L.; Major, S.; Pandya, D. K., *Thin Solid Films* **1983,** *102* (1), 1-46.

158. Yan, C.; Zharnikov, M.; Gölzhäuser, A.; Grunze, M., *Langmuir* **2000,** *16* (15), 6208-6215.

159. Schwartz, J.; Bruner, E. L.; Koch, N.; Span, A. R.; Bernasek, S. L.; Kahn, A., *Synthetic Met* **2003,** *138* (1-2), 223-227.

160. Purvis, K. L.; Lu, G.; Schwartz, J.; Bernasek, S. L., *J Am Chem Soc* **2000,** *122* (8), 1808-1809.

161. Lee, J.; Jung, B.-J.; Lee, J.-I.; Chu, H. Y.; Do, L.-M.; Shim, H.-K., *J Mater Chem* **2002,** *12* (12), 3494-3498.

162. Hillebrandt, H.; Tanaka, M., *J Phys Chem B* **2001,** *105* (19), 4270-4276.

163. Sfez, R.; De-Zhong, L.; Turyan, I.; Mandler, D.; Yitzchaik, S., *Langmuir* **2001,** *17* (9), 2556-2559.

164. Sigaud, P.; Chazalviel, J. N.; Ozanam, F.; Lahlil, K., *Appl Sur Sci* **2003,** *218* (1-4), 54-57.

165. Hyung, K. H.; Han, S. H., *Synthetic Met* **2003,** *137* (1-3), 1441-1442.

166. Oh, S.-Y.; Yun, Y.-J.; Kim, D.-Y.; Han, S.-H., *Langmuir* **1999,** *15* (14), 4690-4692.

167. Kim, C. O.; Hong, S. Y.; Kim, M.; Park, S. M.; Park, J. W., *J Colloid Interface Sci* **2004,** *277* (2), 499-504.

168. Zotti, G.; Schiavon, G.; Zecchin, S.; Berlin, A.; Pagani, G.; Canavesi, A., *Langmuir* **1997,** *13* (10), 2694-2698.

169. Carrara, M.; Nüesch, F.; Zuppiroli, L., *Synthetic Met* **2001,** *121* (1-3), 1633-1634.

170. Armstrong, N. R.; Carter, C.; Donley, C.; Simmonds, A.; Lee, P.; Brumbach, M.; Kippelen, B.; Domercq, B.; Yoo, S. Y., *Thin Solid Films* **2003,** *445* (2), 342-352.

171. Meyer, T. J.; Meyer, G. J.; Pfennig, B. W.; Schoonover, J. R.; Timpson, C. J.; Wall, J. F.; Kobusch, C.; Chen, X.; Peek, B. M., *Inorganic Chemistry* **1994,** *33* (18), 3952-3964.

172. Koh, S. E.; McDonald, K. D.; Holt, D. H.; Dulcey, C. S.; Chaney, J. A.; Pehrsson, P. E., *Langmuir* **2006,** *22* (14), 6249-6255.

173. Hanson, E. L.; Guo, J.; Koch, N.; Schwartz, J.; Bernasek, S. L., *J Am Chem Soc* **2005,** *127* (28), 10058-10062.

174. Besbes, S.; Ltaief, A.; Reybier, K.; Ponsonnet, L.; Jaffrezic, N.; Davenas, J.; Ben Ouada, H., *Synthetic Met* **2003,** *138* (1-2), 197-200.

175. Brewer, S. H.; Brown, D. A.; Franzen, S., *Langmuir* **2002,** *18* (18), 6857-6865.

176. Markovich, I.; Mandler, D., *J Electroanal Chem.* **2001,** *500*, 8.

177. Markovich, I.; Mandler, D., *J Electroanal Chem* **2000,** *484* (2), 194-202.

178. Muthurasu, A.; Ganesh, V., *J Colloid Interface Sci* **2012,** *374* (1), 241-9.

179. Huang, R. F.; Guo, L. H., *Science China-Chemistry* **2010,** *53* (8), 1778-1783.

180. Hyung, K.-H., *J Phys Chem* **2008,** *112*, 18178-18182.

181. Liu, X.; Neoh, K. G.; Kang, E. T., *Langmuir* **2002,** *18* (23), 9041-9047.

182. Jain, V.; Yochum, H.; Wang, H.; Montazami, R.; Hurtado, M. A. V.; Mendoza-Galvan, A.; Gibson, H. W.; Heflin, J. R., *Macromolecular Chemistry and Physics* **2008,** *209* (2), 150-157.

183. Ng, S. W.; Neoh, K. G.; Wong, Y. T.; Sampanthar, J. T.; Kang, E. T.; Tan, K. L., *Langmuir* **2001,** *17* (5), 1766-1772.

184. Xu, B.; Xu, L.; Gao, G.; Yang, Y.; Guo, W.; Liu, S.; Sun, Z., *Electrochim Acta* **2009,** *54* (8), 2246-2252.

185. Wang, N. X.; Damlin, P.; Esteban, B. M.; Aaritalo, T.; Kankare, J.; Kvarnstrom, C., *Electrochim Acta* **2013,** *90*, 171-178.

186. Shimomura, M.; Kasuga, K.; Tsukada, T., *Chem Commun* **1991,** (13), 845.

187. Lee, D. Y.; Lee, M.-S.; Lim, I.; Kang, S. H.; Nah, Y.-C.; Lee, W.; Han, S.-H., *Appl Sur Sci* **2011,** *257* (23), 9879-9884.

188. Wang, J. F.; Hu, J. J.; Sun, X. C.; Agarwal, A. M.; Kimerling, L. C.; Lim, D. R.; Synowicki, R. A., *J Appl Phys* **2008,** *104* (5), 4.

189. Yang, Y.; Bittner, A. M.; Baldelli, S.; Kern, K., *Thin Solid Films* **2008,** *516*, 8.

190. Bain, C. D.; Greene, P. R., *Current Opinion in Colloid & Interface Science* **2001,** *6* (4), 313-320.

191. Parikh, A. N.; Allara, D. L.; Azouz, I. B.; ROndelez, F., *J Phys Chem* **1994,** *98*, 14.

192. Tillman, N.; Ulman, A.; Penner, T. L., *Langmuir* **1989,** *5* (1), 101-111.

193. Bass, M.; DeCusatis, C.; Enoch, J.; Lakshminarayanan, V.; Li, G.; MacDonald, C.; Mahajan, V.; Stryland, E. V., *Hand Book of Optics*. McGraw-Hill: United States, 2009; Vol. I, p 1248.

CHAPTER 2
EXPERIMENTAL

2.1. Materials

All chemicals used in the present experiments are: 11-bomoundecytrichlorosilane (99%) from Gelest, Inc. 97% H_2SO_4 (ultrapure grade), 30% H_2O_2 aqueous solution, 30% NH_3 aqueous solution, dichloromethane, super dehydrated toluene (98%), n-hexane (98 %), Benzene (99.9 %), $NaBH_4$ (95 %), methyl viologen, and 4,4'-bipyridine (99%) were purchased from Wako Pure Chemicals. 1-bromobutane (95 %), 1,4-dibromobutane (98 %) and K_2PtCl_4 (99.9 %) were purchased from Aldrich. Water was purified using a Milli-Q purification system (Millipore). All chemicals were used as received. ITO glass (10 Ωcm^{-2}) were purchased from, Finebrand. A Ag (99.99%) and Pt wires (99.99%) were purchased from Nilaco. The glassware was cleaned in hot H_2SO_4, followed by copious rinsing with Milli-Q water before used.

2.2. Sample preparation
2.2.1. ITO pretreatment

Rectangular ITO-covered glass slides (approx. 2.0×2.0 cm) were ultrasonicated in dichloromethane for 10 min. followed by rinsing with ethanol and Milli-Q water. The pre-cleaned ITO substrate were subjected to an RCA-type cleaning procedure by immersing in the mixture of Milli-Q water + 30% H_2O_2 + 30% aqueous NH_3 (5:1:1 by volume) at 70 °C for 1 hr. The substrates were then rinsed with a copious amount of Milli-Q water and dried with N_2, and then UV-ozone treatment was carried out to remove remaining organic contaminant.

2.2.2. Alkylbromide-terminated monolayer

Silane linker layer formation were performed as shown in Figure 2-1(a). Clean ITO substrates were immersed into 1% (v/v) 11-bromoundecyltrichlorosilane (BUDCS) toluene solution and kept at room temperature (23-25 $^{\circ}$C) for 6 hr. The reaction was performed inside a glove box (humidity = 10-15%) under N_2 atmosphere. After reaction, the substrates were then ultrasonicated in dehydrated n-hexane and toluene, for 10 min, subsequently. Then the bromo-terminated ITO (Br-ITO) was dried under N_2 flow.

2.2.3. Viologen mono- and multilayer preparation and Pt-complex incorporation

Mono- and multi-viologen-layer construction on ITO and Pt incorporation were performed as shown in Figure 2-1. (b) The Br- ITO substrates were kept in a benzene solution saturated with the 4,4`-bipyridine for 12 hr (temperature of oil bath maintained at 70 $^{\circ}$C). The substrates were then placed into a neat solution of 1-bromobutane (c1) and refluxed for another 12 hr to yield 1LV-ITO. On the other hand 1,4-dibromobutane (c2) was used to prepare multi-viologen-layers. (d) After alternately repeating the surface coupling reaction step (b) and (c2) several times, (e) the bipyridine-terminated ITO substrate, was kept in 1-bromobutane atmosphere for 12 hours to yield a 3LV- or 5LV-ITO surface. After completing each surface reactions, the ITO substrates were ultrasonicated in dichloromethane, ethanol and Milli-Q water for 10 min, alternately, then rinsed with a copious amount of Milli-Q water, and dried under N_2 flow. (f) The bromide ions were replaced with $PtCl_4^{2-}$ by ion exchange reaction by immersing the nLV-ITO substrate in 10 mM K_2PtCl_4 aqueous solution for 10 min to obtain 1LV-ITO/Pt-complex.
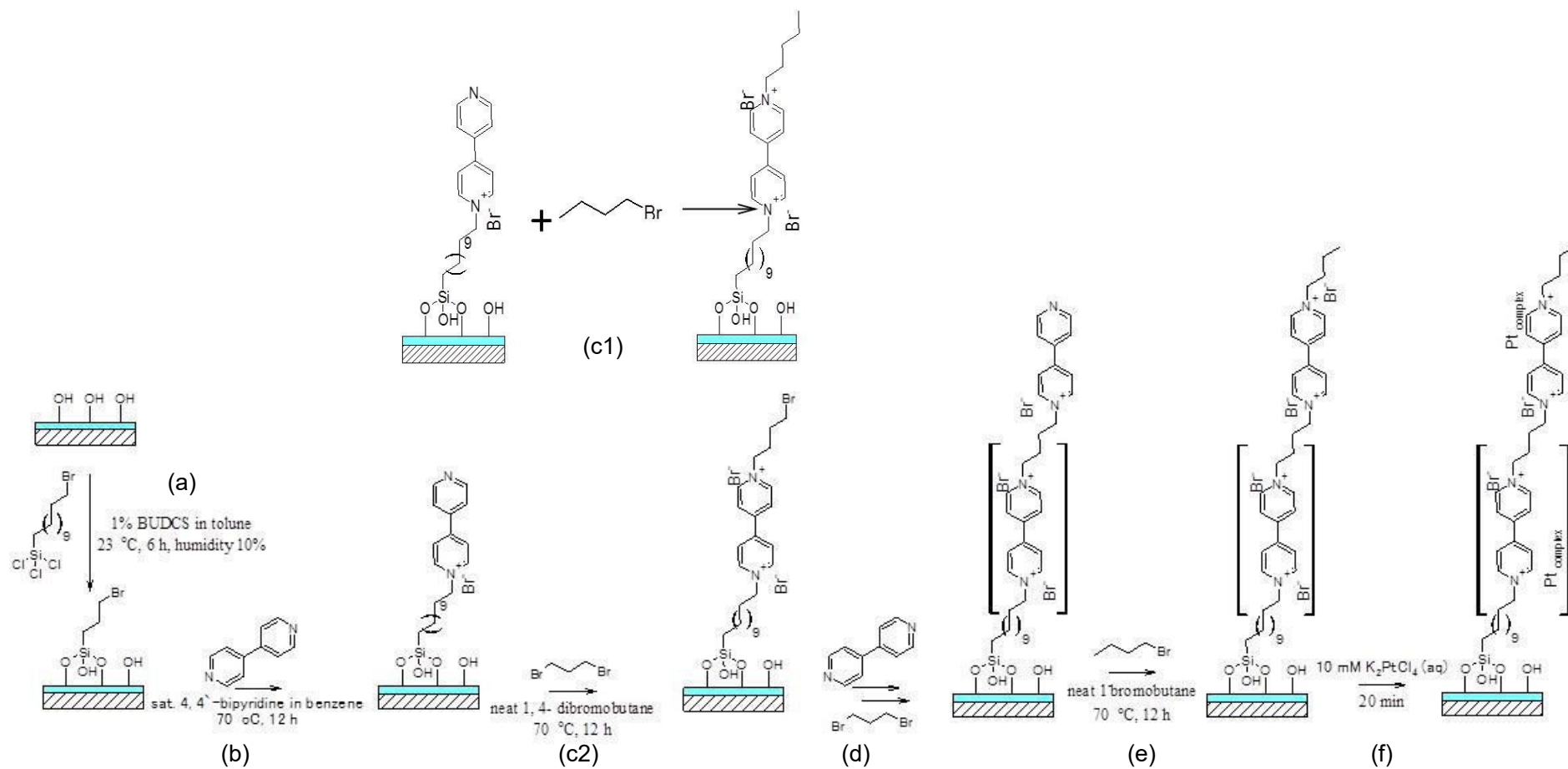
Figure 2-1. Schematic illustration of viologen multilayers constructed on ITO using a stepwise surface coupling and incorporation of Pt-complex within viologen layers.

2.3. Physical characterization

2.3.1. Ellipsometry

Spectroscopic ellipsometry measurements were carried out with a SOPRA GESP 5 spectrometer using a 30 W Xe lamp as a light source. The incident angle was set at 57° and 61°. The Ψ and Δ values were measured between 300 nm and 800 nm with a step of 10 nm. Simulations were carried out using software provided by the manufacturer (SOPRA, WinElli). Measurements taken from single-layer samples for each material yield the optical indices and, therefore, the dielectric function of the molecular layer.
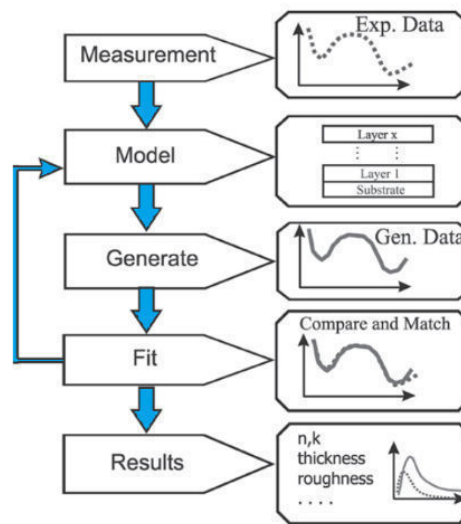

Figure 2-2. Flow chart for the ellipsometry process. The model was adjusted by regression analysis to find the optical constants and layer thickness that generate data curves that best match the experimental data curves.[1]

Data analysis is carried out by creating a model of a given sample, and theoretical values of Ψ_c and Δ_c are calculated. Next the unknown parameters of the model, such as thickness and refractive index are varied until a best fit between the measured Ψ_m and Δ_m and calculated Ψ_c and Δ_c is obtained. The mean squared error is used to measure the goodness of the fit. The solution for the thickness and refractive index is not unique,

therefore a reasonable estimate for the film structure is required to obtain useful information. Then by using regression analysis, the unknown coating properties are found that best generate a theoretical response to match the experimental curves. This process is shown in Figure 2-2 and is referred to as "fitting" the data.

2.3.2. FTIR

FT-IR spectra were measured in reflectance configuration using a Bio-RAD FTS-30 spectrometer equipped with a HgCdTe (mercury cadmium telluride) detector cooled with liquid nitrogen. All the spectra were measured by integrating 128 interferograms with a resolution 2 cm^{-1}, and the spectra of an cleaned ITO was used as a reference.

2.3.3. X-ray photoelectron spectroscopy

Bare ITO, Br-ITO, 1LV-ITO, and 1LV-ITO/Pt-complex were investigated by X-ray photoelectron spectroscopy analysis (Thermo Electron Co.) using an Al-Kα X-ray source (15 keV). Angle-resolved (AR) XPS measurements were performed by changing the take-off angle of the samples at 10, 25, 50, 75 and 90°. Here, we defined the take-off angle as the angle between the sample surface and the analyzer axis.

2.4. Spectroelectrochemical analysis
2.4.1. Spectroelectrochemical cells

Spectroelectrochemical measurements were carried out in a three-electrode configuration as shown in Figure 2-3. A Pt wire and a Ag/AgCl (sat. NaCl) electrodes were used as a counter and a reference electrode, respectively. The working electrode, an ITO glass was attached to the cell via a custom-made Teflon holder interspaced by an O-ring to

prevent electrolyte leakage (Figure 2-3). The current densities were calculated by dividing measured current to geometric area of the electrode ($A = 0.6$ cm^2). Sapphire windows was used on the other side of the cell to transmit the beam light. The electrical contact of the ITO electrode to the potentiostat was established with a piece of aluminum foil.
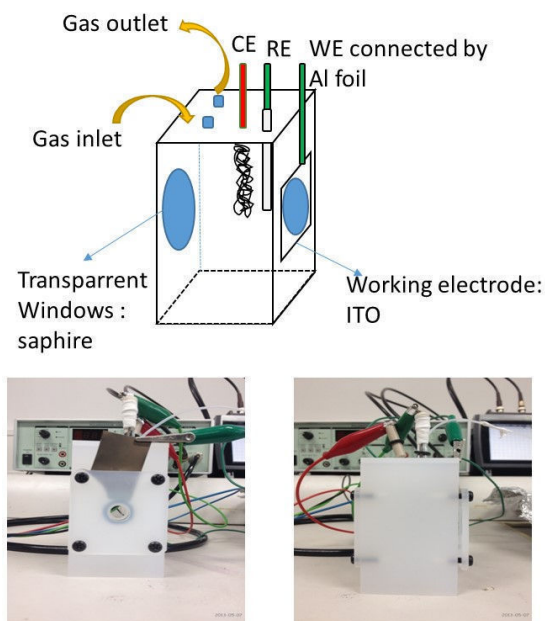

Figure 2-3. (Top) Schematic of spectroelectrochemical cells and (bottom) photograph of the cell front view (left-hand side) and side view (right-hand side).

All electrolytes solutions in electrochemical systems were prepared by using Milli-Q water, and were deaerated with argon (Ar) or nitrogen (N2) gas for about 30 min before measurement. The gas was kept flew during the experiments placed on the top of solution to avoid oxygen intake. The measurements were carried out at room temperature at (23-25 ºC). The 0.1 M Na$_2$SO$_4$ aqueous solution was used as supporting electrolyte for spectroelectrochemical measurements.

The potentiostat (TOHO Technical Research, TTR-2000) was used to control the potential of working electrode. A function generator (Agilent 33120A) was used to control

the speed of the applied potential. The output signals were stored in a digital storage that recorded with an X-Y recorder (Graphtec, GL900).

2.4.2. UV-vis spectrometer

2.4.2.1. Steady state measurement

The UV-vis spectra were measured using Shimadzu UV-2600 spectrometer. The steady state UV-vis spctroelectrochemical measurements were carried out by first record the UV-vis spectra at 0 V (E1) as a reference. Potential was stepped from E1 to E2 (-1.0 < E2 < 0.1 V), then the UV-vis spectra at each E2 steps were measured, as shown in Figure 2-4. Absorbance change at certain wavelength was also measured simultaneously with potential sweep from E1 to E2 and then return to E1 with various sweep rate. The absorbance at 0 V was always used as reference spectra.
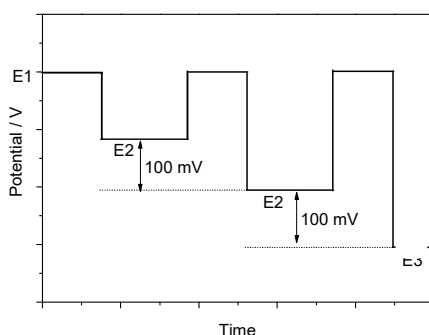

Figure 2-4. Diagram of potential step for steady state absorbance spectra measurements.

2.4.2.2. Transient absorbance UV-vis

Time-resolved spectroelectrochemical measurements was carried out by combining a fast response function generator (Agilent, 33120A) with the potentiostat to provide potential step and to measure the transient current simultaneusly. To monitor the transient absorbance, a Xe-lamp (Ushio, UXL-500D) equipped with a monochromator (Ritsu Oyo Kogaku, MC-

20N) was used to provide monochromatized light, which was split into 50:50 using a beam splitter, and the transmitted light through the spectroelectrochemical cell (signal: I) and the reflected light by the beam splitter (reference: I_0) were simultaneously detected by two Si photodetectors (Hamamatsu, S1227-1010BQ) and the absorbance, A, was calculated as $A = -\log 10(I/I_0)$.
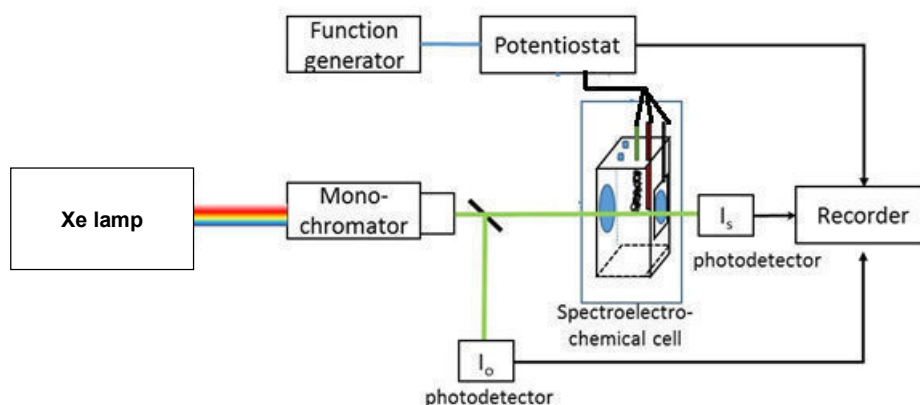

Figure 2-5. Spectrometer setup.

2.5. References

1. Hilfiker, J. N.; Synowicki, R. A.; Tompkins, H. G., Spectroscopic ellipsometry method for thin absorbing coatings. In *51st Annual Technical conference*, Society of vacuum coaters: Chicago, 2008; Vol. II, pp 511-516.

CHAPTER 3

CONSTRUCTION OF MOLECULAR LAYER CONTAINING VIOLOGEN MOIETY AND Pt-COMPLEX ON ITO SURFACE

3.1. Introduction

The attachment of organic moieties to the surface of indium tin oxide (ITO) has been the subject of interest due to the potential applications in fabricating transparent contacts for organic optoelectronic devices,[1, 2] sensors for chemical and/or biological system,[3, 4] and spectroelectroanalytical technique development.[5-7] The majority of ITO functionalization studies have been performed via wet-chemistry using a wide variety of reagents including organic and organometallic alkoxysilanes [8-11], amines [12-15], carboxylic acids [16-19], phosphonic acids[19-22], and thiols[22, 23].

The formation of well-controlled and reproducible SAMs on ITO is not simple, mostly for two main reasons that are, the high roughness of the ITO and the low hydroxyl coverage [17]. Clearly, modification of such a surface requires good wetting by the solvent and a relatively long time of exposure to the coupling reagent to assure full coverage. A pretreatment procedure that will activate the surface, i.e. increase its hydroxyl surface coverage, is also recommended [18, 19].

A number of pretreatments have been examined following previous reports. The methods examined which had been reported previously and provide the best results were obtained by using a mixture of $5:1:1 = H_2O : H_2O_2$ (30%): NH_3 (25%) for one hr at 70°C. No severe damage to the surface was detected using this pretreatment. [17-19] Other parameters that also have an effect on the surface coupling include the time, solvent, and humidity or water content that exist in the silanization mixture solution. Generally, it is

accepted that the presence of low concentrations of water is necessary for the formation of a monolayer from a trichloroalkylsilane precursor.[20-22] However, excess water results in facile polymerization of trichloroalkylsilane in solution and polysiloxane deposition on the surface.[20,22] On the other hand, at a high water content, alkoxysilanes are more stable towards hydrolysis.[23]

The utilization of viologen as a functional unit would require preparative methods that allow its functionality to be exhibited effectively. One of the most common methods is the deposition of Langmuir-Blodgett monolayers on electrode substrates to build interfacial amphiphilic structures.[12] Another approach is based on the self-assembly of lipophilic molecules ending in hydrolytically unstable groups, such as silane, or thiol functional groups, which have strong adsorption on substrates.[9,13] A significant advantage of monolayers prepared by the self-assembly of amphiphilic viologens is the simplicity of their preparation. This chapter dealt with viologen mono- and multi-layer construction on ITO surface using surface coupling reaction.

3.2. Results and discussion

3.2.1. Physical characterization

3.2.1.1. Bromoalkylsilane terminated ITO (Br-ITO)

As-received ITO substrates were inhomogeneous regarding electrical conductivity and contaminated with organic species. The RCA and UV-ozone treatment are expected to provide clean and OH-rich surfaces. This impurities removal contribute to decreasing surface roughness and an increase in the conductivity as well as the homogeneity.[24] Reproducible monolayer formation on ITO is not easy. The time of silane coupling formation on ITO that has been reported using trialkoxysilanes shown a wide range from

less than an hour to several days. Markovich [35, 36] and Muthurasu coworkers [37] prepared trialkoxysilane monolayers on ITO in hexane as a result of refluxing the substrates for hours to several days. Other procedures, which involved either glass or tin oxide, were carried out at room temperature and accomplished within minutes to hours.[47-49]

FTIR has been widely used to determine the required immersion time to form a well-organized monolayer. Figure 3-1(a) shows reflection-absorption IR spectra in C-H region of the ITO surface after being left in 1% BUDCS solution. Monitoring the intensity change and peak positions of CH stretching in a BUDCS is an efficient method to check the monolayer formation on the surface. After 15 min immersion time, two peaks at ca. 2928 and 2857 cm^{-1} was observed indicate the asymmetric and the symmetric CH_2 stretching of BUDCS monolayer The intensity of those two peaks were increased but the peak position were slightly shifted to the lower wavenumber (Figure 3-1(b)). This result suggest that the packing density of BUDCS monolayer was increased. However, after 6 hr, no intensity and position change were observed at the two peaks at ca. 2924 and 2854 cm^{-1}, and the integration of peak area under CH region implying that reaction was completed after 6 hr (Figure 3-1(c)). The CH stretching of the BUDCS monolayer appears in lower intensities and at higher wavenumbers than the OTS monolayer.[25] This means that a more disordered state and low packing density of the BUDCS monolayer are induced due to the steric hindrance of the bulky bromide group.[9, 14, 15]
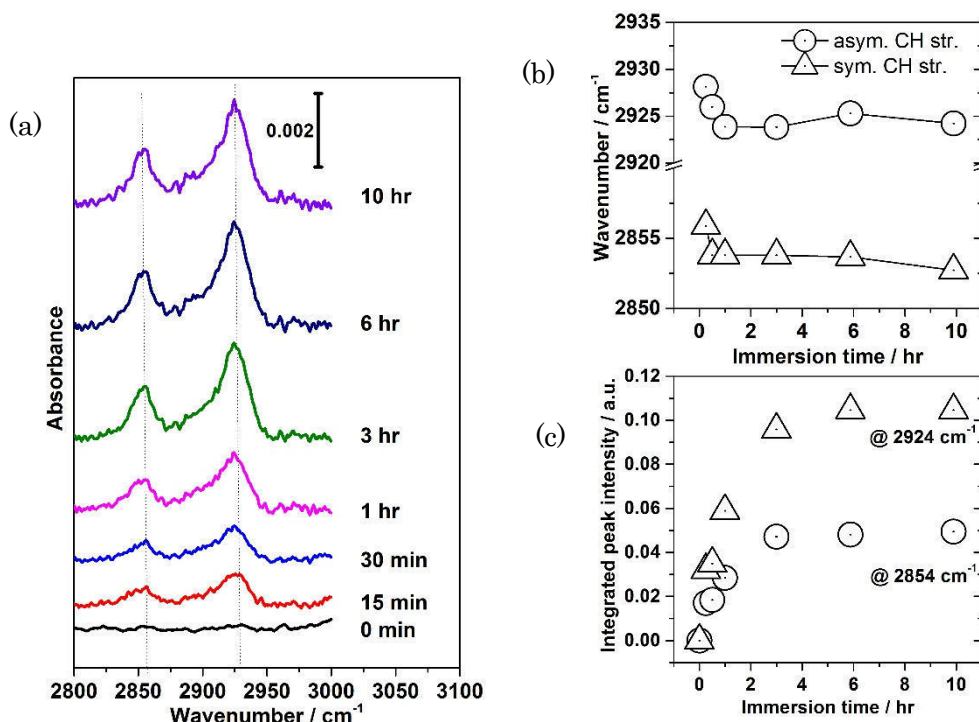
Figure 3-1. (a) FTIR Spectra of Br-ITO at CH region after immersion in 1% BUDCS with bare ITO as a reference, (b) Peak position changes at CH region and (c) plot of absorbance at 2854 (circle) and 2924 cm^{-1} (triangle) as a function of immersion time.

An XPS study of the ITO surface was performed to confirm the formation of Br-ITO surface. Figure 3-3(i)(a) shows a wide scan XP spectra of bare ITO showed a peak at 444.2 eV ($3d_{5/2}$) and at 451.8 eV ($3d_{3/2}$) corresponding to indium (In 3d) and at 486.3 eV ($3d_{5/2}$) and 494.7 eV ($3d_{3/2}$) corresponding to tin, respectively, in addition to the usual carbon and oxygen peaks.[26] Carbon peak (C1s) at 285 eV observed in the wide scan spectra probably be due to the surface contamination during the sample transfer to the XPS apparatus.[26]

The In 3d and Sn 3d intensity were decreased after formation bromoalkylsilane monolayer on ITO. Two new peaks were observed at 71 and 103 eV which corresponding to Br 3d and Si 2p, respectively (Figure 3-3(ii) and 3-3(iii)).This result indicates that the bromoalkylsilane was formed on ITO surface.[27]
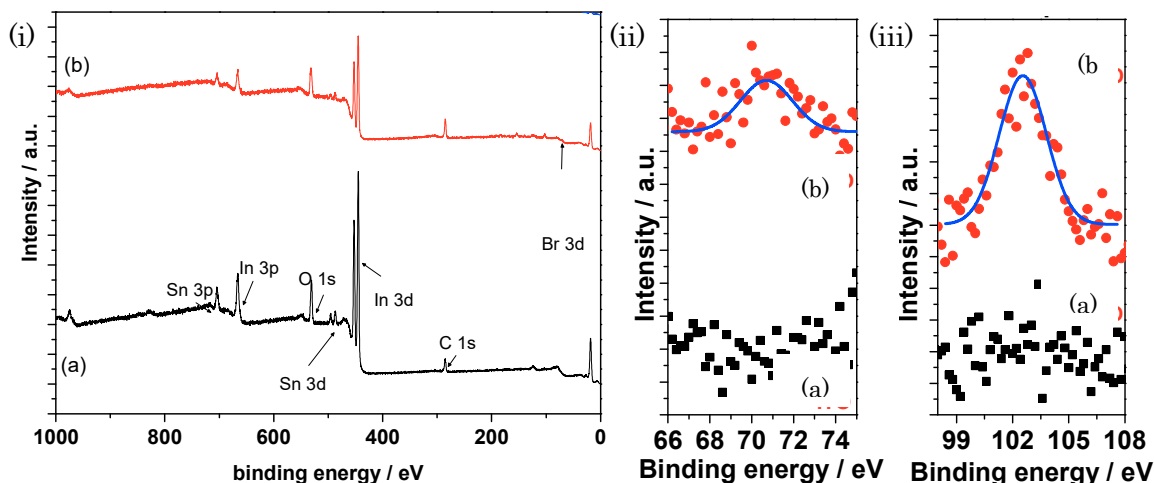
Figure 3-2. (i) XP spectra of Wide scan XP spectra, (ii) Br 3d and (iii) Si 2p region of (a) ITO, (b) Br-ITO.

3.2.1.2. Formation of viologen layers on ITO

FTIR measurements were acquired at viologen modified ITO. For comparison, FTIR measurement was also performed on methyl viologen (MV) which was prepared by drop-casting of MV solution in benzene followed by evaporation of benzene in vacuum for 1 hr. Figure 3-2 presents the FTIR spectra of the 1LV-, 3LV-, 5LV-ITO, and MV on ITO substrates. The Strong peak at 1219, 1407, and 1593 cm^{-1} were observed on IR spectra of MV. These bands correspond to the ring vibrational mode of bipyridine. The peak at ca. 2890 and 3029 cm^{-1} were implied the CH stretching mode from CH_3 and aromatic ring vibration, respectively. On the other hand, peak at 1467 cm^{-1} was employed and the intensity was increased from 1LV- to 5LV-ITO (Figure 3-3). This peak was assigned to the bipyridine ring vibration mode. Another peak was also observed at 2853 and 2923 cm^{-1} which were assigned as the asymmetric and the symmetric CH_2 stretching, respectively. The peak position was not much changed in compare to Br-ITO surface. This indicates that viologen layer has a low packing density.
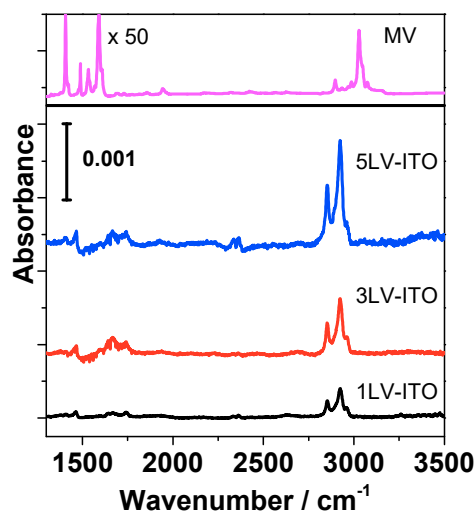
55

Figure 3-3. FTIR Spectra of (a) Drop-casted methyl viologen on ITO, (b) Br-ITO, (c) 1LV-ITO, (d) 3LV-ITO, and (e) 5LV-ITO.

Figure 3-4 shows the XP spectra at O 1s, C 1s and N 1s region of bare ITO, Br-ITO, and 1LV-ITO. Figure 3-4(i)(a) shows O 1s spectrum of ITO containing a maximum around 530 eV suggesting the presence of electrons from oxygen in the O^{2-} state from ITO. Further, in the case of Br-ITO, the deconvolution of O1s peak shows binding energy peak around at 532 eV indicating O^{2-} state from Si-O (Figure 3-4(i)(b)). These peaks were then decreased after viologen constructed on ITO. At the C 1s region (Figure 3-4(i)(b)), the peak at 285 and 289 eV assigned to the binding energy of electron from C-H and C=O, respectively. Figure 3-4(iii) shows the peak at N 1s region. The peak at 400 nm was observed at both ITO and Br-ITO probably due to the surface contamination. The peak was then significantly employed indicating the bipyridine ring was on the surface.
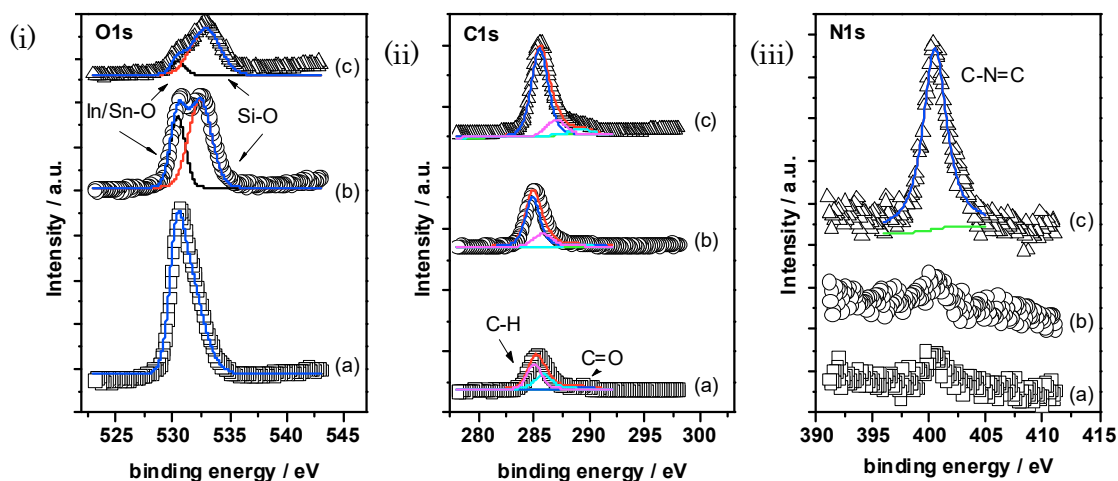
Figure 3-4. XP Spectra evolution at (i) O 1s region, (ii), C 1s region and (iii) N 1s region of (a) ITO, (b) Br-ITO, and (c) 1LV-ITO.

3.2.1.3 Attachment of the Pt-complex

Figure 3-5(i) and (ii) shows XP spectra of Pt 4f region and Cl 2p region of the 1LV-ITO, respectively. At XP spectra of 1LV-ITO (Figure 3-5(i)(a)) no peak was observed at this surface. After the 1LV-ITO substrate was immersed in K_2PtCl_4 aqueous solution 1LV-ITO/Pt-complex, peaks were observed at 72.9 and 76.2 eV that corresponds to Pt $4f_{7/2}$ and $4f_{5/2}$, respectively. The XP spectra of 1LV-ITO/Pt-complex after hydrogen evolution reaction (HER) was shown in Figure 3-5(i)(c). The peak was observed at similar position. This result indicates the Pt redox state after HER was similar to Pt redox state before HER. In order to clarify the Pt state, the Pt complex was reduced into metallic state by immersing within 10 mM $NaBH_4$ aqueous solution for 1 min (denoted as chemical treatment). The XP spectra of chemically treated 1LV-ITO/Pt-complex was shown in Figure 3-5(i)(d). The peak at 71.6 and 75 eV was observed and no peak was observed at Cl 2p suggesting that Pt-complex was reduced into Pt (0).[28] These result also indicate that before and after HER, redox state of Pt was +2 or Pt(II).
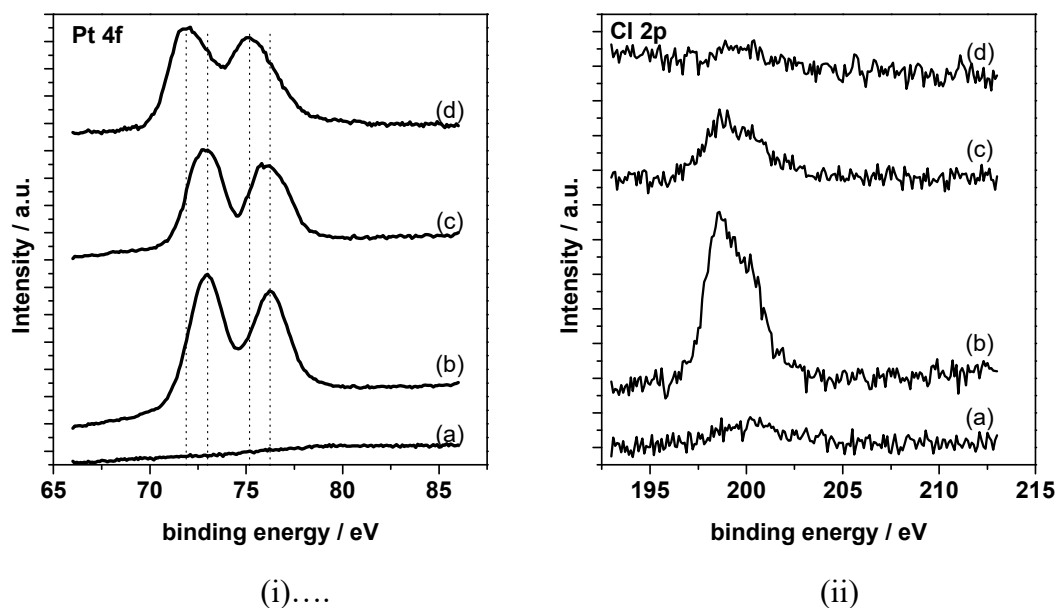
Figure 3-5. XP spectra at (i) Pt 4f region (ii) Cl region of (a) 1LV-ITO surface, (b) 1LV-ITO/Pt-complex surface after immersion in K_2PtCl_4 aqueous solution, (c) 1LV-ITO/Pt-complex surface after electrochemical treatment, and (d) 1LV-ITO/Pt after immersed in 2 mM $NaBH_4$ for 1 min.

Figure 3-5(ii) shows the peak at Cl region. Immediately after 1LV-ITO was immersed in K_2PtCl_4 aqueous solution, peak at 198.6 eV was employed. This strongly suggests that $PtCl_4^{2-}$ ions were incorporated into the 1LV-ITO surface (Figure 3-5(ii)(b)). After HER, the peak then decreased. This result is in agreement with previously reported by our group which suggesting the ligand exchange during HER.[29] It was also demonstrated that in the equilibrium condition of an aqueous solution containing $PtCl_4^{2-}$, Cl^- ligands can be partly exchanged to aquo ligands, taking for a few days, yielding $PtCl_3(H_2O)^-$, $PtCl_2(H_2O)_2$ and $PtCl(H_2O)_3^+$.[30-36]

3.2.1.4. Pt positions on the monolayer

The angle-resolved (AR) XPS measurement was carried out to investigate the position of Pt in viologen monolayers. Our group reported that incorporation of Pt complex within viologen layers provide a well-controlled Pt position. By controlling the Pt position, then Pt-complex can efficiently perform as a molecular catalyst.[37, 38]

Figure 3-6 shows the AR-XP spectra of 1LV-ITO/Pt-complex surface in (a) In 3d (b) N 1s and (c) Pt 4f region measured at take-off angles of 10, 25, 50, 75 and 90 °. As the take-off angle decreased, the intensity of In 3d peak decreased but those of N 1s and Pt 4f peaks slightly increased, suggesting that the ITO substrate was covered with an organic monolayer with viologen moieties and that Pt-complex was immobilized within viologen molecular layer.

More quantitative analysis can be carried out utilizing the relation between the XPS signal intensity from a thin-film-covered substrate and take-off angle, θ, as follows[39, 40]

$$ln(I) = \frac{-d}{\lambda \sin(\theta)} + ln(I_0)$$

(3-1)

where I_0 and I represent the intensity of the photoelectrons from a bare substrate and a substrate covered with a thin film of thickness d, respectively, and λ is the photoelectron mean free path.

According to the Eq. (3-1), *ln(I)* should be linearly related to *1/sinθ* with a slope of -*d/λ* and an intercept of *ln(I$_0$)*. Figure 3-6(d) shows *ln*(relative integrated intensity between In 3d and N 1s peaks) and *ln*(relative integrated intensity between N 1s and Pt 4f peaks) of the 1LV-ITO/Pt-complex surfaces as a function of *1/sinθ*. It is difficult to determine the terminal group on viologen modified ITO surfaces since there are two N atoms in two different pyridine rings. However, the calculated distance between the ITO surface to N atom on

pyridine rings were calculated to be 2.8 nm by using the slope of $ln(I_{In3d}/I_{N1s})$ in Figure 3-6(d), $-d/\lambda = 0.5$, and mean free path, λ, for In 3d photoelectrons as 5.6 nm. This value close to the distance of ITO to outermost bipyridine ring that theoretically calculated as 2.3 nm. The slope of $ln(I_{N1s}/I_{Pt4f})$ (open circles in Figure 3-6(d)) is almost 0, indicating that the Pt is the same as that outermost N bipyridine ring.
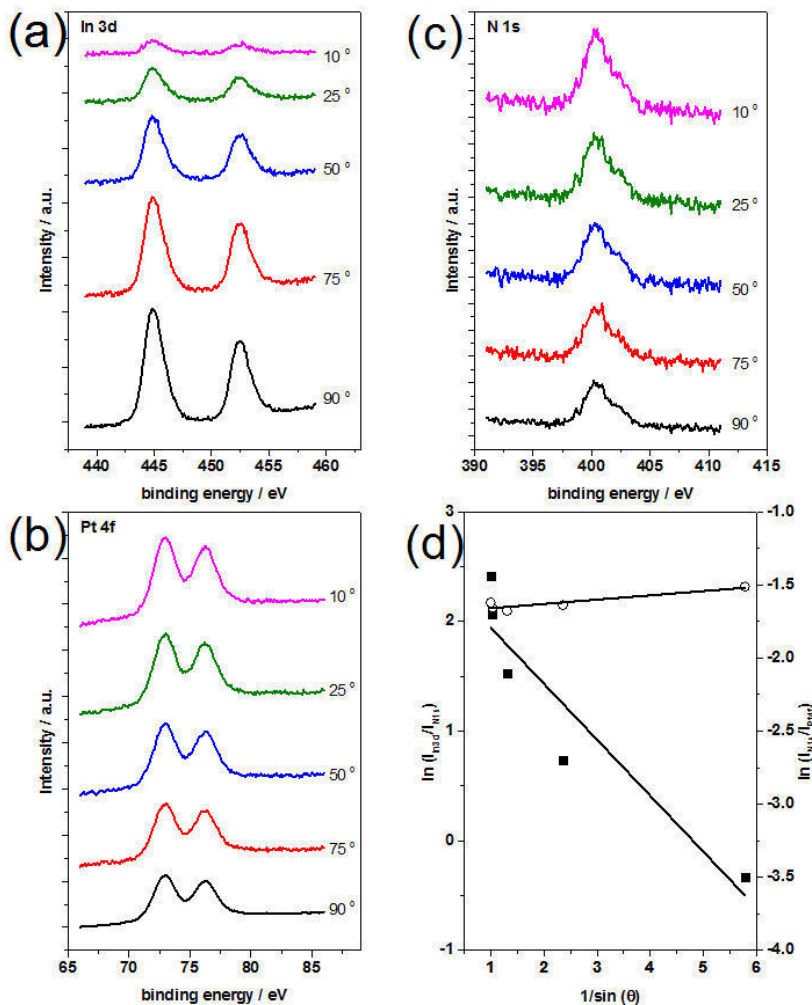

Figure 3-6. A series of XP spectra in (a) In 3d, (b) N 1s and (c) Pt 4f region of the 1LV-ITO/Pt-complex surface measured at take-off angles of 10, 25, 50, 75 and 90 ° and (d) take off angle dependencies of ln(relative integrated intensity between In 3d and N1s peaks) (black square) and ln(relative integrated intensity between N1s and Pt 4f peaks) (open circles) of the 1LV-ITO/Pt-complex surfaces.

3.2.2 Voltammetric response of $[Fe(CN)_6]^{3-/4-}$ on the modified ITO electrodes

3.2.2.1 Bromoalkylsilane terminated ITO electrodes

The redox response of $Fe(CN)_6^{3-/4-}$ was preferred to be used as an electrochemical probe for examining the quality of BUDCS monolayer on ITO, such as pinhole or defect structure, insulating property and the density of the BUDCS.[41] Figure 3-7 shows the CVs of bare and a Br-ITO electrode in 0.1 M Na_2SO_4 aqueous solution containing 1 mM $K_3[Fe(CN)_6]$.
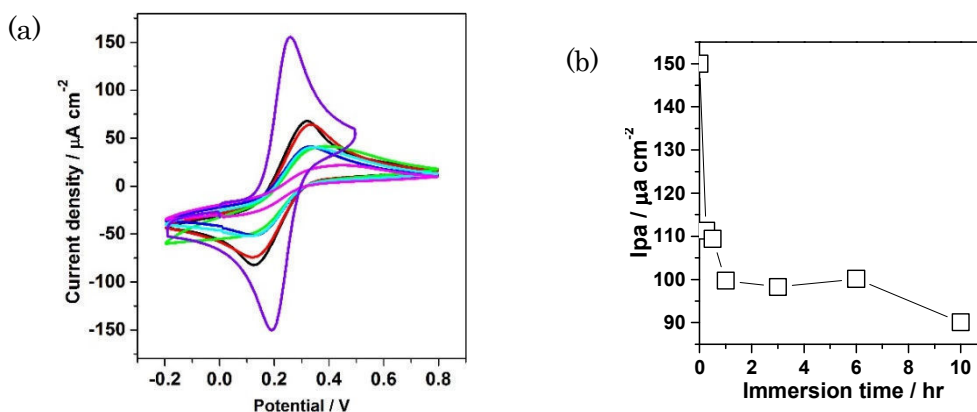

Figure 3-7. (a) Cyclic voltammograms of 0.1 M Na_2SO_4 aqueous solution containing 1 mM $K_3Fe(CN)_6$ at bare ITO (purple) and BUDCS modified ITO after 0.25 (black), 0.5 (red), 1 (blue), 3 (green), 6 (light blue) and 10 hr (pink) immersion within 1% BUDCS solution, scan rate of 50 mVs^{-1}. (b) The plot of anodic current vs immersion time.

The $[Fe(CN)_6]^{3-/4-}$ couple peaks were used to identify the electron-transfer efficiency through the SAMs. A reversible redox peaks were observed on the bare ITO electrode ($E_{1/2}$= 0.23V, and peak separation, ΔEp = 60 mV). After ITO electrode was immersed within BUDCS solution for 15 minutes, a reversible redox peak due to $[Fe(CN)_6]^{3-/4-}$ was still observed ($E_{1/2}$= 0.22 V) but the peak current was decreased and peak separation ΔEp ca. 100 mV. At longer immersion time, the redox peak was still observed and peak current relatively

constant (Figure 3-7(b)). These results indicate that silane coupling on ITO surface was completed. The redox response of $[Fe(CN)_6]^{3-/4-}$ still observed at longer immersion time, suggesting that the pinhole or structural defect existed on BUDCS monolayer modified ITO.

3.2.2.2 Viologen terminated ITO surfaces

The CVs of the 1LV-, 3LV-, and 5LV-ITO electrodes in the 0.1 M Na_2SO_4 aqueous solution containing 1mM $K_3Fe(CN)_6$ electrolyte solution shows in Figure 3-8. A reversible redox pair due to $[Fe(CN)_6]^{3-/4-}$ were observed at all modified ITO electrode. This indicates that viologen layers cannot perfectly block the electron transfer of $[Fe(CN)_6]^{3-/4-}$. Nakamura and co-workers demonstrated that in binary SAMs of a viologen thiol and a phospholipid, viologens can act as an electron-transfer mediator for $[Fe(CN)_6]^{3-/4-}$ to "gated" access to the electrode surface across the phospholipid monolayer.[42]

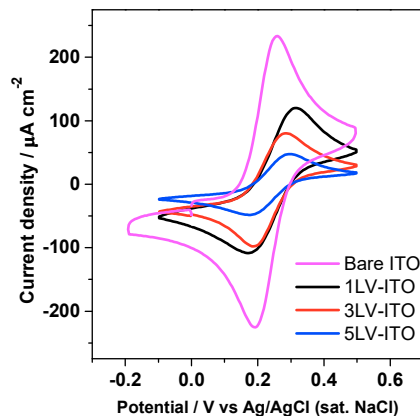Figure 3-8. Cyclic voltammogram of 1 mM $K_3Fe(CN)_6$ at bare ITO (line), 1LV-ITO (dashed line), 3LV-ITO (dotted line) and 5LV-ITO (dot-dashed line), recorded in 0.1 M Na_2SO_4 aqueous solution with a scan rate of 50 mVs^{-1}.

However, by increasing the viologen layers, the current response was decreased. This electrochemical property indicates that redox behaviors $[Fe(CN)_6]^{3-/4-}$ are closely related to a number of viologens. The $[Fe(CN)_6]^{3-/4-}$ can access the electrode or have an electron transfer to/from electrode when the viologen concentration is high; conversely, the ion cannot access or transfer electrons.[42]

3.3. Conclusion

Viologen mono- and multi-layers has been constructed on an ITO surface. The reproducible preparation of mono- and multi-layers achieved by controlling the reaction time of silane coupling as a linker layer for the next surface coupling reaction with bipyridine. The silane coupling and viologen construction were confirmed by FTIR and XPS study. Further, the XPS study shows that the incorporated Pt-complex state was not changed due to the electrochemical treatment. The $Fe(CN)_6^{3-/4-}$ redox response in solution shows that molecular organic layer constructed on ITO block the electron transfer from the ITO electrode to the redox species in solution.

3.4. References

1. Kavei, G.; Gheidari, A. M., *J Mater Process Technol* **2008,** *208* (1-3), 514-519.

2. Malval, J. P.; Morand, J. P.; Lapouyade, R.; Rettig, W.; Jonusauskas, G.; Oberle, J.; Trieflinger, C.; Daub, J., *Photochem photobiol Sci* **2004,** *3* (10), 939-48.

3. Hotta, H.; Tatsuno, K.; Hattori, Y.; Hashimoto, T.; Uehara, M.; Tsunoda, K.-i., *Electrochem Commun* **2008,** *10* (9), 1351-1354.

4. HyungSupported by the Brain Korea, K.-H.; Kim, D.-Y.; Han, S.-H., *New J Chem* **2005,** *29* (8), 1022.

5. Komorsky-Lovrić, Š.; Mirčeski, V.; Kabbe, C.; Scholz, F., *J Electroanal Chem* **2004,** *566* (2), 371-377.

6. Osawa, M.; Yoshii, K.; Ataka, K.; Yotsuyanagi, T., *Langmuir* **1994,** *10* (3), 640-642.

7. Yu, H. Z.; Zhang, H. L.; Liu, Z. F.; Ye, S.; Uosaki, K., *Langmuir* **1998,** *14* (3), 619-624.

8. Lee, J.; Jung, B.-J.; Lee, J.-I.; Chu, H. Y.; Do, L.-M.; Shim, H.-K., *J Mater Chem* **2002,** *12* (12), 3494-3498.

9. Hillebrandt, H.; Tanaka, M., *J Phys Chem B* **2001,** *105* (19), 4270-4276.

10. Sfez, R.; De-Zhong, L.; Turyan, I.; Mandler, D.; Yitzchaik, S., *Langmuir* **2001,** *17* (9), 2556-2559.

11. Sigaud, P.; Chazalviel, J. N.; Ozanam, F.; Lahlil, K., *Appl Surf Sci* **2003,** *218* (1-4), 54-57.

12. Hyung, K. H.; Han, S. H., *Synthetic Met* **2003,** *137* (1-3), 1441-1442.

13. Oh, S.-Y.; Yun, Y.-J.; Kim, D.-Y.; Han, S.-H., *Langmuir* **1999,** *15* (14), 4690-4692.

14. Kim, C. O.; Hong, S. Y.; Kim, M.; Park, S. M.; Park, J. W., *J Colloid Interface Sci* **2004,** *277* (2), 499-504.

15. Zotti, G.; Schiavon, G.; Zecchin, S.; Berlin, A.; Pagani, G.; Canavesi, A., *Langmuir* **1997,** *13* (10), 2694-2698.

16. Carrara, M.; Nüesch, F.; Zuppiroli, L., *Synth. Met.* **2001,** *121* (1-3), 1633-1634.

17. Armstrong, N. R.; Carter, C.; Donley, C.; Simmonds, A.; Lee, P.; Brumbach, M.; Kippelen, B.; Domercq, B.; Yoo, S. Y., *Thin Solid Films* **2003,** *445* (2), 342-352.

18. Meyer, T. J.; Meyer, G. J.; Pfennig, B. W.; Schoonover, J. R.; Timpson, C. J.; Wall, J. F.; Kobusch, C.; Chen, X.; Peek, B. M., *Inorg Chem* **1994,** *33* (18), 3952-3964.

19. Koh, S. E.; McDonald, K. D.; Holt, D. H.; Dulcey, C. S.; Chaney, J. A.; Pehrsson, P. E., *Langmuir* **2006,** *22* (14), 6249-6255.

20. Hanson, E. L.; Guo, J.; Koch, N.; Schwartz, J.; Bernasek, S. L., *J Am Chem Soc* **2005,** *127* (28), 10058-10062.

21. Besbes, S.; Ltaief, A.; Reybier, K.; Ponsonnet, L.; Jaffrezic, N.; Davenas, J.; Ben Ouada, H., *Synthetic Met* **2003,** *138* (1-2), 197-200.

22. Brewer, S. H.; Brown, D. A.; Franzen, S., *Langmuir* **2002,** *18* (18), 6857-6865.

23. Yan, C.; Zharnikov, M.; Gölzhäuser, A.; Grunze, M., *Langmuir* **2000,** *16* (15), 6208-6215.

24. Cerruti, M.; Rhodes, C.; Losego, M.; Efremenko, A.; Maria, J.-P.; Fischer, D.; Franzen, S.; Genzer, J., *J Phys D: Appl Phys* **2007,** *40* (14), 4212-4221.

25. Mori, T.; Morimoto, T.; Nishikawa, T., *Appl Phys Express* **2011,** *4* (11).

26. Muilenberg, G. E., *Handbook of X-Ray Photoelectron Spectroscopy*. Perkin-Elmer: Minnesota, 1978.

27. Zhou, X. L.; Solymosi, F.; Blass, P. M.; Cannon, K. C.; White, J. M., *Surf Sci* **1989,** *219* (1-2), 294-316.

28. Wagner, C. D.; Riggs, W. M.; Davis, L. E.; Moulder, J. F.; Muilenberg, G. E., *Handbook of X-Ray Photoelectron Spectroscopy*. Perkin-Elmer: Minnesota, 1979.

29. Masuda, T.; Fukumitsu, H.; Takakusagi, S.; Chun, W. J.; Kondo, T.; Asakura, K.; Uosaki, K., *Adv Mater* **2012,** *24* (2), 268-72.

30. Grantham, L. F.; Elleman, T. S.; Martin, D. S., *J Am Chem Soc* **1955,** *77* (11), 2965-2971.

31. Elding, L. I., *Acta Chem Scand* **1970,** *24* (5), 1527-&.

32. Elding, L. I., *Acta Chem Scand* **1970,** *24* (4), 1331-&.

33. Elding, L. I., *Acta Chem Scand* **1970,** *24* (4), 1341-&.

34. Drougge, L.; Elding, L. I.; Gustafso.L, *Acta Chem Scand* **1967,** *21* (6), 1647-&.

35. Elding, L. I.; Leden, I., *Acta Chem Scand* **1966,** *20* (3), 706-&.

36.   Elding, L. I., *Acta Chem Scand* **1966,** *20* (9), 2559-&.

37.   Yanagida, M.; Kanai, T.; Zhang, X. Q.; Kondo, T.; Uosaki, K., *B Chem Soc Jpn* **1998,** *71* (11), 2555-2559.

38.   Kondo, T.; Yanagida, M.; Shimazu, K.; Uosaki, K., *Langmuir* **1998,** *14* (19), 5656-5658.

39.   Fadley, C. S.; Baird, R. j.; Siekhaus, W.; Novakov, T.; Bergstrom, S. A. L., *J. Electron Spectrosc Relat Phenom* **1974,** *4*, 93.

40.   Fraser, W. A.; Florio, J. V.; Delgass, W. N.; Robertson, W. D., *Surf Sci* **1973,** *36* (2), 661.

41.   Porter, M. D.; Bright, T. B.; Allara, D. L.; Chidsey, C. E. D., *J Am Chem Soc* **1987,** *109* (12), 3559-3568.

42.   Nakamura, N.; Huang, H.-X.; Qian, D.-J.; Miyake, J., *Langmuir* **2002,** *18* (15), 5804-5809.

CHAPTER 4

VOLTAMMETRIC AND UV-VIS SPECTROELECTROCHEMICAL INVESTIGATION OF REDOX PROCESSES OF VIOLOGEN MOLECULAR LAYERS ON ITO

4.1. Introduction

Numerous investigations of chemically modified electrodes and schemes for modification of electrode surfaces has been reported for various application including fundamental studies. The self-assembled viologen moiety and its redox-functionality on solid electrodes have been widely investigated by cyclic voltammetry,[1-3] UV-vis-absorption,[4] vibrational spectroscopy (IR and Raman),[5] quartz crystal microbalance (QCM),[6] electroreflectance,[7-9] and STM.[10]

The efforts have been made to fabricate the modified electrode based on viologen layer as well polyviologen-polyanion complexes,[11, 12] viologen-substituted conducting polymers,[13] electropolymerized films,[14] mono- and multi-viologen layers[15-17] and molecular wires,[18] Viologen-modified electrode have been proposed for electrochromic devices,[19, 20] electrocatalytic activity,[21, 22] stabilization of nanoparticles or metal complexes[23], and for sensitization of solar energy conversion.[24] Viologen is a well-known electrochromic material[25-27] and electron transfer mediator [28-33] due to its reversible redox behavior. Although the viologen moiety was successfully confined on the electrode surfaces, the spectroelectrochemical properties on ITO surface, were less studied.[34-36]

After successfully construct viologen molecular layers on ITO surfaces (Chapter 3), this chapter deals with in situ spectroelectrochemistry based on a surface confined viologen (V^{2+}) and aqueous solution-phase methyl viologen (MV^{2+}) for comparison.

4.2. Result and Discussions

4.2.1. Cyclic voltammetry (CVs) of methyl viologen in solution

Figure 4-1(a) shows CVs of an ITO in 0.1 of Na_2SO_4 aqueous solution containing 1 mM $MVCl_2$, scanned from 0.1 to -1.1 V with different scan rate in the range 0.01–1.00 Vs^{-1}. The peaks a and a` which observed at -0.57 and -0.52 V, respectively, were due to $MV^{2+}$ + e$^-$ $\rightleftarrows$ $MV^{+\bullet}$. At more negative potentials, peak b and b` correspond to MV^{2+} + e$^-$ $\rightleftarrows$ MV^0 were observed at -0.92 and -0.85 V, respectively. Peak-to-peak separations of $MV^{2+}/MV^{\bullet+}$ are rather constant at 60 mV up to 0.5 Vs^{-1}. These results indicate that $MV^{\bullet+}$ formation is a reversible process. Figure 4-1(b) shows the resulting plot of the Randles-Sevcik analysis performed on these peaks where it is clear that the peak currents observed for both peaks have a linear dependence on the square root of the scan rate that implies that these peaks arise from a diffusion controlled process.[37]
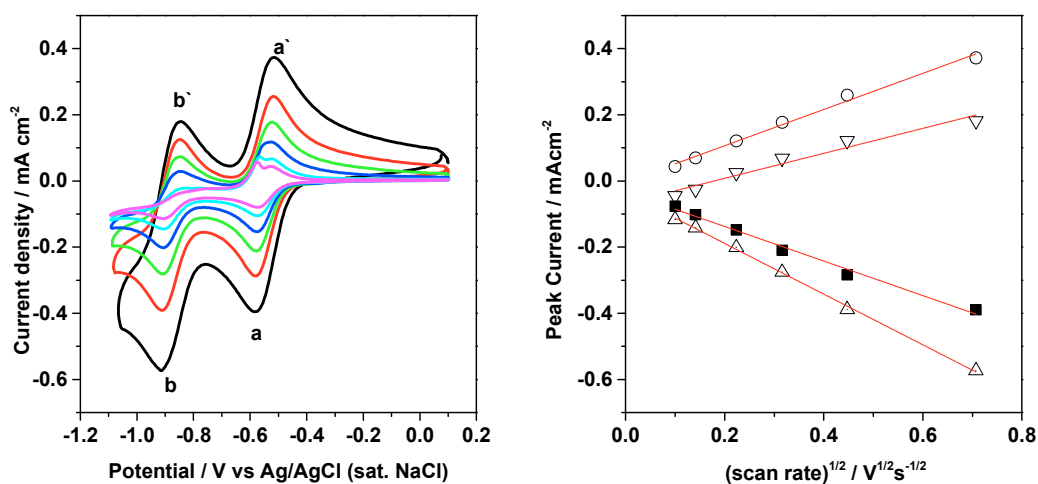

Figure 4-1(a) CVs of methyl viologen dichloride ($MVCl_2$) in 0.1 M Na_2SO_4 aqueous solution at scan rates of 0.01 (pink line), 0.02 (light blue line), 0.05 (blue line), 0.1 (green line), 0.2 (red line) and 0.5 Vs^{-1} (black line). The characteristic current peaks are labeled a/a` and b/b`. (b) Randles-Sevcik plot of peak a/a` (black square/circle) and b/b`(down-pointing triangle /up-pointing triangle) observed in (a).

4.2.2. Cyclic voltammetry of viologen constructed on ITO

Figure 4-2 (a) shows the CVs of bare ITO and mono- and multi-viologen layers constructed on ITO electrode, measured on 0.1 M Na_2SO_4 aqueous solution and scan rate 50 mVs^{-1}. Before viologen moiety was constructed on ITO, no redox peak was observed, then two well-defined redox peak for were observed after viologen constructed on ITO substrate. In compare to the MV^{2+} solution, the first redox pair corresponds to $V^{2+/\bullet+}$ and the second redox pair corresponds to $V^{\bullet+/0}$ redox process. The formal potential ($E_{1/2}$), surface coverage (Γ), electron transfer rate constant (k_{app}), peak separation (ΔE) and peak current (i_p) of $V^{2+/\bullet+}$ and $V^{\bullet+/0}$ formation was shown in Table 4-1 and Table 4-2, respectively.
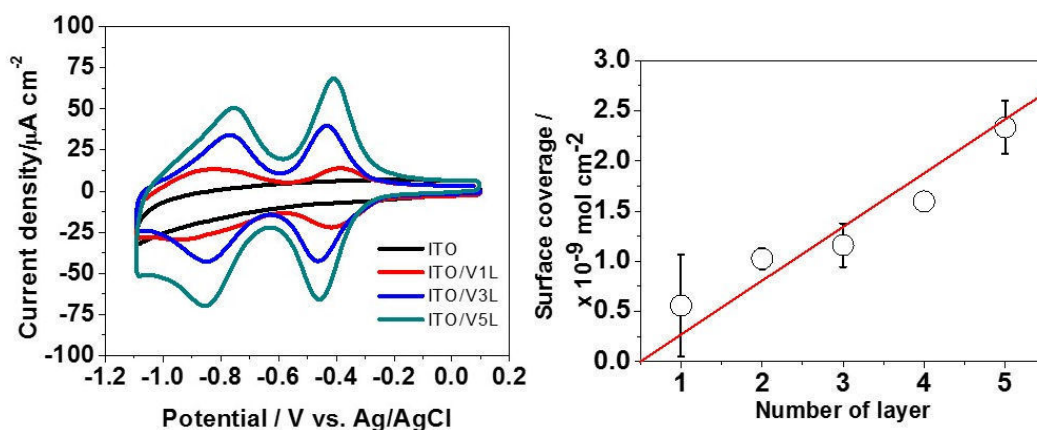
Figure 4-2(a) CVs of ITO after stepwise surface coupling reaction to construct viologen layers in 0.1 M Na_2SO_4 aqueous solution at scan rates of 0.05 Vs^{-1}. (b) The surface coverage calculated from the anodic current of the first cathodic charge ($V^{+\bullet}/V^{2+}$).

Figure 4-3(a), (b), and (c) shows the CVs of 1LV-, 3LV- and 5LV-ITO recorded at different scan rates (10 ~ 500 mV s^{-1}), and plots of the peak currents and potentials vs. the scan rate. The peaks current are proportional to the scan rate (v), rather than the $v^{1/2}$. These results indicate that viologen mono- and multi-layers was formed and covalently bond to the ITO surface.
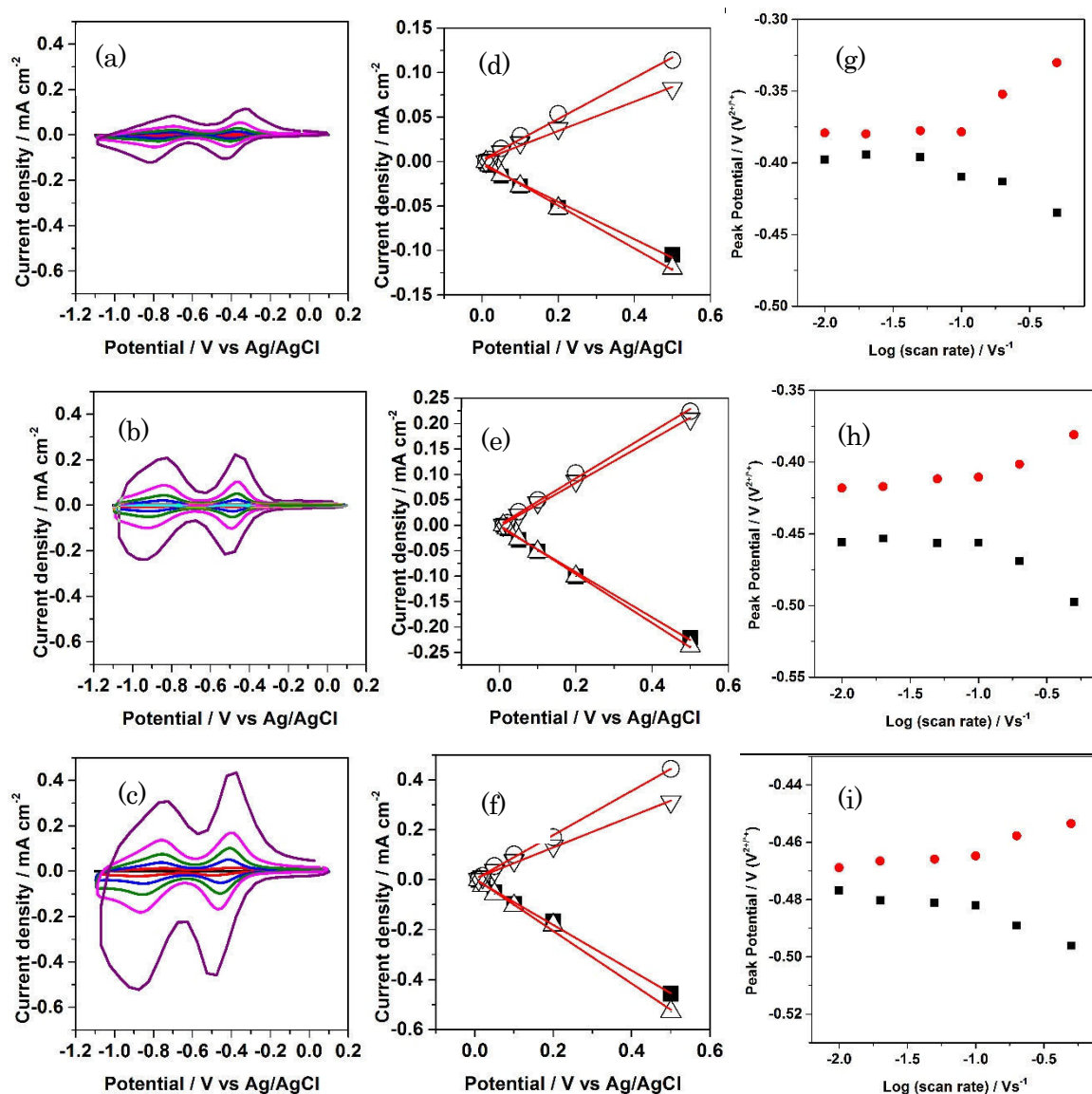
69

Figure 4-3. CVs of (a) 1LV-, (b) 3LV- and (c) 5LV-ITO electrode in 0.1 M Na_2SO_4, pH ~ 5.8. The scan rates range from 10 ~ 500 Vs^{-1};(d), (e) and (f)scan rate dependencies of the peak currents for $V^{2+}/V^{+\bullet}$ redox process (black square/circle) and for $V^{+\bullet}/V^0$ redox process (up-pointing triangle/down-pointing triangle) of 1LV-, 3LV- and 5LV-ITO, respectively. (g), (h), and (i) Relationship between Ep values and log scan rate of 1LV-, 3LV- and 5LV-ITO, respectively.

Apparent rate constants, k_{app}, were calculated for all modified surfaces according to the standard Laviron method expressed as eq 4-1.

$$k_{app} = \frac{(1-\alpha)nFv_a}{RT} \qquad (4\text{-}1)$$

the transfer coefficient α (a measure of the energy barrier symmetry) was approximated as 0.5.[14] The peak potentials $E_{p,a}$ and $E_{p,c}$ were plotted versus log(v) (Figure 4-3(g),(h) and (i)), and $E_{p,a}$ and $E_{p,c}$ were plotted separately to determine the convergent intercept of the anodic and cathodic linear regions. The potential of the convergence point (v_a in eq. 4-1) was then used in the standard Butler−Volmer theory analysis. The result is shown in Table 4-1 and Table 4-2. The formation of $V^{\bullet+}$ almost not depends on the number of viologen layer. However, the formation of V^0 was affected by the number of viologen layer. This probably implies that V^0 formation not only via $V^{\bullet+} + e \rightarrow V^0$ but also probably via $V^{2+} + 2e \rightarrow V^0$. However, the rate constant formation of V^0 still needs to be clarified. The electron transfer coefficients are clearly too small, a phenomenon which k_{app} been attributed to defectiveness in the viologen layers.[13,15] Nevertheless, the values are given in Table 4-1 and 4-2 are acceptable in comparison to those reported by Chidsey [12] for ferrocene, immobilized at the alkyl thiol monolayers. Further, these data show that the rate of transferring electrons from the ITO electrode to the viologen moiety within the mono- and multi-layers are quite fast, suggesting that conditions can be found in which the cross-reaction rate constant limits the overall current.

The viologen coverage was calculated from the integrated charge of first cathodic current ($V^{2+/\bullet+}$). The coverage as a function of viologen layer was shown in Figure 4-2(b). The coverage of viologen was increased linearly with number of layers ($\pm 5 \times 10^{-10}$ mol cm^{-2} per layer). This value was larger than viologen coverage on viologen [16]. Similar surface coverage was also observed from the SAMs of some other viologens on the Au electrode,[12,16] and from the viologen LB films on ITO electrode surface. However, the increase of viologen coverage indicates that viologen mono- and multi-layer successfully constructed via surface coupling reaction, by using alkyl silane as a linker layer.

Table 4-1. Electrochemical parameters for the viologen modified ITO for the $V^{\bullet+}$ formation ($V^{2+/\bullet+}$).

	$\Gamma \times 10^{-9}$/mol cm^{-2}	$k_{app}{}^{a}$/s^{-1}	$E_{1/2}{}^{b}$/V	$\Delta E_{p}{}^{b}$/mV
1LV-	0.55	42.1	-0.40	49
3LV-	1.21	45.8	-0.43	60
5LV-	2.25	44.8	-0.42	63

Table 4-2. Electrochemical parameters for the viologen modified ITO for the V^{0} formation ($V^{\bullet+/0}$).

	$\Gamma \times 10^{-9}$/mol cm^{-2}	$k_{app}{}^{a}$/s^{-1}	$E_{1/2}{}^{b}$/V	$\Delta E_{p}{}^{b}$/mV
1LV-	0.37	12.5	-0.88	90
3LV-	0.93	25.2	-0.80	72
5LV-	1.89	24.3	-0.79	60

Note to Table 1 and 2: [a]Average of measurements with different scan rate. [b]Scan rate: 100 mV s^{-1}; $\Delta E_{1/2}$ is the total width at half-height of the wave.

From Table 4-1, it can be seen that $E_{1/2}$ was slightly shifted to the more negative potential as the number viologen layer increased. Such potential shifted have been also reported for polyelectrolyte complexes containing viologen.[38, 39] The slightly shifted in $V^{2+/\bullet+}$ potential region may be due to slow ion transport within the multilayer or a dimerization reaction between the $V^{\bullet+}$ formed after the first reduction, as postulated by Bird and Kuhn.[40]. The dimer formation has been reported in the LB films of viologens with short alkyl chains[41] and in the SAMs of $CH_3V^{2+}(CH_2)_nSH$ (n = 10, 12, 14).[42] The similar behavior was also observed in a solution containing a high concentration of MV^{2+}. The dimer formation will cause reorientation or recrystallization in the viologen layer.[40] Another possibility is that viologen layers behaving as a membrane creating a Donnan potential.[43] The redox probe appears to be able to penetrate the membrane with relative ease. The

membrane is then generating a different ionic environment, shifting the effective potential at the electrode surface.

4.2.3. Spectroelectrochemistry of methyl viologen in solution

The study of methyl viologen both electrochemically and spectroscopically has been well-known. Figure 4-7 shown the UV-vis spectra of MV^{2+} measured in 0.1 M Na_2SO_4 aqueous solution. MV^{2+} in solution are colorless and absorb strongly in the UV region at maxima 267 nm), When the potential was introduced into solution via ITO electrode, some peaks was observed at absorbance spectra in the visible region. The broad absorbance peak with a maximum at ca. 603 nm and the narrow absorbance peak centered at 394 nm start to be observed during application of -0.4 V. Another absorbance peak at 367 nm and 550 nm was also observed. The presence of this peak is due to the formation of diradical formation or dimer $(MV)_2^{2+}$. This result is in good agreement with previously reported. [10-17,22,24] At more negative potentials (less than -0.6 7), this absorbance peak was observed to be increased. Based on the CVs (Figure 4-1), at potential region -0.4 to -0.7 V, $MV^{\bullet+}$ species was formed. Then the steady state UV-vis spectra correspond to $MV^{\bullet+}$. At potential more negative than -0.8V, the absorbance at 600 nm was decreased but the absorbance at 400 nm was continuously increased. The absorbance at 400 nm was then assigned to the viologen radical formation $V^{2+/\bullet+}$ [17] as it confirmed from the potential region of MV^0 formation (Figure 4-1). The results suggest that both $MV^{\bullet+}$ and MV^0 were observed from the UV-vis spectra and their formation depended on the potentials.
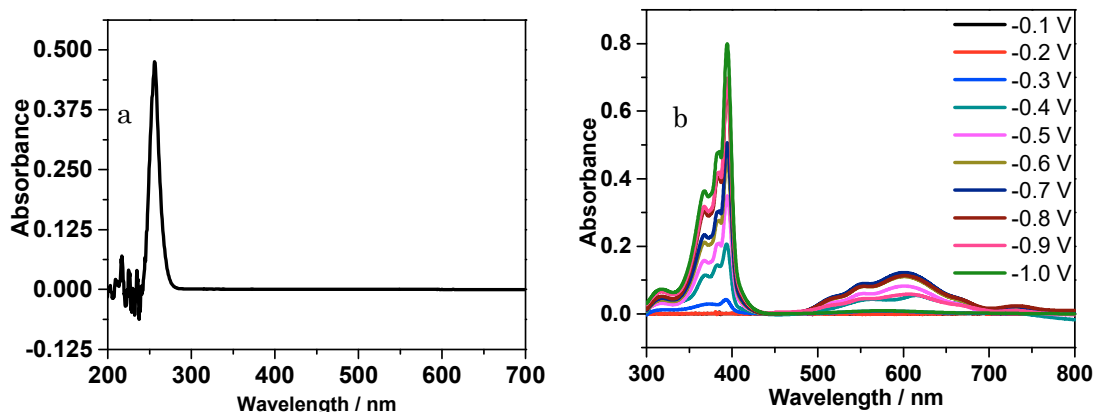
Figure 4-6. (a) UV-vis spectra of 0.1 M Na₂SO₄ aqueous solution containing 1 mM MVCl₂ within quartz cell and (b) steady state UV-vis spectra measured of MVCl₂ on ITO electrode by applying potential from -0.1 to1.0 V for each 0.1 V.

Figure 4-7 shows the absorbance changes at 400 and 600 nm simultaneously measured with current change during the potential sweep. The absorbance at 0 V was used as a reference. The result shows that the first cathodic current was observed and the absorbance at 400 and 600 nm start to increase at potential more negative than -0.6 V. The current responses indicate that the MV^{2+} was reduced to form $MV^{\bullet+}$. The absorbance changes at 400 and 600 than implied the presence of $MV^{\bullet+}$ in solution. When the second cathodic current was observed, the absorbance at 600 nm then slightly increases at the more negative potential. The CVs confirm that neutral species formation starts from -0.85 V. However, the absorbance at 600 nm remains, indicates that in solution, $MV^{\bullet+}$ still exist at more negative potentials. The reason is that in solution after $MV^{\bullet+}$ was formed on the electrode, some of $MV^{\bullet+}$ was then moved away and stable in solution.

As the potential was positively scanned, the anodic current was observed. At this potential, the MV^0 was oxidized to form $MV^{\bullet+}$. The remaining $MV^{\bullet+}$ in solution was causing the absorbance at 600 is higher than before MV^0 was formed. These results suggest that

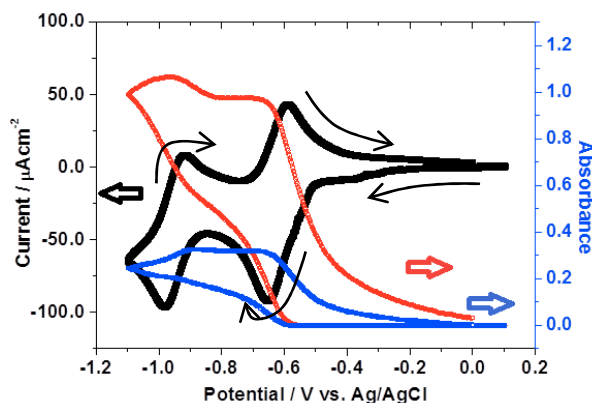MV$^{\bullet+}$ is stable in solution.

Figure 4-7. Absorbance changes at 400 (red line) and 600 nm (blue line) measured simultaneously with cyclic voltammetry (black line) of 0.1 M Na$_2$SO$_4$ aqueous solution containing MV^{2+}.

4.2.4. Spectroelectrochemistry of viologen mono- and multi-layers

4.2.4.1. Viologen monolayer on ITO electrode (1LV-ITO)

Figure 4-8(a) shows the in situ UV–vis spectra of the 1LV-ITO under potentiostatic conditions recorded at every 0.1 V from -0.1 to -1.0 V, measured in 0.1 M Na$_2$SO$_4$ aqueous solution. At potential -0.1 V, no peak was observed in the absorbance spectra, suggesting that viologen exists in the dication state (V^{2+}). The peaks were then observed at maxima 400 nm and 600 nm when the potential was kept at above -0.4 V and the peaks were increased up to potentials -0.6V. Compare to absorbance spectra of MV^{2+} in solution, the absorbance spectra were then in agreement with V$^{\bullet+}$ formation. At more negative potential (-0.7 to -0.9 V), the absorbance at 600 was decreased but the peak at 400 nm was increased. This result implies that V$^{\bullet+}$ was reduced to form V^0. When the 1LV-ITO was kept at -1.0V, the peak at 600 nm was not observed while the peak at 400 nm was reached maxima.
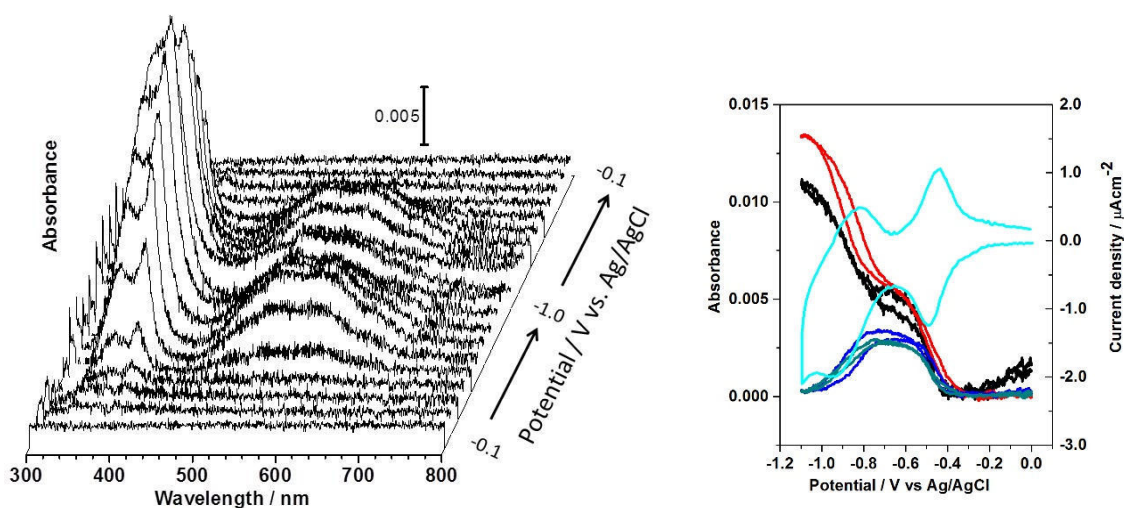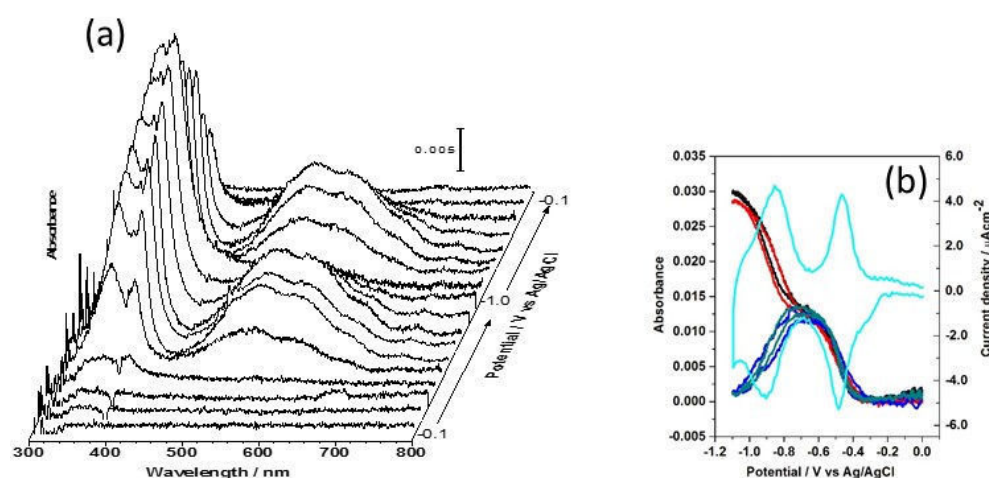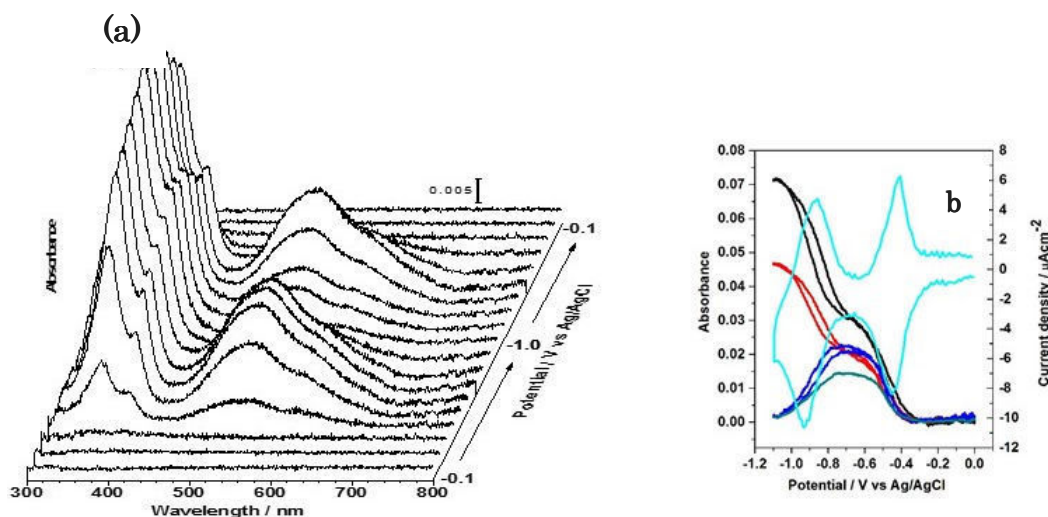
Figure 4-8 (a) Steady state UV-vis spectra of 5LV-ITO, measured at -0.1 to 1.0 V for every 0.1 V (spectra at 0 V as a reference), and (b) current and absorbance response at 375 (black line), 400 (red line), 550 (green line) and 600 nm (blue line). The 0.1 M Na$_2$SO$_4$ aqueous solution was used as an electrolyte and the scan rate was 10 mVs^{-1}.

The absorbance at 375, 40, 550 and 600 nm simultaneously measured with a potential sweep as shown in Figure 4-8(b). When the potential sweep from 0 to negative potentials, first cathodic current flow, the absorbance at all observed wavelength were started to increase from -0.3 to -0.6 V. This indicate that the V$^{\bullet+}$ was formed. Then, the absorbance relatively constant up to -0.7V, indicating that V$^{\bullet+}$ exist at this potential region. When the potential was sweep to the more negative, second cathodic current was observed, at the same time the absorbance at 550 and 600 nm was decreased while the absorbance at 375 and 400 nm was continuously increased. At this potential region, V$^{\bullet+}$ was reduced to form V^0 species. The continuous increase in absorbance throughout the whole reduction can be explained that both the viologen V$^{\bullet+}$ and the neutral species absorb the light at 400 nm. The V^0 species absorbs the light at 400 nm stronger than the V$^{\bullet+}$ species resulting in the further increase of absorbance at higher negative potentials. At the reverse direction potential sweep,

76

absorbance at 400 nm is decreasing while absorbance at 600 nm was increased, suggesting that V^0 was oxidized to form $V^{\bullet+}$. Then the absorbance return to initial value, showing that the $V^{\bullet+}$ was oxidized to form V^{2+} species. This result implies that the absorbance spectra was depend on the potential at which electrogenerated viologen species were formed.

4.2.4.2. Viologen multi-layer on ITO

Figure 4-9(a) shows the steady state UV–vis spectra of the 3LV-ITO. At potential -0.4 to -0.7 V, the peak at 370, 400, 550 and 600 nm were observed. The last three main peaks position was similar to the 1LV-ITO UV-vis spectra while the first peak was blue-shifted compared to the 1LV-ITO. In the case of 3LV-ITO, the absorbance ratio at 370 and 550 nm was higher than absorbance ratio at 400 and 600 nm. The shift and increase at 375 suggested the formation of dimer.[44]

Figure 4-9 (a) Steady state UV-vis spectra of 3LV-ITO, measured at -0.1 to 1.0 V for every 0.1 V (spectra at 0 V as a reference), and (b) current and absorbance response at 370 (black line), 400 (red line), 550 (green line) and 600 nm (blue line). The 0.1 M Na_2SO_4 aqueous solution was used as an electrolyte and the scan rate was 10 mVs^{-1}.

(a)

Figure 4-10 (a) Steady state UV-vis spectra of 5LV-ITO, measured at -0.1 to 1.0 V for every 0.1 V (spectra at 0 V as a reference), and (b) current and absorbance response at 365 (black line), 400 (red line), 550 (green line) and 600 nm (blue line). The 0.1 M Na₂SO₄ aqueous solution was used as an electrolyte and the scan rate was 10 mVs⁻¹.

The formation of dimer at higher viologen concentration was also observed in steady state UV-vis spectra of 5LV-ITO, as shown in Figure 4-10(a). The peak position was slightly compared to 1LV- and 3LV-ITO. To compare the peak shapes and position, the steady state spectra at -0.6 V was presented in Figure 4-11.
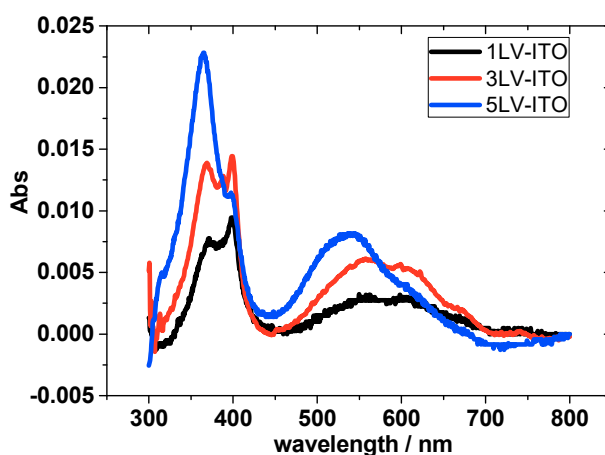
Figure 4-11. The steady state UV-vis spectra of 1LV- (black line), 3LV- (red line), and 5LV-ITO (blue line) at potential -0.6V.

The molar absorptivity values for monomer ($\varepsilon_{M600nm} = 14.049$ and $\varepsilon_{M520nm} = 4.307$) and dimer ($\varepsilon_{D600nm} = 11.989$ and $\varepsilon_{D520nm} = 23.045$) for reduced methyl viologen were reported by Komers.[49] For the three electrogenerated viologen species, the percentage dimerization was 90% or greater, provided the ratio of the molar absorptivities of the viologenated dendrimer monomer and dimer are the same as those of methyl viologen. In the case of confined viologen on ITO surface, the calculated % dimer at -0.6 V for 1LV-, 3LV- and 5LV- were 49%, 68%, and 88% respectively. This result implies that the dimer formation was due to high viologen coverage on ITO surface.

4.2.5. Time-resolved UV-vis spectroelectrochemistry of viologen monolayer on ITO

The double potential step chronoamperometry is then carried out to investigate both current and absorbance response of viologen on ITO. The potential was stepped to the more negative potentials. When the potential was stepped from 0 V (E1) to the potential $E_2 = -0.24$ V, -0.28V, and -0.32 V (Figure 4-12(a), 4-13(a), and 4-14(a) respectively), the transient current shows a spike current or charging current then decay to the baseline. The spike current was also observed when the potential was stepped back to 0 (Figure 4-12(b), 4-13(b), and 4-14(b) respectively). At these potentials (E_2) no absorbance change was observed (Figure 4-12(c), 4-13(c), and 4-14(c) respectively). This indicates that viologen still in the dication state (V^{2+}).

At more negative potentials (E_2), the spike current response was observed and immediately decays. Simultaneously, the absorbance was changed as the potential was stepped to -0.4V <E_2<-0.6 V (Figure 4-15, 4-16, and 4-17) and stay stable until the potential was stepped back to 0V. The contour spectra show the absorbance change profile at a various wavelength, and the transient spectra at the certain time show in agreement with steady state spectra of $V^{\bullet+}$ at -0.6V.

At more negative potential, -0.7 V < E_2 < -1.0V, as in the steady state spectra of neutral viologen species was observed, the absorbance at 400 nm was increased as the potential was stepped from 0 to E_2, and stay constant or stable until the potential was stepped back to 0V. On the other hand, the absorbance at 600 nm becomes lower and not changed at E_2=-1.0V. The transient spectra are in agreement with steady state spectra of neutral viologen species. It was also observed that the V^0 was directly formed via two electron reduction reaction of V^{2+} and no $V^{\bullet+}$ spectra were not observed in the transient spectra.
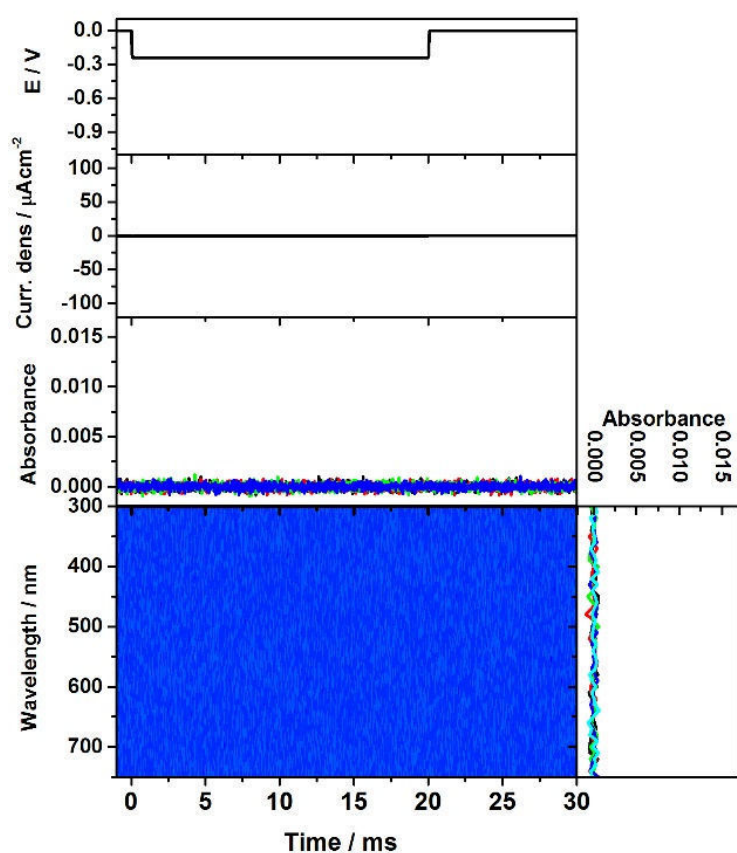
Figure 4-12. (a) Potential profile (stepped from 0 to -0.24V) and (b) the corresponding current response at both the 1LV-ITO electrodes. (c) Corresponding absorbance response at 375 (black line), 400 (red line), 550 (green line), and 600 nm (blue line), (d) contour of the absorbance as functions of probe wavelength and time after the potential step, and (e) time-resolved spectra at -0.5 (black line), 0 (red line), 1 (green line), 5 (blue line), and 10 ms (light blue line) after the potential step.
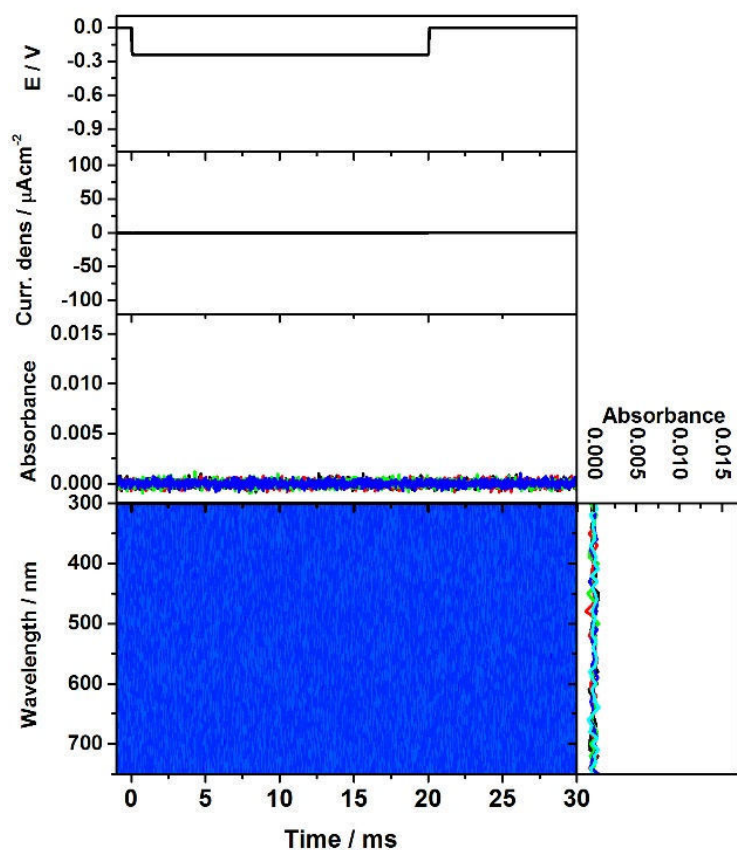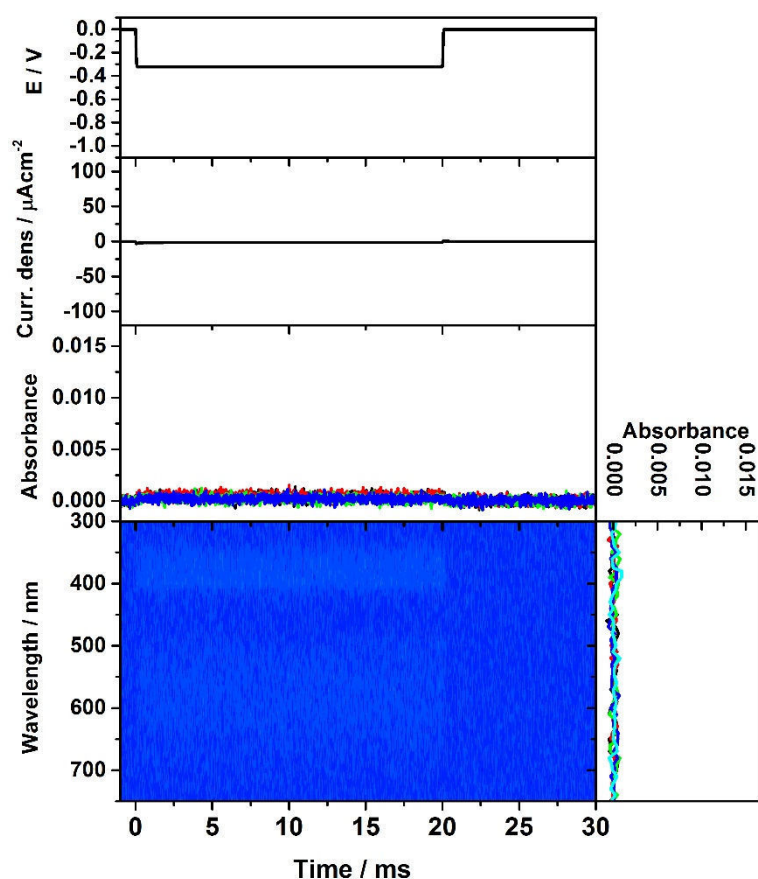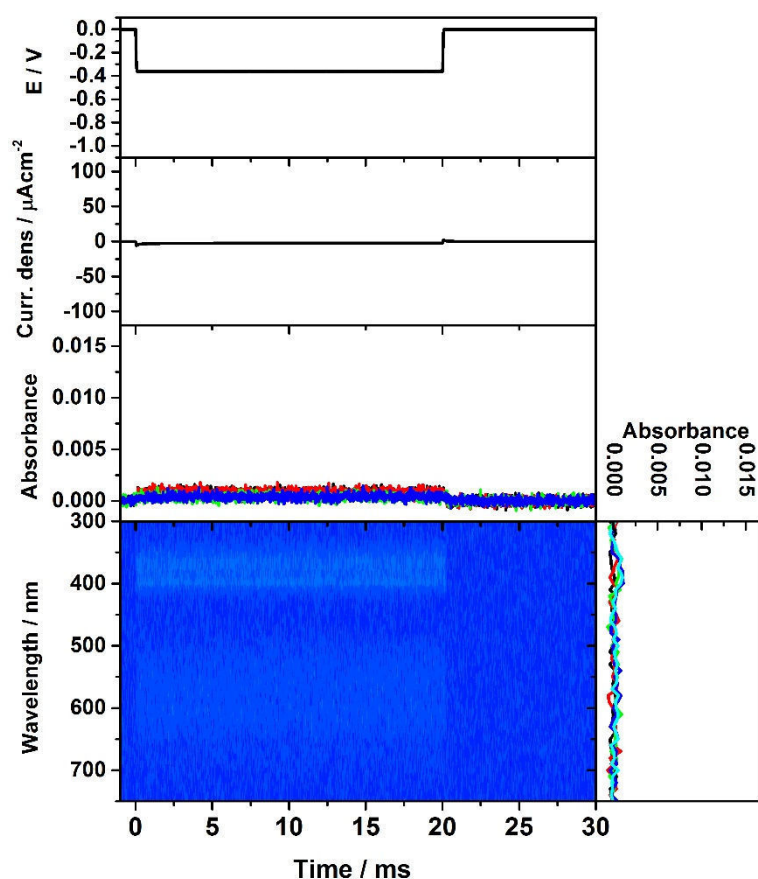
Figure 4-13. (a) Potential profile (stepped from 0 to -0.28V) and (b) the corresponding current response at both the 1LV-ITO electrodes. (c) Corresponding absorbance response at 375 (black line), 400 (red line), 550 (green line), and 600 nm (blue line), (d) contour of the absorbance as functions of probe wavelength and time after the potential step, and (e) time-resolved spectra at -0.5 (black line), 0 (red line), 1 (green line), 5 (blue line), and 10 ms (light blue line) after the potential step.

Figure 4-14. (a) Potential profile (stepped from 0 to -0.32V) and (b) the corresponding current response at both the 1LV-ITO (black line) and 1LV-ITO/Pt-complex (red line) electrodes. (c) Corresponding absorbance response at 375 (black line), 400 (red line), 550 (green line), and 600 nm (blue line), (d) contour of the absorbance as functions of probe wavelength and time after the potential step, and (e) time-resolved spectra at -0.5 (black line), 0 (red line), 1 (green line), 5 (blue line), and 10 ms (light blue line) after the potential step of 1LV-ITO.
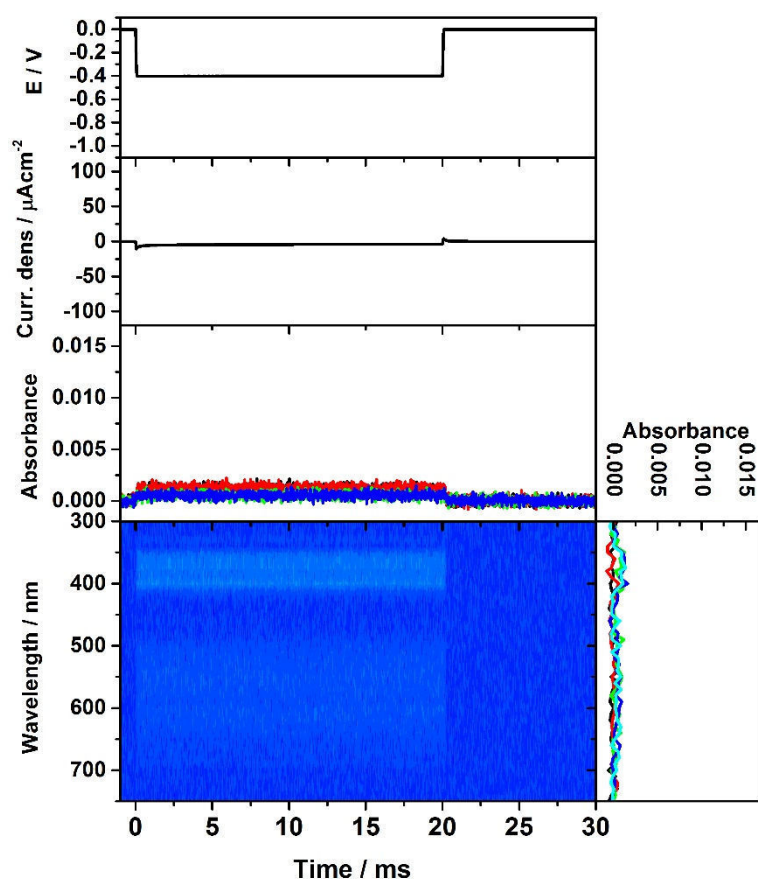
Figure 4-15. (a) Potential profile (stepped from 0 to -0.36V) and (b) the corresponding current response at both the 1LV-ITO electrodes. (c) Corresponding absorbance response at 375 (black line), 400 (red line), 550 (green line), and 600 nm (blue line), (d) contour of the absorbance as functions of probe wavelength and time after the potential step, and (e) time-resolved spectra at -0.5 (black line), 0 (red line), 1 (green line), 5 (blue line), and 10 ms (light blue line) after the potential step.
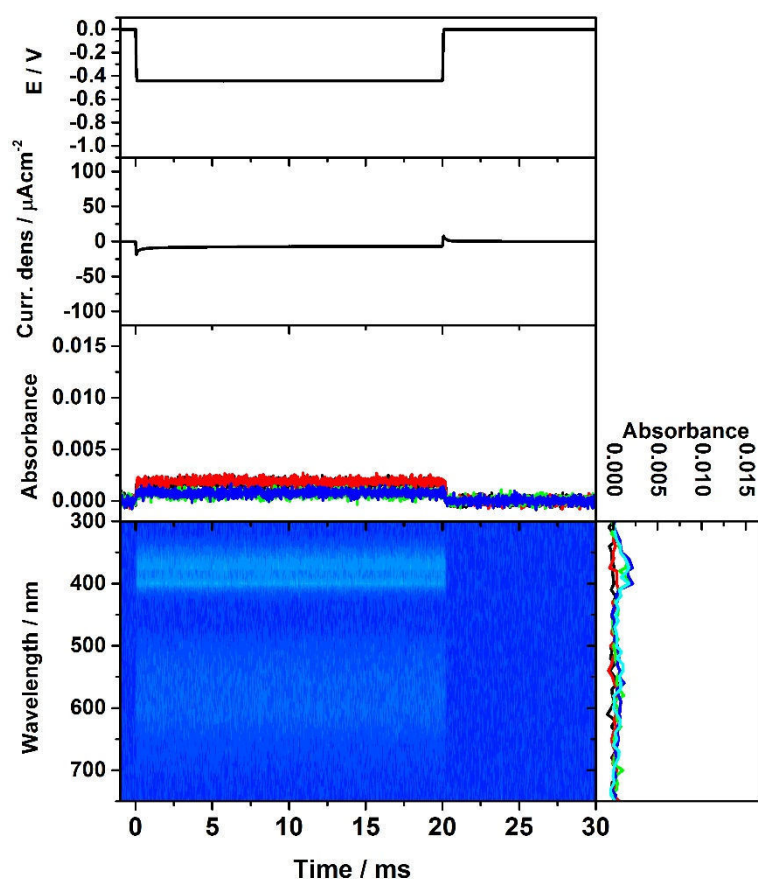
Figure 4-16. (a) Potential profile (stepped from 0 to -0.40V) and (b) the corresponding current response at both the 1LV-ITO electrodes. (c) Corresponding absorbance response at 375 (black line), 400 (red line), 550 (green line), and 600 nm (blue line), (d) contour of the absorbance as functions of probe wavelength and time after the potential step, and (e) time-resolved spectra at -0.5 (black line), 0 (red line), 1 (green line), 5 (blue line), and 10 ms (light blue line) after the potential step.
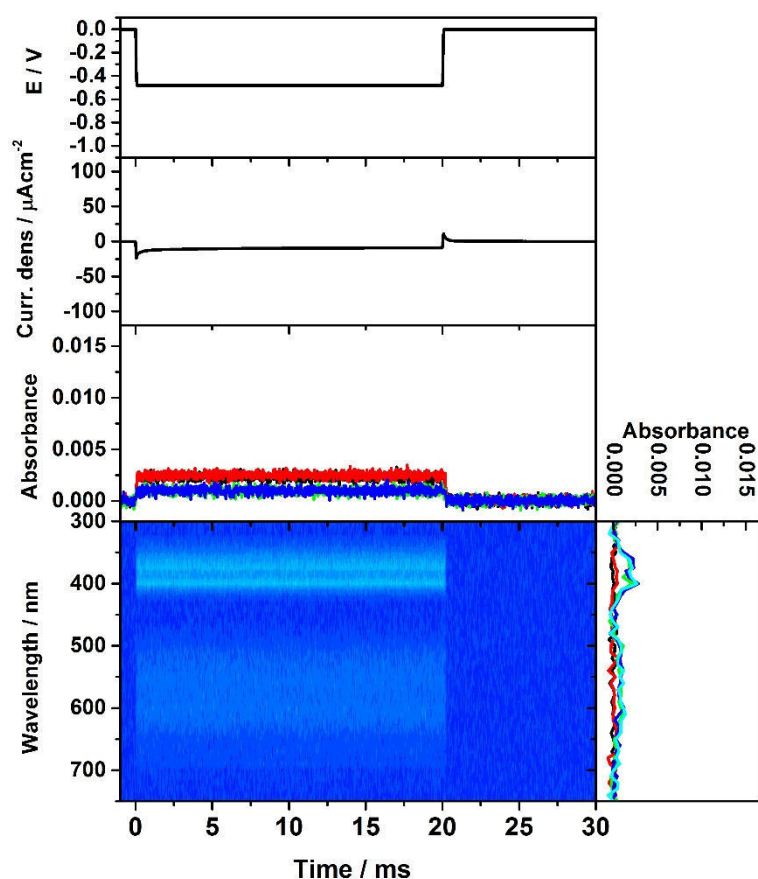
84

Figure 4-17. (a) Potential profile (stepped from 0 to -0.44V) and (b) the corresponding current response at both the 1LV-ITO electrodes. (c) Corresponding absorbance response at 375 (black line), 400 (red line), 550 (green line), and 600 nm (blue line), (d) contour of the absorbance as functions of probe wavelength and time after the potential step, and (e) time-resolved spectra at -0.5 (black line), 0 (red line), 1 (green line), 5 (blue line), and 10 ms (light blue line) after the potential step.
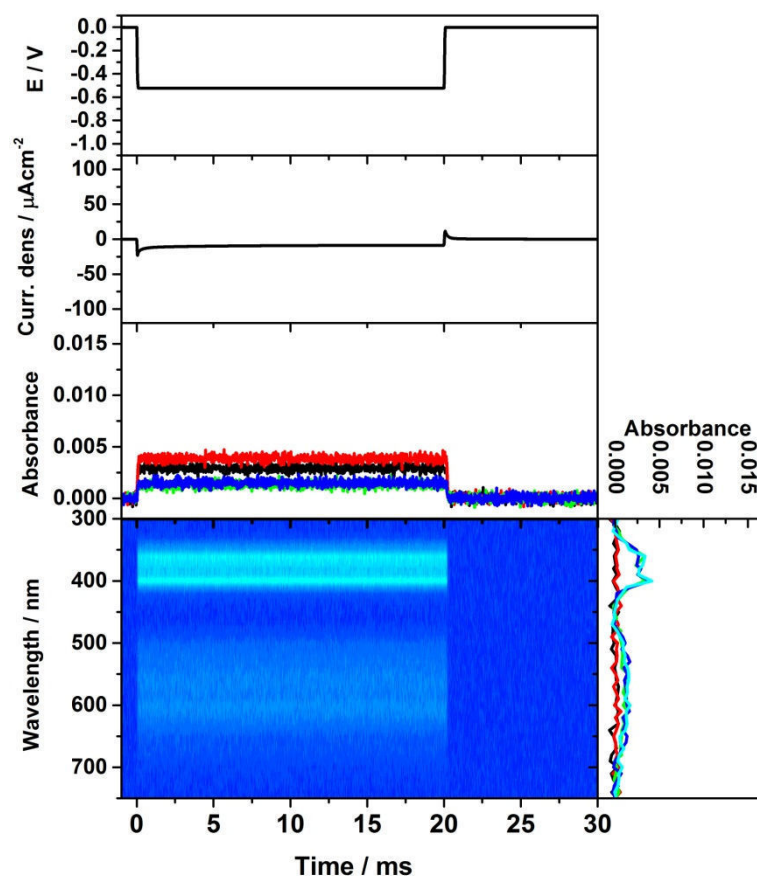
Figure 4-18. (a) Potential profile (stepped from 0 to -0.48V) and (b) the corresponding current response at both the 1LV-ITO electrodes. (c) Corresponding absorbance response at 375 (black line), 400 (red line), 550 (green line), and 600 nm (blue line), (d) contour of the absorbance as functions of probe wavelength and time after the potential step, and (e) time-resolved spectra at -0.5 (black line), 0 (red line), 1 (green line), 5 (blue line), and 10 ms (light blue line) after the potential step.
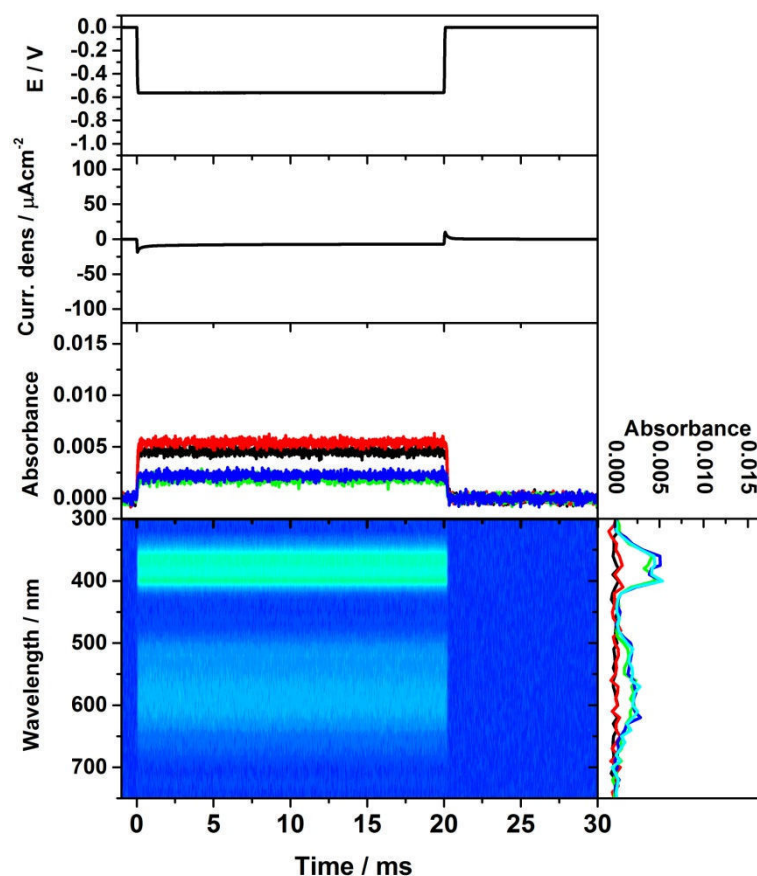
Figure 4-19. (a) Potential profile (stepped from 0 to -0.52V) and (b) the corresponding current response at both the 1LV-ITO electrodes. (c) Corresponding absorbance response at 375 (black line), 400 (red line), 550 (green line), and 600 nm (blue line), (d) contour of the absorbance as functions of probe wavelength and time after the potential step, and (e) time-resolved spectra at -0.5 (black line), 0 (red line), 1 (green line), 5 (blue line), and 10 ms (light blue line) after the potential step.

Figure 4-20. (a) Potential profile (stepped from 0 to -0.56V) and (b) the corresponding current response at both the 1LV-ITO electrodes. (c) Corresponding absorbance response at 375 (black line), 400 (red line), 550 (green line), and 600 nm (blue line), (d) contour of the absorbance as functions of probe wavelength and time after the potential step, and (e) time-resolved spectra at -0.5 (black line), 0 (red line), 1 (green line), 5 (blue line), and 10 ms (light blue line) after the potential step.
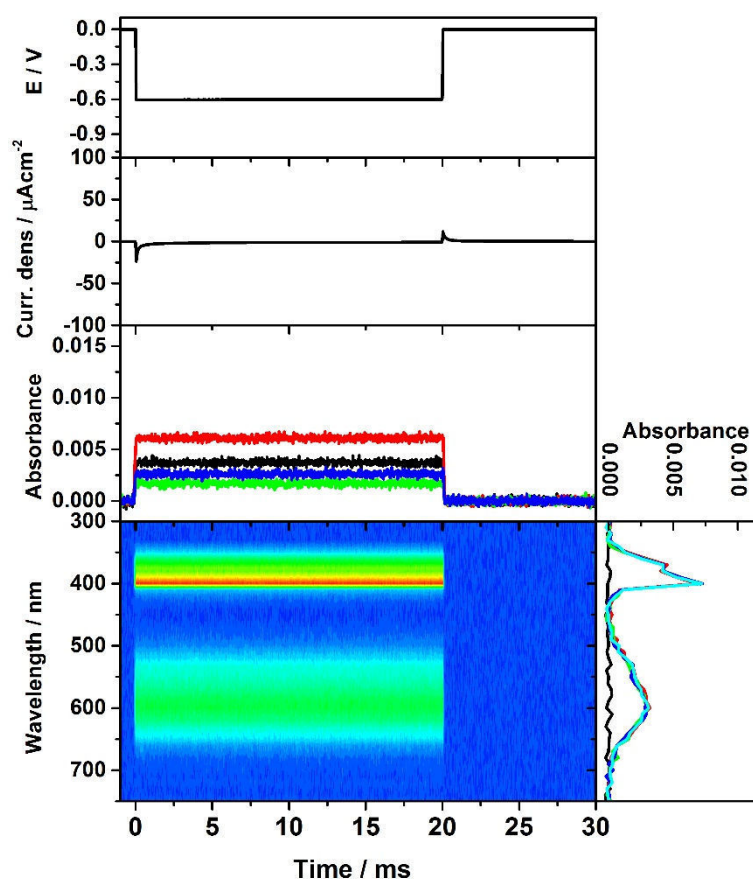
Figure 4-21. (a) Potential profile (stepped from 0 to -0.60V) and (b) the corresponding current response at both the 1LV-ITO electrodes. (c) Corresponding absorbance response at 375 (black line), 400 (red line), 550 (green line), and 600 nm (blue line), (d) contour of the absorbance as functions of probe wavelength and time after the potential step, and (e) time-resolved spectra at -0.5 (black line), 0 (red line), 1 (green line), 5 (blue line), and 10 ms (light blue line) after the potential step.
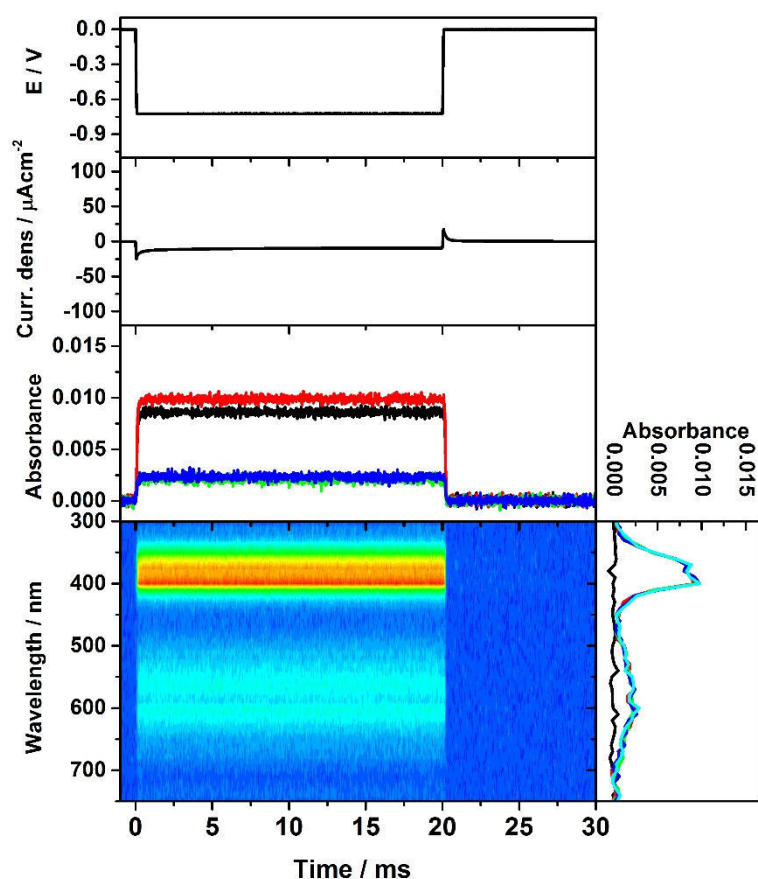
Figure 4-22. (a) Potential profile (stepped from 0 to -0.72V) and (b) the corresponding current response at both the 1LV-ITO electrodes. (c) Corresponding absorbance response at 375 (black line), 400 (red line), 550 (green line), and 600 nm (blue line), (d) contour of the absorbance as functions of probe wavelength and time after the potential step, and (e) time-resolved spectra at -0.5 (black line), 0 (red line), 1 (green line), 5 (blue line), and 10 ms (light blue line) after the potential step.
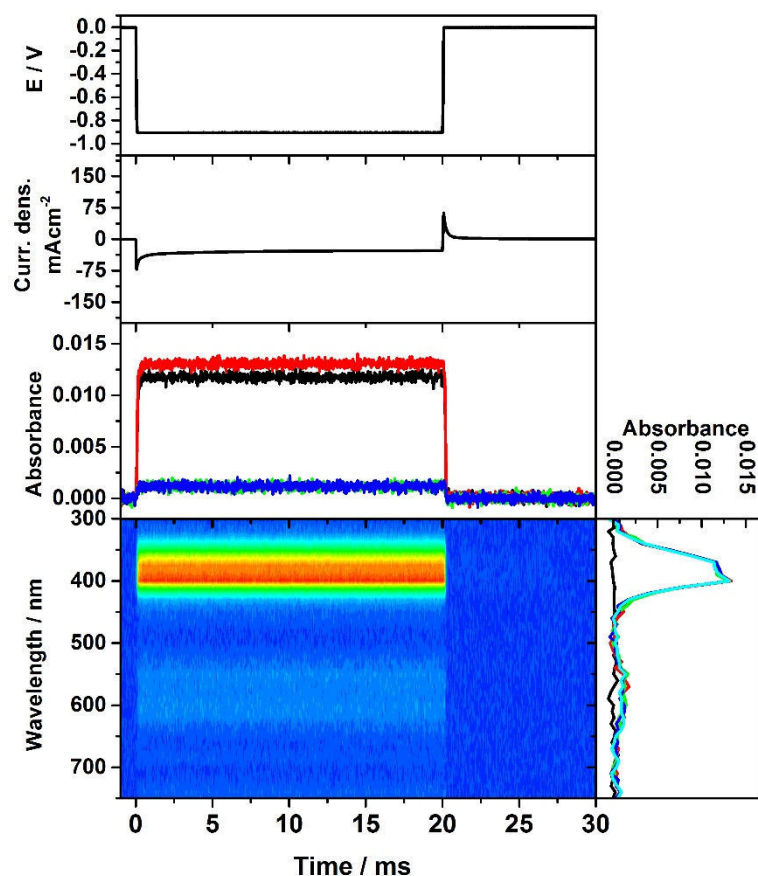
90

Figure 4-23. (a) Potential profile (stepped from 0 to -0.90V) and (b) the corresponding current response at both the 1LV-ITO electrodes. (c) Corresponding absorbance response at 375 (black line), 400 (red line), 550 (green line), and 600 nm (blue line), (d) contour of the absorbance as functions of probe wavelength and time after the potential step, and (e) time-resolved spectra at -0.5 (black line), 0 (red line), 1 (green line), 5 (blue line), and 10 ms (light blue line) after the potential step.
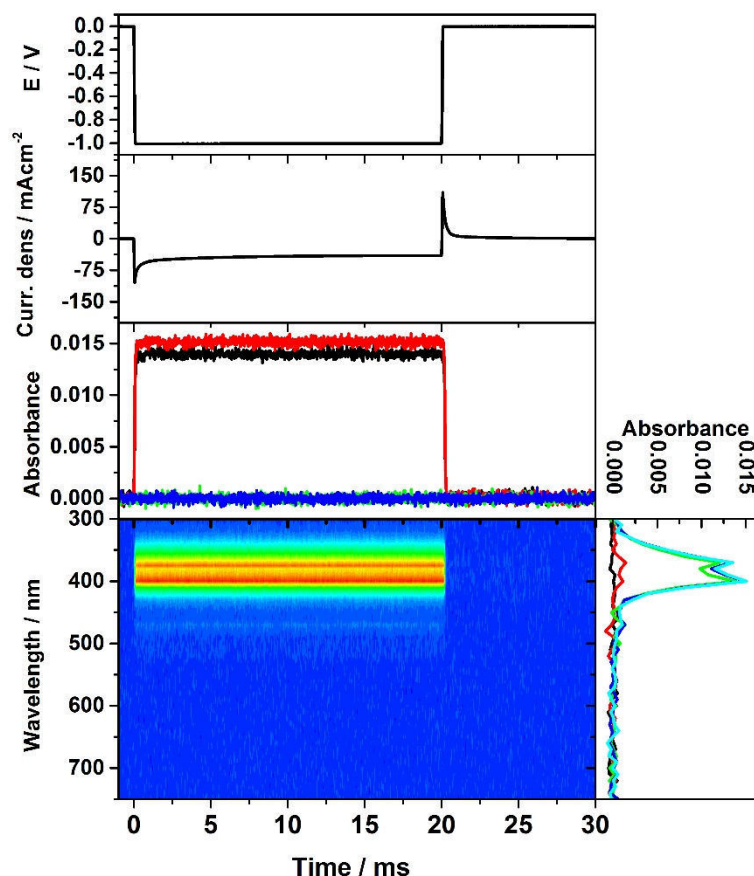
Figure 4-24. (a) Potential profile (stepped from 0 to -1.00V) and (b) the corresponding current response at both the 1LV-ITO electrodes. (c) Corresponding absorbance response at 375 (black line), 400 (red line), 550 (green line), and 600 nm (blue line), (d) contour of the absorbance as functions of probe wavelength and time after the potential step, and (e) time-resolved spectra at -0.5 (black line), 0 (red line), 1 (green line), 5 (blue line), and 10 ms (light blue line) after the potential step.

Potential dependence of electrogenerated viologen species was confirmed by using potential step experiment coupled with UV-vis absorbance spectroscopy. The absorbance response, as the potential was stepped from 0 to negative potential, were very fast. These results suggest that the formation of $V^{\bullet+}$ and V^0 directly from V^{2+} were very fast. This indicates that electron transfer from ITO to viologen and vice versa was very fast.

4.3. Conclusion

Viologen are existed in three different redox states. In compare to methyl viologen in solution, the viologen species on ITO electrode is confirmed both from CVs and UV-vis spectra. The electronic structure of electrogenerated viologen species was clarified from the steady state UV-vis spectra and also from transient spectra. Dimer of viologen was also observed both from the CV and UV-vis spectra. Dimer species were increased as the viologen number increase.

4.4. Reference

1. De Long, H. C.; Buttry, D. A., *Langmuir* **1992,** *8*, 6.

2. Zen, J. M.; Lo, C. W., *Anal Chem* **1996,** *68* (15), 2635-2640.

3. Snover, J. L.; Thompson, M. E., *J Am Chem Soc* **1994,** *116* (2), 765-766.

4. Lee, C.; Moon, M. S.; Park, J. W., *J Inclus Phenom Mol* **1996,** *26* (4), 219-232.

5. Kim, J. H.; Lee, K. A. B.; Uphaus, R. A.; Cotton, T. M., *Thin Solid Films* **1992,** *210* (1-2), 825-827.

6. Lee, C.; Lee, Y. K.; Lee, Y.; Jeon, I. C., *J Electroanal Chem* **1999,** *463* (2), 224-231.

7. Sagara, T.; Maeda, H.; Yuan, Y.; Nakashima, N., *Langmuir* **1999,** *15*, 8.

8. Higashi, T.; Shigemitsu, Y.; Sagara, T., *Langmuir* **2011,** *27* (22), 13910-13917.

9. Sagara, T.; Kato, N.; Toyota, A.; Nakashima, N., *Langmuir* **2002,** *18* (18), 6995-7001.

10. Lee, N.-S.; Shin, H.-K.; Qian, D.-J.; Kwon, Y.-S., *Jpn J Appl Phys* **2007,** *46* (4B), 2745-2748.

11. Xu, B.; Xu, L.; Gao, G.; Yang, Y.; Guo, W.; Liu, S.; Sun, Z., *Electrochim Acta* **2009,** *54* (8), 2246-2252.

12. Jain, V.; Yochum, H.; Wang, H.; Montazami, R.; Hurtado, M. A. V.; Mendoza-Galvan, A.; Gibson, H. W.; Heflin, J. R., *Macromol Chem Physic* **2008,** *209* (2), 150-157.

13. Young Jo, M.; Eun Ha, Y.; Hyun Kim, J., *Sol Energ Mat Sol C* **2012,** *107*, 1-8.

14. Cheng, K. C.; Chen, P. Y., *Electroanal* **2008,** *20* (2), 207-210.

15. Masuda, T.; Fukumitsu, H.; Takakusagi, S.; Chun, W. J.; Kondo, T.; Asakura, K.; Uosaki, K., *Adv Mater* **2012,** *24* (2), 268-72.

16. Masuda, T.; Uosaki, K., *Chem Lett* **2004,** *33* (7), 788-789.

17. Sun, Y.; Masuda, T.; Uosaki, K., *Chem Lett* **2012,** *41* (3), 328-330.

18. Kolivoska, V.; Gal, M.; Pospisil, L.; Valasek, M.; Hromadova, M., *Phys Chem Chem Phys* **2011,** *13* (23), 11422-9.

19. Mortimer, R. J.; Reynolds, J. R., *Displays* **2008,** *29* (5), 424-431.

20. Tieke, B., *Curr Opin Colloid In* **2011,** *16* (6), 499-507.

21. Abe, M.; Masuda, T.; Kondo, T.; Uosaki, K.; Sasaki, Y., *Angew Chemie* **2005,** *44* (3), 416-9.

22. Hara, K.; Akiyama, R.; Takakusagi, S.; Uosaki, K.; Yoshino, T.; Kagi, H.; Sawamura, M., *Angew Chem Int Edit* **2008,** *47* (30), 5627-5630.

23. Fukumitsu, H.; Masuda, T.; Qu, D.; Waki, Y.; Noguchi, H.; Shimazu, K.; Uosaki, K., *Chem Lett* **2010,** *39* (7), 768-770.

24. Imahori, H.; Hasobe, T.; Yamada, H.; Nishimura, Y.; Yamazaki, I.; Fukuzumi, S., *Langmuir* **2001,** *17* (16), 4925-4931.

25. Gadgil, B.; Damlin, P.; Aaritalo, T.; Kvarnstrom, C., *Electrochim Acta* **2014,** *133*, 268-274.

26. Mortimer, R. J., *Electrochim Acta* **1999,** *44* (18), 2971-2981.

27. Wang, G. M.; Fu, X. K.; Deng, J.; Huang, X. M.; Miao, Q., *Chem Phys Lett* **2013,** *579*, 105-110.

28. Bookbinder, D. C.; Lewis, N. S.; Wrighton, M. S., *J Am Chem Soc* **1981,** *103* (25), 7656-7659.

29. Chandrasekaran, K.; Whitten, D. G., *J Am Chem Soc* **1981,** *103* (24), 7270-7275.

30. Ghica, M. E.; Brett, C. M. A., *Anal Chim Acta* **2005,** *532* (2), 145-151.

31. Gunther, H.; Paxinos, A. S.; Schulz, M.; Vandijk, C.; Simon, H., *Angew Chem Int Edit* **1990,** *29* (9), 1053-1055.

32. Karatani, H.; Wada, N.; Sugimoto, T., *Bioelectrochemistry* **2003,** *60* (1-2), 57-64.

33. Lymar, S. V.; Hurst, J. K., *J Am Chem Soc* **1992,** *114* (24), 9498-9503.

34. Blubaugh, E. A.; Yacynych, A. M.; Heineman, W. R., *Anal Chem* **1979,** *51* (4), 561-565.

35. Martínez, A.; Colina, A.; Dryfe, R. A. W.; Ruiz, V., *Electrochim Acta* **2009,** *54* (22), 5071-5076.

36. Mortimer, R. J.; Varley, T. S., *Sol Energ Mat Sol C* **2012,** *99*, 213-220.

37. Bard A.J.; Faulkner, L. R., *Electrochemical Methods: Fundamentals and Applications.* John Wiley & Sons, Inc.: New York, 2001.

38. Ohno, H.; Hosoda, N.; Tsuchida, E., *Die Makromolekulare Chemie* **1983,** *184* (5), 1061-1070.

39. Huang, H.-X.; Qian, D.-J.; Nakamura, N.; Nakamura, C.; Wakayama, T.; Miyake, J., *Electrochimica Acta* **2004,** *49* (9-10), 1491-1498.

40. Bird, C. L.; Kuhn, A. T., *Chem Soc Rev* **1981,** *10* (1), 49-82.

41. Qian, D. J.; Nakamura, C.; Noda, K.; Zorin, N. A.; Miyake, J., *Appl Biochem Biotech* **2000,** *84-6*, 409-418.

42. Tang, X.; Schneider, T. W.; Walker, J. W.; Buttry, D. A., *Langmuir* **1996,** *12* (24), 5921-5933.

43. Redepenning, J.; Tunison, H. M.; Finklea, H. O., *Langmuir* **1993,** *9* (5), 1404-1407.

44. Stargardt, J. F.; Hawkridge, F. M., *Anal Chim Acta* **1983,** *146*, 8.

CHAPTER 5

VOLTAMMETRIC AND UV-VIS SPECTROELECTROCHEMICAL INVESTIGATION OF ELECTRON TRANSFER STEP AT VIOLOGEN MOLECULAR LAYER AND INCORPORATED Pt-COMPLEX

5.1 Introduction

Hydrogen evolution reaction (HER) is one of the most important and fundamental electrochemical processes, and the understanding of the HER process is important for applications such as hydrogen fuel cells and storage of energy via H_2 production.[1, 2] Recently, our group have reported the significant enhancement of (photo)electrochemical HER rate by incorporation of Pt species to the mono- and multi-layer with viologen group constructed on a hydrogen-terminated H-Si electrode.[3, 4] as shown in Figure 5-1. Si electrode, covalently attached viologen moieties and Pt species act as electron donor and photosensitizer, electron relay and catalyst, respectively, in this system. In order to understand the mechanism of HER catalytic reactions and to improve their efficiency, it is important to characterize both Pt-complex and viologen layers. The structure of Pt in viologen-modified Si electrode have been precisely studied.

On the other hand, viologen is a well-known electron transfer mediator. However, to date, no evidence which directly probe the electron transfer steps was mediated via viologen moiety (Figure 5-1(a)) or electron was transferred directly to Pt-complex (Figure 5-1(b)). In Chapter 4, the confined viologen moiety on ITO surfaces was successfully observed using UV-vis spectroelectrochemical technique. Thus, the two possibilities of electron transfer step process shown in Figure 5-1 could be clarified.
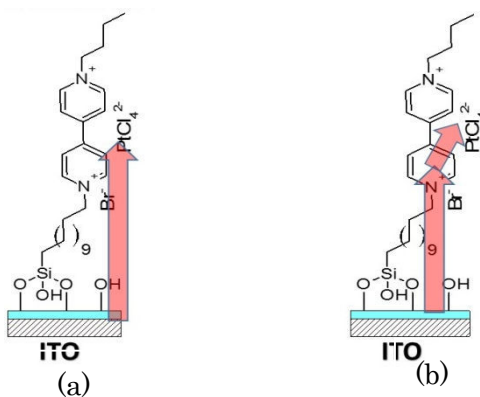
Figure 5- 1. Illustration of electron transfer process (a) direct electron transfer and (b) viologen-mediated electron transfer.

5.2 Results and discussion

5.2.1. Electrochemical hydrogen evolution reaction of Pt incorporated within viologen mono- and multi-layer

In order to study the catalytic activity of Pt-complex incorporated within viologen layer, the cyclic voltammogram of 1LV-, 3LV-, 5LV-ITO/Pt-complex electrodes were measured as shown in Figure 5-1. The voltammograms show a generation of cathodic current due to HER. The inset in Figure 5-1 shows the enlarged area of CVs showing that no redox peak related to the viologen species were observed. When the potential was swept back to positive potential, the peak current was observed this anodic current is related to the adsorption of hydrogen. These results clearly show that (1) the confinement of the Pt-complex accelerates HER significantly as observed before at Si(111) electrode,[14] (2) HER rates of the 1LV-, 3-LV, and 5LV-ITO/Pt-complex were significantly enhanced with the increase in number of the viologen layers.[5, 6] However, no evidence that electron transfer was mediated by viologen moiety.
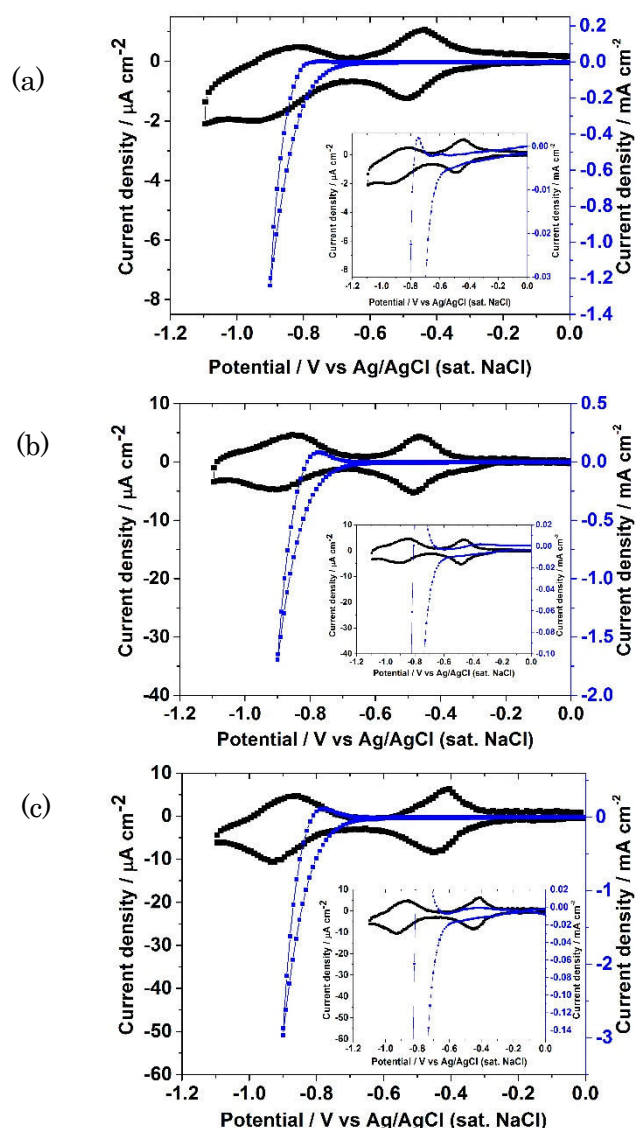
Figure 5- 2. Cyclic voltammetry of (a) 1LV-, (b) 3LV-, and (c) 5LV-ITO without Pt (black line) and with Pt-complex (blue line) measured in 0.1 M Na2SO4 aqueous solution, scan rate of 10 mV s^{-1}.

The catalytic activity of incorporated Pt-complex within viologen layers also measured in acidic and alkaline solutions (Figure 5-2(a) and (b)). The cathodic current due to HER shows that cathodic current were flew without any plateau as compared to the basic solution (Figure 5-2(c)). Auinger and co-workers explain both from theoretical and experimental work that in the unbuffered environment, the cyclic voltammetry of Pt exhibit one current

plateau region for surface pH-value between 5 and 12. The plateau current depends on the pH value and reflects the efforts required to change the surface pH-value.[7] The HER are considered as fast electrochemical reactions, meaning that only small perturbation from thermodynamic equilibrium, i.e. overpotential, is required to enhance the reaction rate. So that, the observed plateau domain does not correspond to a kinetic hindrance of the reaction, but rather to a drastic change of the surface pH with respect to the pH-value of the solution due to the reaction.[7, 8]

The cathodic current generated at 3LV- and 5LV-ITO/Pt-complex electrode larger that in 1LV-ITO/Pt-complex. This indicates that the generated current depend on the viologen layers, particularly with number of Pt-complex incorporated within viologen layers. The amount of Pt atoms expected from the number of viologen moieties at the 1LV-, 3LV-, and 5LV-ITO/Pt-complex surface was about 3.0×10^{13}, 7.2×10^{14}, and 1.3×10^{15} atoms cm^{-2}, respectively, (number of Pt atom was calculated by: number of viologen moiety x N_A, N_A = 6.02 x 10^{23} atom/mol)). Those Pt numbers are lower than previously reported on polyviologen layers on silicon.[9] However, the highly efficient HER current is comparable with that of previously.[4, 9, 10]
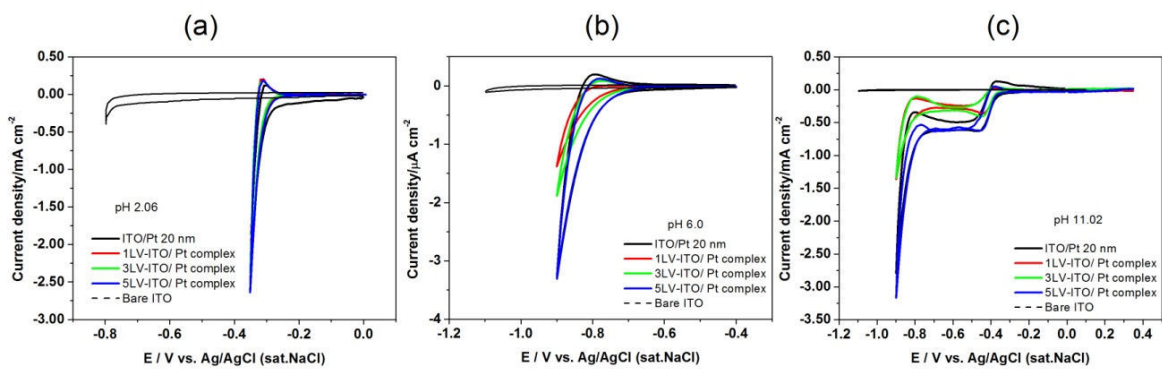

Figure 5- 3. The CVs of bare ITO (dashed-line), 1LV- (red line), 3LV- (green line) 5LV-ITO/Pt-complex and Pt deposited on ITO (black line) at various pH (a) 2.06, (b) 6.0, and (c) 11.02, scan rates of 10 mV s^{-1}.

5.2.2 Steady state UV-vis spectra of nLV-ITO/Pt-complex system

The UV-vis spectra of 1LV-, 3LV-, and 5LV-ITO after Pt-complex incorporation obtained by applying potential from -0.1 to -0.9 V were shown in Figure 5-4. The features of UV-vis absorbance peaks of $V^{\bullet+}$ or V^0 species were not observed, in all potential, after Pt incorporated (Figure 5-3(a)-(c)).
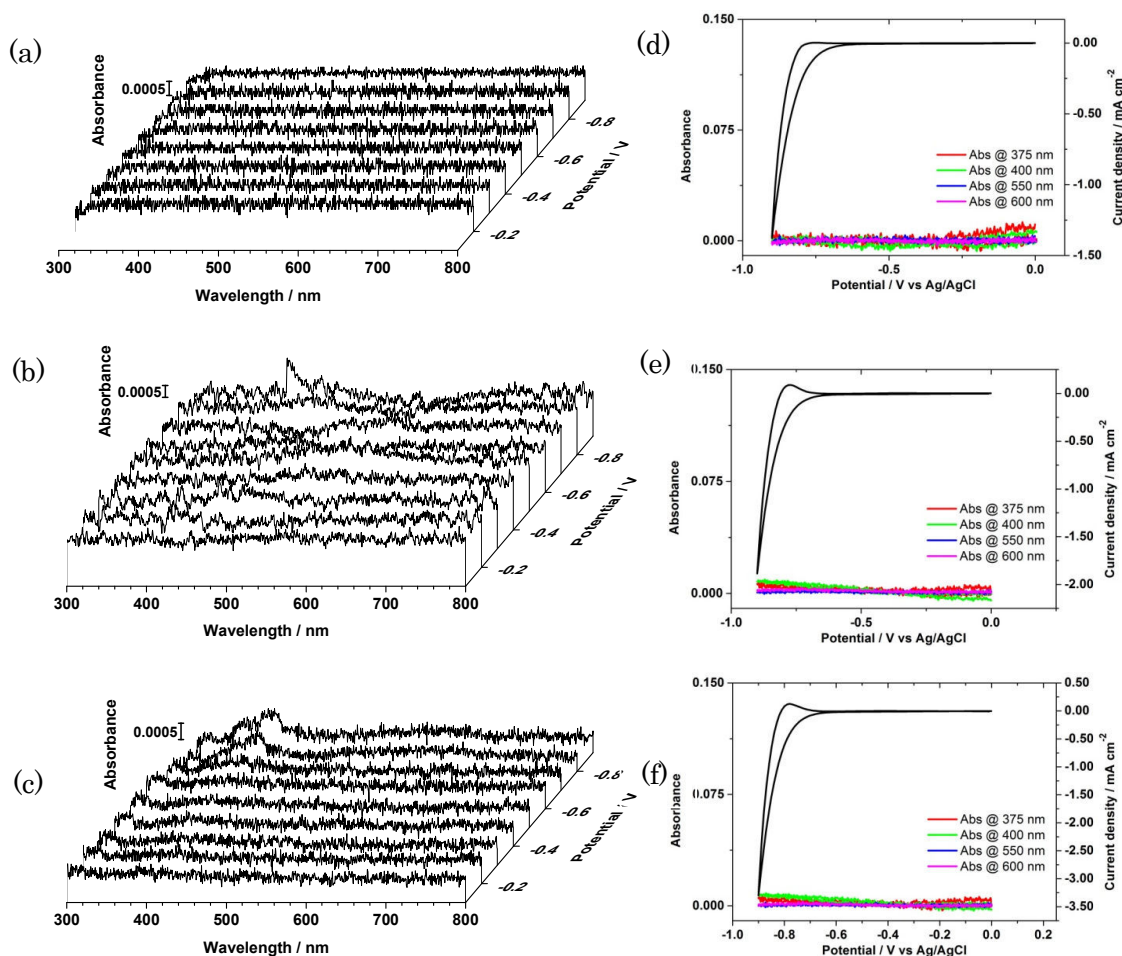

Figure 5-4. Steady state UV-vis spectra of (a) 1LV-, (b) 3LV- and (c) 5LV-ITO/Pt-complex as function of potential.

The $V^{\bullet+}$ and V^0 can be monitored by the absorbance changes at 375, 400, 550, and 600 nm as a characteristic peak of electrogenerated viologen species as it discussed in Chapter 4. Figure 5-3(d-f) shows the absorbance changes simultaneously measured with CVs. No

absorbance changes were observed at 1LV-, 3LV- and 5LV-ITO after Pt-complex incorporation. Both from CVs and steady state UV-vis spectra of nLV-ITO/Pt-complex, the electron transferred steps is still cannot be clarified whether the electron is transferred very fast from viologen to Pt-complex species or electron is directly transferred to Pt-complex.

5.2.3 Time-resolved UV-vis spectroelectrochemistry of 1LV-ITO/Pt complex

If the electron transferred very fast via viologen moiety, thus the intermediate of viologen species could be monitored from their spectra. Since the steady state and potential sweep coupling with UV-vis spectra cannot probe the viologen intermediate, then UV-vis spectroscopy coupled with double step potential chronoabsorptometry was carried out. Viologen monolayer was used in double potential steps measurement since it provides the simplest structure compared to multilayer structure.

Figure 5-5 shows the time profile of (a) potential, (b) current, and (c) absorbance at 375, 400, 550, and 600 nm of 1LV-ITO/Pt-complex when the potential stepped from $E_1= 0.0$ to $E_2= -0.24$ V. Current profile of 1LV-ITO showed a cathodic spike current and immediately recover to ca. 0 mA/cm^2. The absorbance intensity at 375, 400, 550, and 600 nm was also not changed. Similar current and absorbance profile were also observed when potential stepped to -0.28 V (Figure 5-6), -0.32 V (Figure 5-7). This result implies that, at these potential regions, HER has not been taken place yet, and viologen was in V^{2+} state.

The spike current was also observed when the potential was stepped to the more negative potential. The absorbance response at 375 and 400 nm were slightly increased when the potential was stepped to -0.36 V (Figure 5-8) and -0.4 V (Figure 5-9), then decay within ca. 2 ms. Although the absorbance at 600 nm was not observed in the transient spectra at these potential, as it observed in 1LV-ITO without Pt-complex (Figure 4-14 and Figure 4-15), the spectra has confirmed the appearance of $V^{\bullet+}$ species.

At more negative potential steps (-0.48, -0.52, -0.56, and -0.60 V), as shown in Figure 5-10, 5-11, and 5-12, and 5-13, respectively), the spike current observed and decayed, then keep flow (steady). This steady state current indicate that HER was taken place. The spike current was then formed when the potential was stepped back. The transient absorbance spectra of $V^{\bullet+}$ was then observed when the potential step to those potentials, then immediately decay within 1 ms. The transient spectra at the initial time were shown the absorbance peak at 400 and 600 nm. Based on the CVs and steady state UV-vis spectra (Figure 4-17, 4-18, and 4-19 in Chapter 4), at this potential range, the $V^{\bullet+}$ was formed.

In addition, to the cathodic spike were observed upon the negative potential steps (from 0 to -0.65, -0.72, -0.8 and -0.9V), steady state but gradually declining cathodic current due to HER flowed at -0.65, -0.72, -0.8 and -0.9V. Figure 5-14, 5-15, 5-16, and 5-17 (f), (g), and (h) show the absorbance response of the initial 5 ms to the potential step at 375 (black), 400 (red), 550 (green), and 600 nm (blue), contour of the absorbance as functions of probe wavelength and time (initial 5 ms) after the potential step, and (e) time-resolved spectra at -0.5 (black), 0 (red), 0.1 (green), 0.2 (blue), 0.5 (light blue), and 2 ms (pink) after the potential step at the 1LV-ITO/Pt-complex electrode. Absorbance transients of various wavelength and transient spectra at various times show that $V^{\bullet+}$ species were formed within the first 0.1 ms after potential was stepped to -0.72 V and then disappeared with a half-life of ca. 0.3 ms. No absorption was observed after 1 ms in whole wavelength region as is the steady state spectra, showing viologen is in V^{2+} state. This shows that $V^{\bullet+}$ is generated immediately after the potential is stepped to the potential more negative than the $V^{\bullet+}$ formation potential but its concentration decreases as an electron is transferred from $V^{\bullet+}$ to the Pt complex and $V^{\bullet+}$ is converted to V^{2+}, which again accepts an electron to become $V^{\bullet+}$. The reduced state of the Pt complex is consumed by reducing H+ and/or water to hydrogen and the oxidized state of the Pt complex is regenerated to accept an electron from $V^{\bullet+}$ as schematically shown in Figure 5-19.
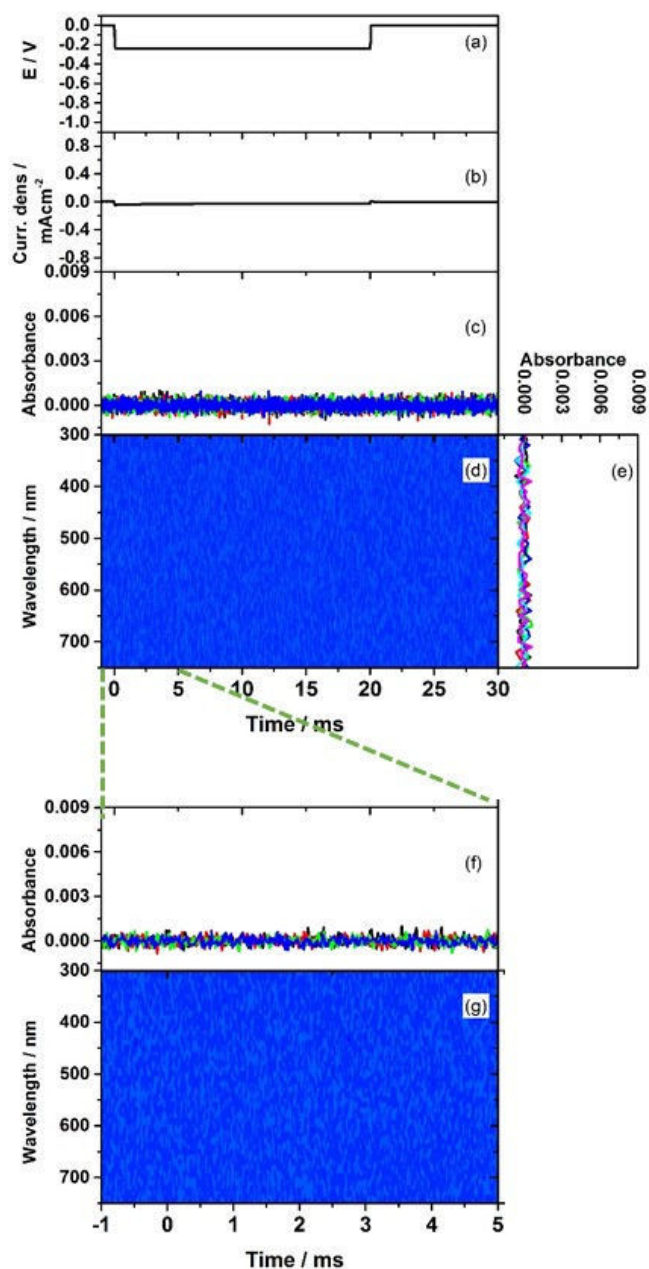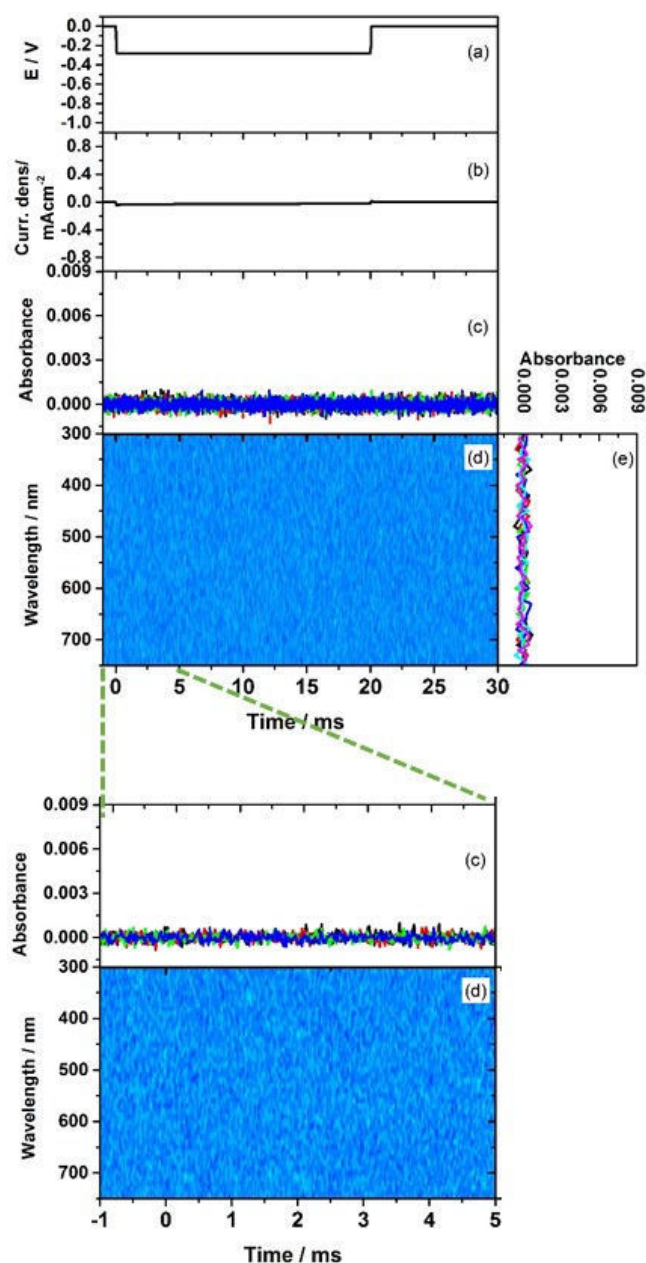
Figure 5-5. (a) potential profile (from 0 to -0.24 V), (b) current response, (c) absorbance response at 375 (black), 400 (red), 550 (blue), and 600 nm (green), (d) contour of the absorbance as functions of probe wavelength and time after the potential step, and (e) time resolved spectra at -0.5 (black), 0 (red), 0.1 (green), 0.2 (blue), 0.5 (light blue) and 2 ms (pink) after the potential step of 1LV-ITO/Pt-complex. (f) Absorbance response 375 (black), 400 (red), 550 (green), and 600 nm (blue), and (g) contour of the absorbance as functions of probe wavelength and time after the potential step of the initial 5ms to the potential step.
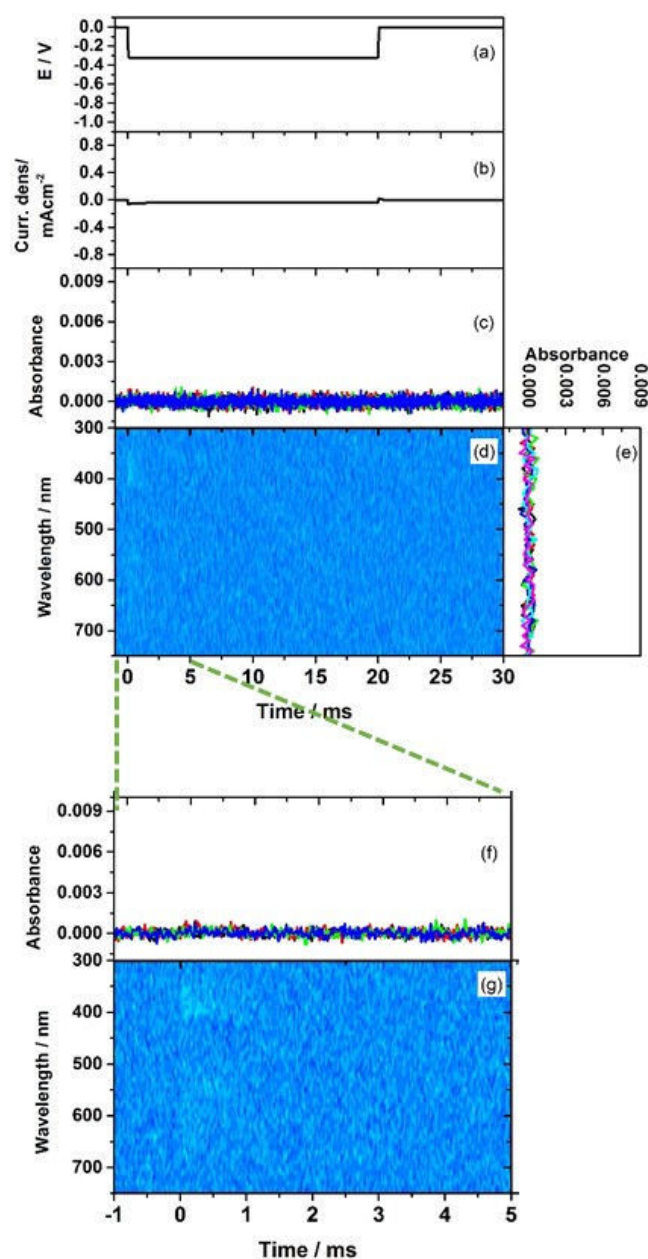
Figure 5-6. (a) potential profile (from 0 to -0.28 V), (b) current response, (c) absorbance response at 375 (black), 400 (red), 550 (blue), and 600 nm (green), (d) contour of the absorbance as functions of probe wavelength and time after the potential step, and (e) time resolved spectra at -0.5 (black), 0 (red), 0.1 (green), 0.2 (blue), 0.5 (light blue) and 2 ms (pink) after the potential step of 1LV-ITO/Pt-complex. (f) Absorbance response 375 (black), 400 (red), 550 (green), and 600 nm (blue), and (g) contour of the absorbance as functions of probe wavelength and time after the potential step of the initial 5ms to the potential step.
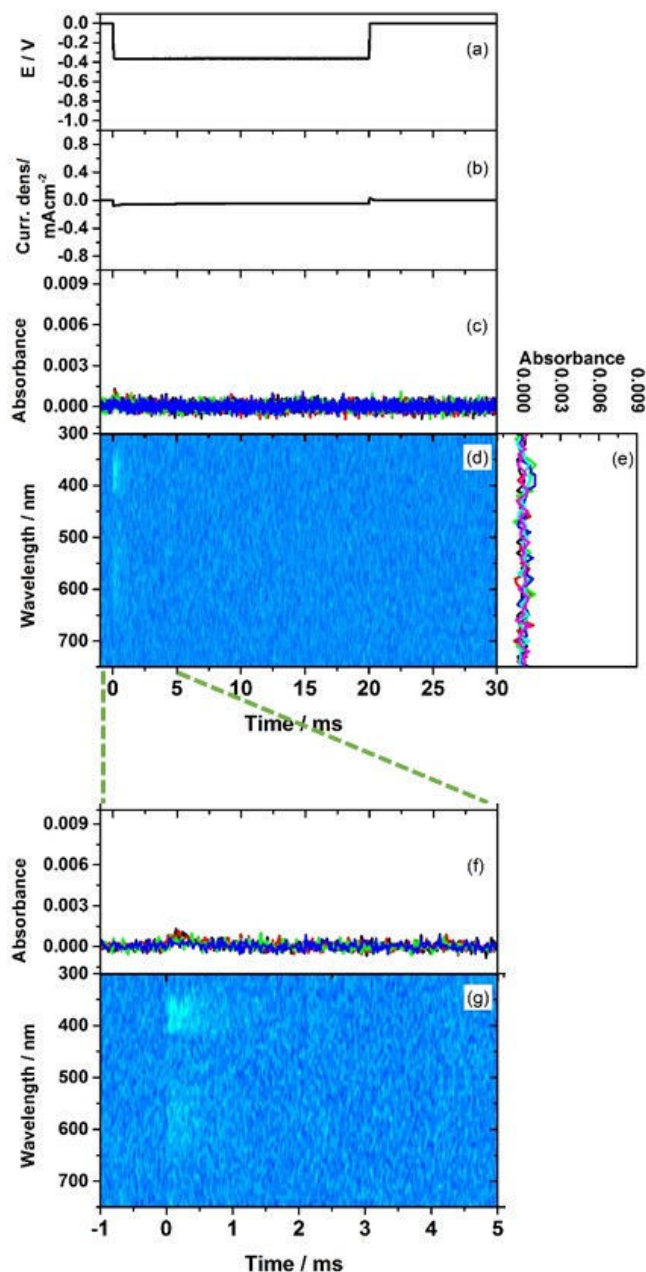
105

Figure 5-7. (a) potential profile (from 0 to -0.32 V), (b) current response, (c) absorbance response at 375 (black), 400 (red), 550 (blue), and 600 nm (green), (d) contour of the absorbance as functions of probe wavelength and time after the potential step, and (e) time resolved spectra at -0.5 (black), 0 (red), 0.1 (green), 0.2 (blue), 0.5 (light blue) and 2 ms (pink) after the potential step of 1LV-ITO/Pt-complex. (f) Absorbance response 375 (black), 400 (red), 550 (green), and 600 nm (blue), and (g) contour of the absorbance as functions of probe wavelength and time after the potential step of the initial 5ms to the potential step.
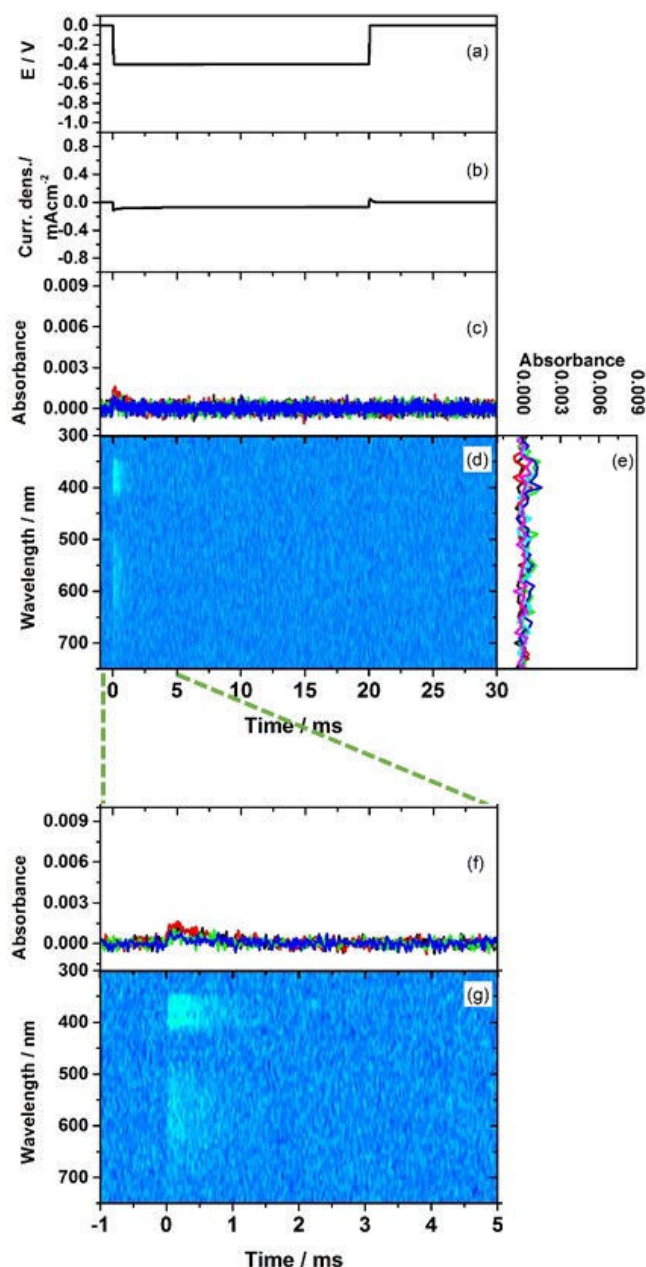
Figure 5-8. (a) potential profile (from 0 to -0.36 V), (b) current response, (c) absorbance response at 375 (black), 400 (red), 550 (blue), and 600 nm (green), (d) contour of the absorbance as functions of probe wavelength and time after the potential step, and (e) time resolved spectra at -0.5 (black), 0 (red), 0.1 (green), 0.2 (blue), 0.5 (light blue) and 2 ms (pink) after the potential step of 1LV-ITO/Pt-complex. (f) Absorbance response 375 (black), 400 (red), 550 (green), and 600 nm (blue), and (g) contour of the absorbance as functions of probe wavelength and time after the potential step of the initial 5ms to the potential step.

107

Figure 5-9. (a) potential profile (from 0 to -0.40 V), (b) current response, (c) absorbance response at 375 (black), 400 (red), 550 (blue), and 600 nm (green), (d) contour of the absorbance as functions of probe wavelength and time after the potential step, and (e) time resolved spectra at -0.5 (black), 0 (red), 0.1 (green), 0.2 (blue), 0.5 (light blue) and 2 ms (pink) after the potential step of 1LV-ITO/Pt-complex. (f) Absorbance response 375 (black), 400 (red), 550 (green), and 600 nm (blue), and (g) contour of the absorbance as functions of probe wavelength and time after the potential step of the initial 5ms to the potential step.
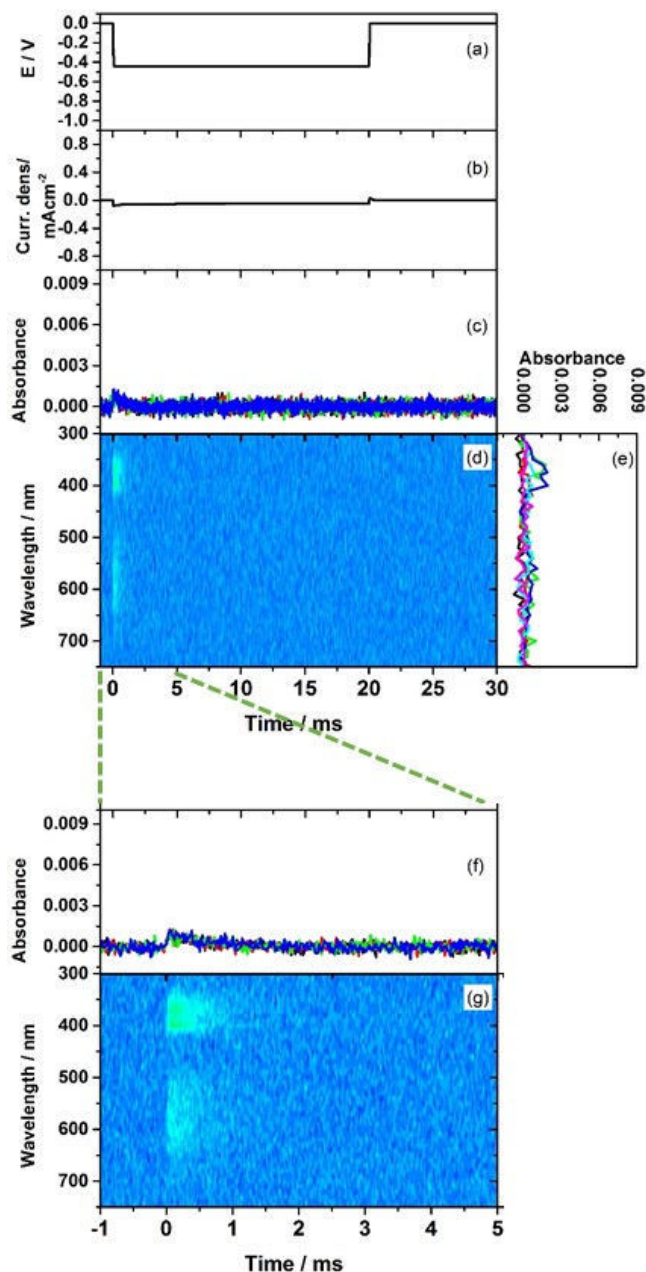
Figure 5-10. (a) potential profile (from 0 to -0.44 V), (b) current response, (c) absorbance response at 375 (black), 400 (red), 550 (blue), and 600 nm (green), (d) contour of the absorbance as functions of probe wavelength and time after the potential step, and (e) time resolved spectra at -0.5 (black), 0 (red), 0.1 (green), 0.2 (blue), 0.5 (light blue) and 2 ms (pink) after the potential step of 1LV-ITO/Pt-complex. (f) Absorbance response 375 (black), 400 (red), 550 (green), and 600 nm (blue), and (g) contour of the absorbance as functions of probe wavelength and time after the potential step of the initial 5ms to the potential step.
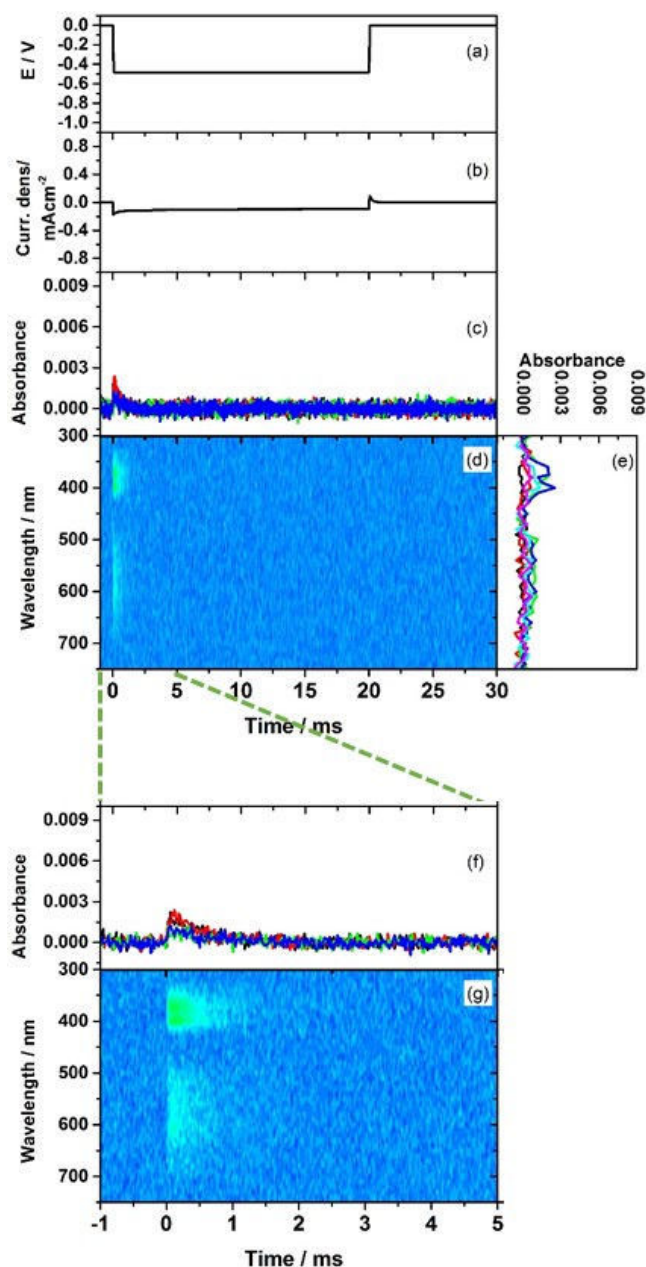
Figure 5-11. (a) potential profile (from 0 to -0.48 V), (b) current response, (c) absorbance response at 375 (black), 400 (red), 550 (blue), and 600 nm (green), (d) contour of the absorbance as functions of probe wavelength and time after the potential step, and (e) time resolved spectra at -0.5 (black), 0 (red), 0.1 (green), 0.2 (blue), 0.5 (light blue) and 2 ms (pink) after the potential step of 1LV-ITO/Pt-complex. (f) Absorbance response 375 (black), 400 (red), 550 (green), and 600 nm (blue), and (g) contour of the absorbance as functions of probe wavelength and time after the potential step of the initial 5ms to the potential step.
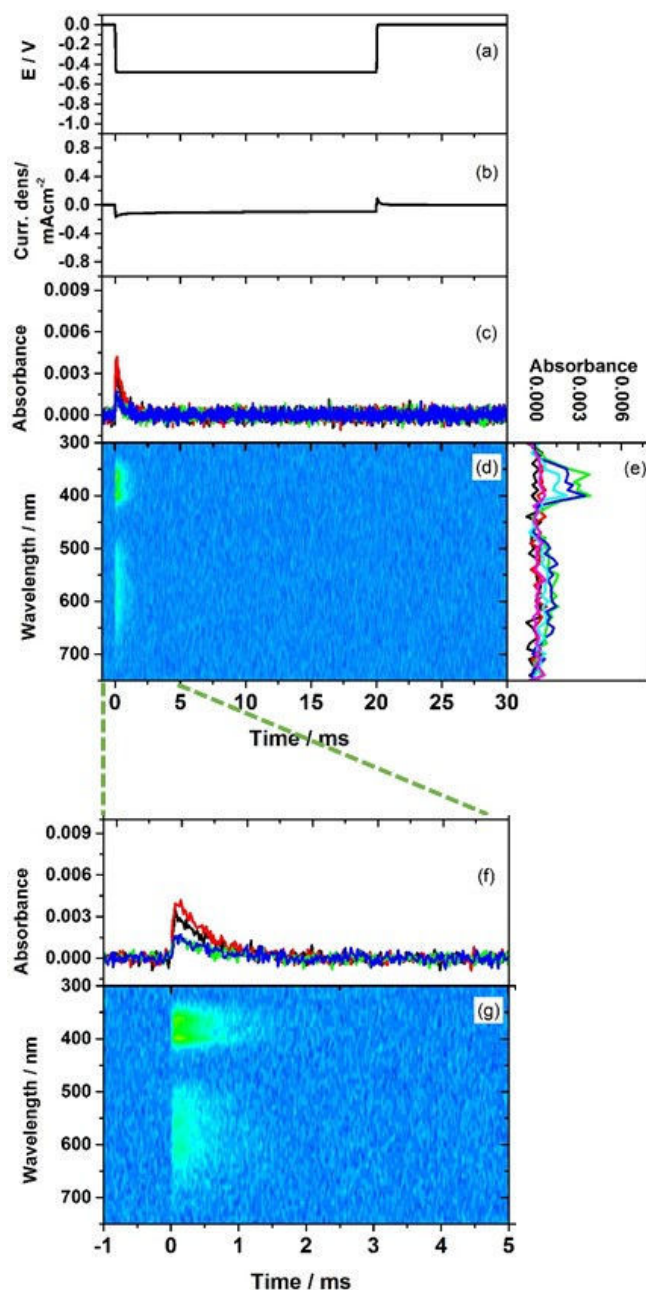
110

Figure 5-12. (a) potential profile (from 0 to -0.52 V), (b) current response, (c) absorbance response at 375 (black), 400 (red), 550 (blue), and 600 nm (green), (d) contour of the absorbance as functions of probe wavelength and time after the potential step, and (e) time resolved spectra at -0.5 (black), 0 (red), 0.1 (green), 0.2 (blue), 0.5 (light blue) and 2 ms (pink) after the potential step of 1LV-ITO/Pt-complex. (f) Absorbance response 375 (black), 400 (red), 550 (green), and 600 nm (blue), and (g) contour of the absorbance as functions of probe wavelength and time after the potential step of the initial 5ms to the potential step.
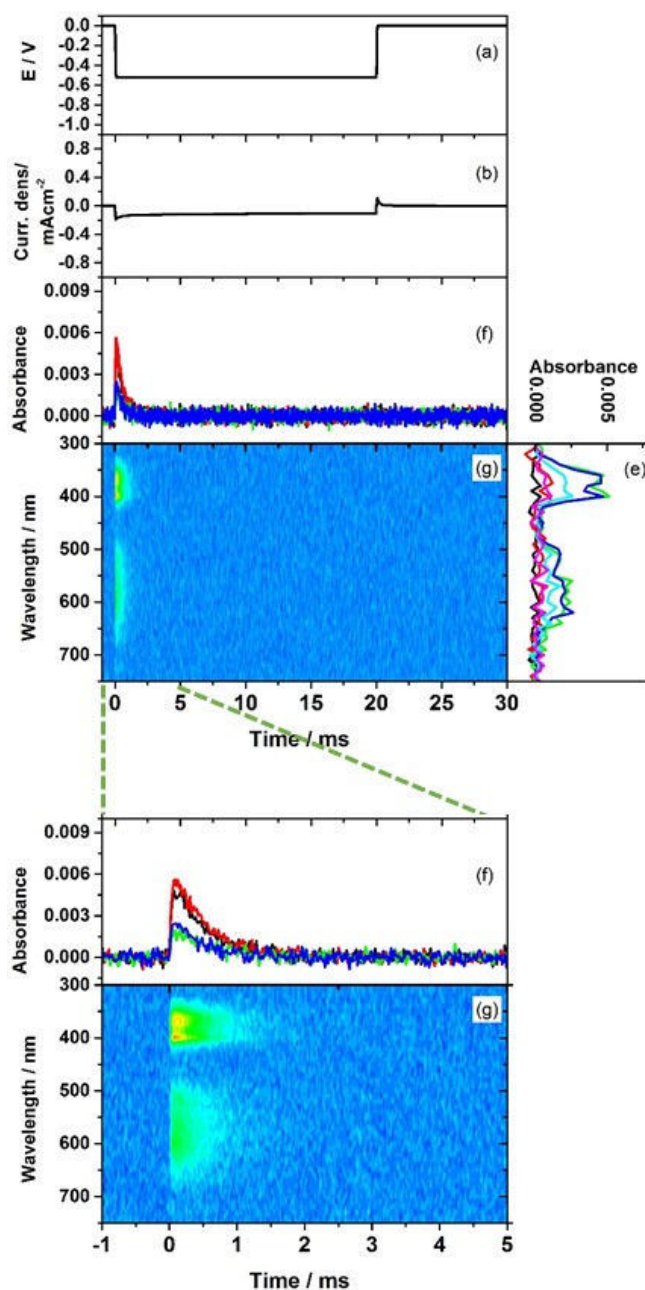
Figure 5-13. (a) potential profile (from 0 to -0.56 V), (b) current response, (c) absorbance response at 375 (black), 400 (red), 550 (blue), and 600 nm (green), (d) contour of the absorbance as functions of probe wavelength and time after the potential step, and (e) time resolved spectra at -0.5 (black), 0 (red), 0.1 (green), 0.2 (blue), 0.5 (light blue) and 2 ms (pink) after the potential step of 1LV-ITO/Pt-complex. (f) Absorbance response 375 (black), 400 (red), 550 (green), and 600 nm (blue), and (g) contour of the absorbance as functions of probe wavelength and time after the potential step of the initial 5ms to the potential step.
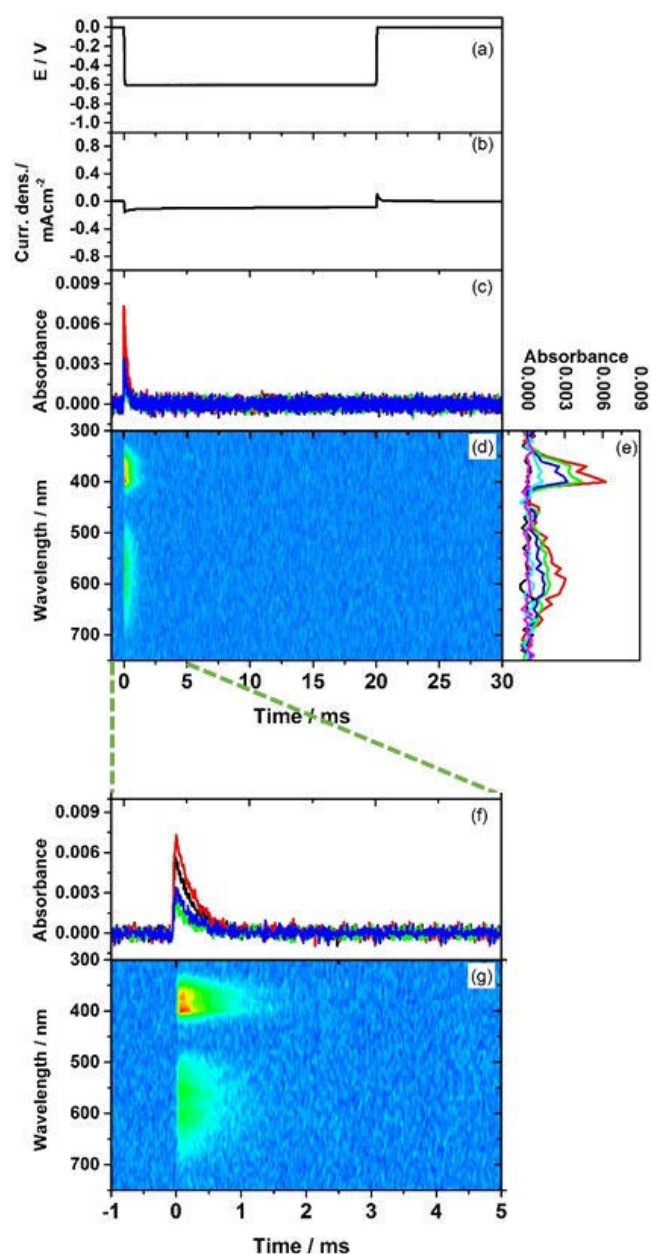
112

Figure 5-14. (a) potential profile (from 0 to -0.60 V), (b) current response, (c) absorbance response at 375 (black), 400 (red), 550 (blue), and 600 nm (green), (d) contour of the absorbance as functions of probe wavelength and time after the potential step, and (e) time resolved spectra at -0.5 (black), 0 (red), 0.1 (green), 0.2 (blue), 0.5 (light blue) and 2 ms (pink) after the potential step of 1LV-ITO/Pt-complex. (f) Absorbance response 375 (black), 400 (red), 550 (green), and 600 nm (blue), and (g) contour of the absorbance as functions of probe wavelength and time after the potential step of the initial 5ms to the potential step.
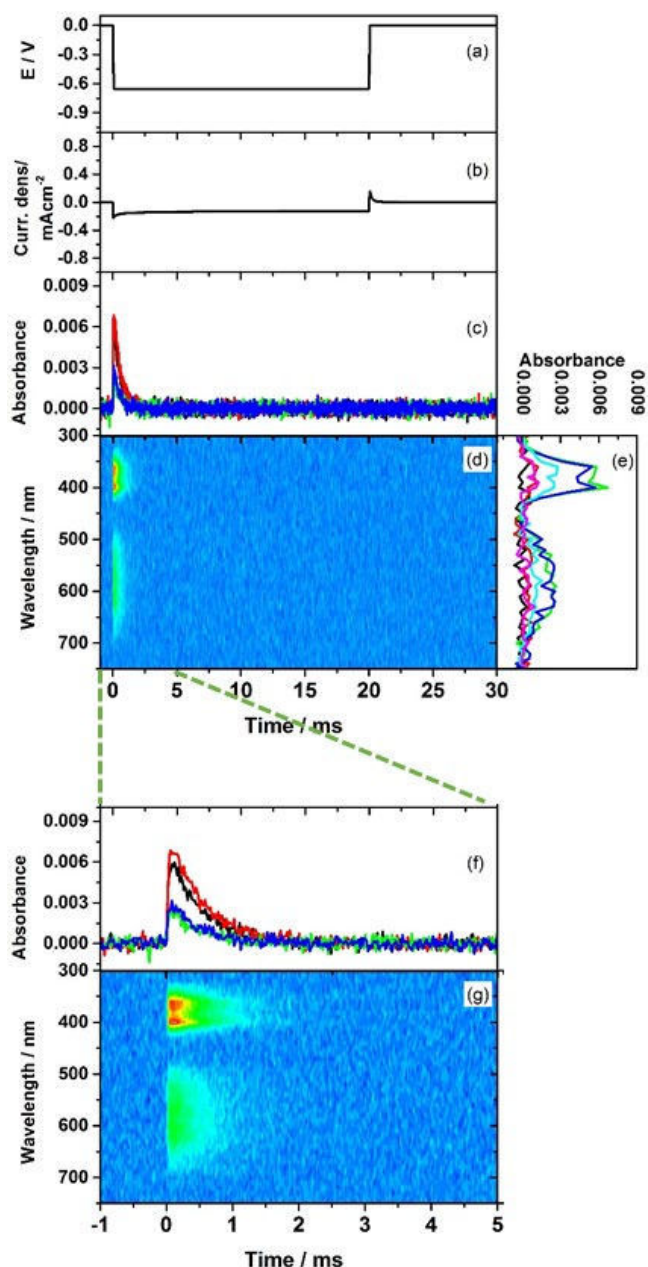
113

Figure 5-15. (a) potential profile (from 0 to -0.65 V), (b) current response, (c) absorbance response at 375 (black), 400 (red), 550 (blue), and 600 nm (green), (d) contour of the absorbance as functions of probe wavelength and time after the potential step, and (e) time resolved spectra at -0.5 (black), 0 (red), 0.1 (green), 0.2 (blue), 0.5 (light blue) and 2 ms (pink) after the potential step of 1LV-ITO/Pt-complex. (f) Absorbance response 375 (black), 400 (red), 550 (green), and 600 nm (blue), and (g) contour of the absorbance as functions of probe wavelength and time after the potential step of the initial 5ms to the potential step.
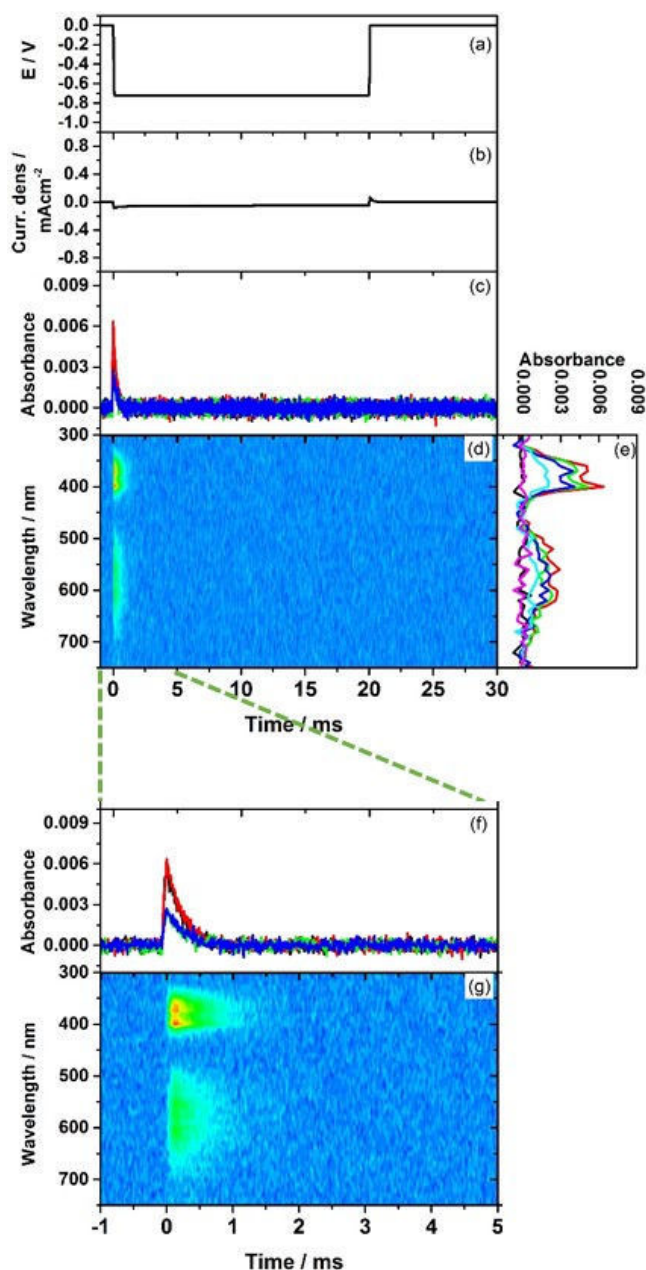
114

Figure 5-16. (a) potential profile (from 0 to -0.72 V), (b) current response, (c) absorbance response at 375 (black), 400 (red), 550 (blue), and 600 nm (green), (d) contour of the absorbance as functions of probe wavelength and time after the potential step, and (e) time resolved spectra at -0.5 (black), 0 (red), 0.1 (green), 0.2 (blue), 0.5 (light blue) and 2 ms (pink) after the potential step of 1LV-ITO/Pt-complex. (f) Absorbance response 375 (black), 400 (red), 550 (green), and 600 nm (blue), and (g) contour of the absorbance as functions of probe wavelength and time after the potential step of the initial 5ms to the potential step.
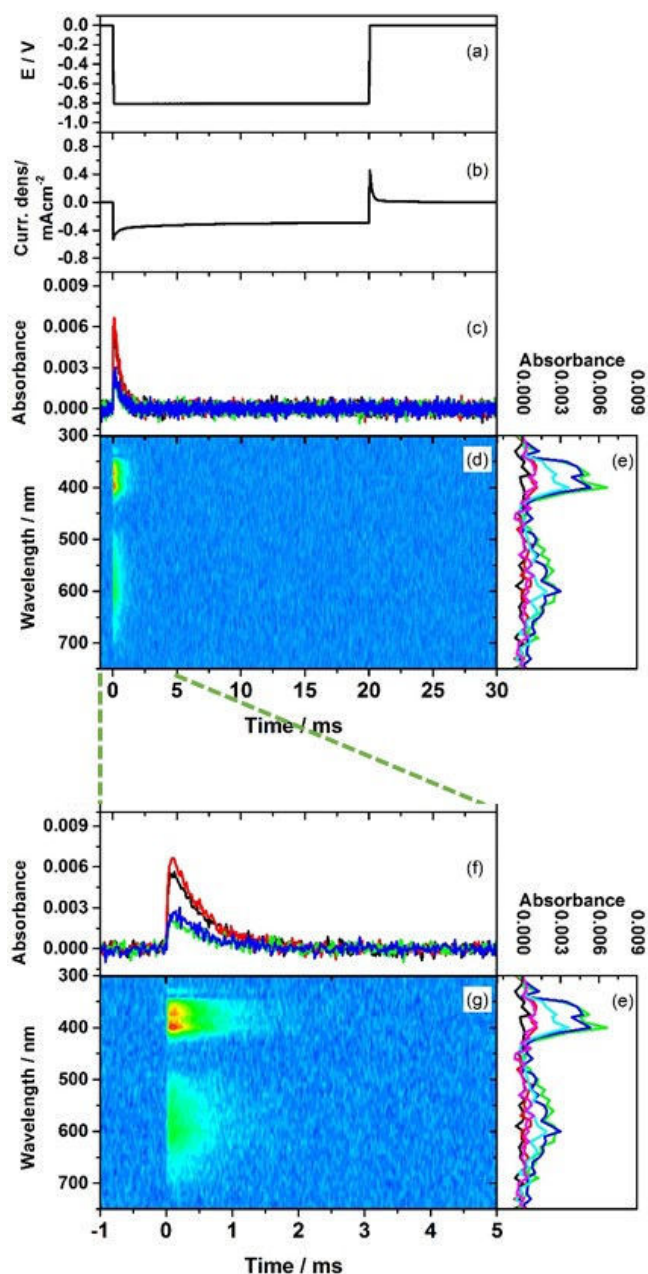
Figure 5-17. (a) potential profile (from 0 to -0.8 V), (b) current response, (c) absorbance response at 375 (black), 400 (red), 550 (blue), and 600 nm (green), (d) contour of the absorbance as functions of probe wavelength and time after the potential step, and (e) time resolved spectra at -0.5 (black), 0 (red), 0.1 (green), 0.2 (blue), 0.5 (light blue) and 2 ms (pink) after the potential step of 1LV-ITO/Pt-complex. (f) Absorbance response 375 (black), 400 (red), 550 (green), and 600 nm (blue), and (g) contour of the absorbance as functions of probe wavelength and time after the potential step of the initial 5ms to the potential step.
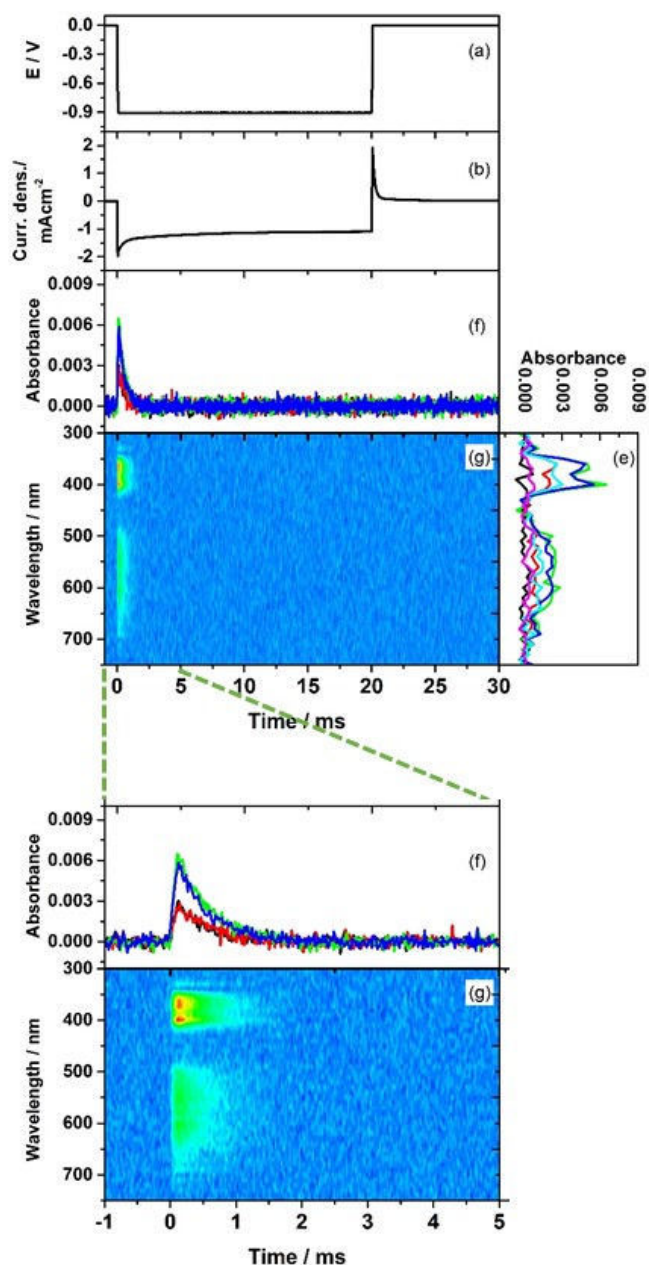
Figure 5-18. (a) potential profile (from 0 to -0.90 V), (b) current response, (c) absorbance response at 375 (black), 400 (red), 550 (blue), and 600 nm (green), (d) contour of the absorbance as functions of probe wavelength and time after the potential step, and (e) time resolved spectra at -0.5 (black), 0 (red), 0.1 (green), 0.2 (blue), 0.5 (light blue) and 2 ms (pink) after the potential step of 1LV-ITO/Pt-complex. (f) Absorbance response 375 (blue), 400 (green), 550 (red), and 600 nm (black), and (g) contour of the absorbance as functions of probe wavelength and time after the potential step of the initial 5ms to the potential step.
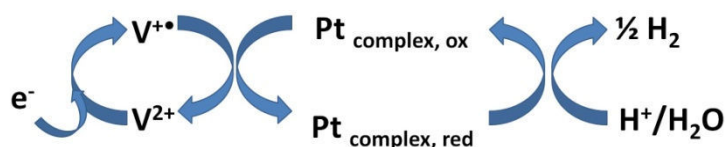
117

Figure 5-19. Schematic of electron transfer steps mediated viologen moiety during HER catalyzed by Pt-complex.

5.3. Conclusion

Pt-complex incorporated within viologen layers act as a hydrogen evolution reaction catalyst at various pH. The large cathodic current increased as the number of viologen layer increase which means that the number of incorporated Pt-complex also increase. The viologen species cannot be observed via steady state UV-vis spectra measurement in the presence of Pt-complex. However, the formation of $V^{\bullet+}$ was confirmed from the transient absorbance spectra upon potential step measurement. These results provided a direct evidence of electron transfer step was mediated by viologen moiety.

5.4. References

1. Kiwi, J.; Grätzel, M., *Nature* **1979,** *281* (5733), 657-658.

2. Heyrovsky, M., *Collection of Czechoslovak Chemical Communications* **2001,** *66* (1), 67-80.

3. Masuda, T.; Uosaki, K., *Chem Lett* **2004,** *33* (7), 788-789.

4. Masuda, T.; Shimazu, K.; Uosaki, K., *J Phys Chem C* **2008,** *112* (29), 10923-10930.

5. Haiss, W.; van Zalinge, H.; Hobenreich, H.; Bethell, D.; Schiffrin, D. J.; Higgins, S. J.; Nichols, R. J., *Langmuir* **2004,** *20* (18), 7694-7702.

6. Gittins, D. I.; Bethell, D.; Neeichols, R. J.; Schiffrin, D. J., *J Mat Chem* **2000,** *10* (1), 79-83.

7. Auinger, M.; Katsounaros, I.; Meier, J. C.; Klemm, S. O.; Biedermann, P. U.; Topalov, A. A.; Rohwerder, M.; Mayrhofer, K. J., *Phys Chem Chem Phys* **2011,** *13* (36), 16384-94.

8. Katsounaros, I.; Meier, J. C.; Klemm, S. O.; Topalov, A. A.; Biedermann, P. U.; Auinger, M.; Mayrhofer, K. J. J., *Electrochem Commun* **2011,** *13* (6), 634-637.

9. Abruna, H. D.; Bard, A. J., *J Am Chem Soc* **1981,** *103* (23), 6898-6901.

10. Masuda, T.; Fukumitsu, H.; Takakusagi, S.; Chun, W. J.; Kondo, T.; Asakura, K.; Uosaki, K., *Adv Mater* **2012,** *24* (2), 268-72.

CHAPTER 6
GENERAL CONCLUSION AND FUTURE PROSPECTS

The construction of mono- and multi-layers of viologen molecules on ITO surfaces and demonstration of their functionalities such as electron transfer mediator for very highly efficient hydrogen evolution electrocatalysts were performed in this thesis.

In Chapter 3, viologen moiety was constructed on ITO surface via step by step surface coupling reactions consist of silane coupling, 4,4`-bipyridine coupling, and terminal alkylbromide coupling reactions. Then Pt complex was incorporated within viologen layers by ion exchange reaction. Each step was confirmed by FTIR and cyclic voltammetry of $Fe(CN)_6^{3-/4-}$ system to confirm the molecular layer formation. The XP spectra result suggest that viologen layer was constructed on ITO surface. The angle-resolved XPS spectra confirm that the Pt complex was attached at the distance as similar as N atom of pyridine ring on viologen moieties.

In Chapter 4, cyclic voltammetry characterization of viologen both in solution and confined molecules was investigated. The in situ UV-vis spectroelectrochemical properties of viologen on ITO electrode was also studied. The two redox waves on viologen modified ITO surfaces were in a good agreement with redox characteristic of dissolved methyl viologen related to the formation of radical cation and neutral viologen species. The coverage of viologen moiety was increased by 5.5×10^{-10} mol cm^{-2} per layer. Further, the steady state UV-vis spectra were confirmed the potential dependent of viologen species formation. Viologen radical cation shows the main peak at 400 and 600 nm while neutral viologen only shows absorbance peak at 400 nm. The absorbance changes during double potential steps measurement shows that electrogenerated viologen species switch very fast

(ca. 200 us) from its dication to radical cation or neutral species.

In Chapter 5, electron transfer mediation capability of viologen moiety was demonstrated at viologen-modified ITO surface. Hydrogen evolution reaction (HER) rate was improved by incorporation of Pt complex on the viologen-modified ITO surface. In advanced, an improvement of HER rate was achieved at the viologen multilayer modified ITO electrode with platinum complex. In the presence of Pt complex, both CV and steady state UV-vis spectra cannot probe the viologen species. However, the time-resolved UV-vis spectra coupled with double potential shows the evidence of the viologen radical cation from very fast absorbance change and then decay within 1 ms. The radical cation species was observed from the transient absorbance spectra. These results clarify the viologen monolayers roles as an electron transfer mediator in the electrocatalytic process.

In this thesis, time-resolved UV-vis spectroelectrochemistry technique has been used to monitor the intermediate species generated during HER catalyzed by Pt complex, so the electron transfer mediation properties of viologen moiety confined on ITO surface can be directly proved. The study was carried out on monolayer viologen constructed on ITO in neutral pH solution.

In future, the time resolution can be improved so that the electrogenerated intermediate species could be precisely detected. In the present research, the viologen dimer can only probe during steady state. Then, the effect of viologen layer will also be investigated, since in the dimer species strongly observed at high viologen coverage. After all, the spectroelectrochemical technique will be extended to investigate the structural changes of viologen species using surface enhanced Infra-Red absorption (SEIRA). These studies are expected to provide a better understanding of the electrocatalytic by the molecular catalyst.